ANALYSIS OF LINKED AIRCRAFT AERODYNAMICS AND FLIGHT DYNAMICS

A Dissertation

Presented to the Faculty of the Graduate School

of Cornell University

In Partial Fulfillment of the Requirements for the Degree of

Doctor of Philosophy

by

Edgar Adrian Cuji

August 2011

ANALYSIS OF LINKED AIRCRAFT AERODYNAMICS AND FLIGHT DYNAMICS

Edgar Adrian Cuji, Ph. D.

Cornell University 2011

In this research, I have analyzed different aircrafts with nonconventional wings. The analyses have included aerodynamic modeling, flight dynamics and trajectory optimization. Two different nonconventional aircrafts are analyzed, a V-shape morphing wings and a Linked UAV system. A modern adaptation of Prandtl's lifting-line method is utilized to analyze the aerodynamics of both systems. This method can compute the aerodynamic forces for a system of lifting surfaces with arbitrary camber, sweep, dihedral, position and orientation. The V-shape morphing wings consist of a wing configuration that has two panels, an out-of-plane dihedral section and a horizontal section. An analysis of the aircraft turning dynamics shows that by manipulating the dihedral angles, of the V-shape wings, either by symmetric or asymmetric wing shape changes, can affect the turning capabilities of an aircraft to perform a variety of different missions depending on the importance of each of the turning performance measurements.

A linked UAV concept, where individual UAVs link at high altitude, creates an aerodynamically efficient system of aircraft which has long endurance capabilities and can cruise for extended periods with significantly reduced power loads. This dissertation presents an analysis of close proximity aerodynamics and aircraft dynamics of two Linked UAVs. As the UAVs approach each other for wingtip

docking there are strong aerodynamic coupling between their wings tips. An aerodynamic disturbance intensity field has been generated, utilizing both simulation and wind tunnel data, to determine a trajectory for the two UAVs to approach each other for midair docking. Finally, two optimal trajectories, a 2-D and 3-D docking trajectories are generated and compared. Dynamic wind tunnel test are performed to compare different midair wingtip docking trajectories. The results of the optimization concludes that a trajectory with a span-wise approach is more desirable since it goes through the least aerodynamic disturbances and requires less control effort to perform the midair docking maneuver.

BIOGRAPHICAL SKETCH

Edgar Adrian Cuji was born in 1983 in Gualaceo, Ecuador. In 1994 he moved to the United States, where he graduated from Manhattan Center High School in 2001. He attended the University of Rochester where he received a Bachelor of Science in Mechanical Engineering with High Distinction in the Major and a Certificate of Management with a concentration in Accounting. Upon graduating, Edgar continued into the doctoral program at Cornell University where he joined Dr. Ephrahim Garcia's Laboratory for Intelligent Machine Systems (LIMS). There he received an Olin Graduate Fellowship, a Sloan Graduate Fellowship and Provost's Diversity Fellowship. In May 2009, he received a Master of Science in Aerospace Engineering. Following graduation, he will begin his professional career at The Charles Stark Draper Laboratory.

To my parents.

ACKNOWLEDGMENTS

I would like to first thank my graduate adviser Ephrahim Garcia of Cornell University. Under his guidance, I have received advice and great words of wisdom academically, professional, and otherwise.

I would like to acknowledge my graduate committee: Dr. David Caughey and Dr. Brandon Hencey of Cornell University. I appreciate all of their support and insight throughout this process.

I would also like to thank all of the members of the Laboratory on Intelligent Machines Systems (LIMS) at Cornell University, namely Adam Wickenheiser, Justin Manzo, Tim Reissman, John Dietl, Allen Hurst, Matt Bryant and Mitch Walters. Also, I would like to thank the students that worked under my guidance, particularly Sarah Leung, Trent Lukaczyk, and David Hartino.

I would like to thank my colleagues and friends in Cornell University's Mechanical and Aerospace Engineering graduate program, notably, Bernardo Cordovez, Justin Atchison, Vishal Tandon, Alex Barbati, Michael Kalontarov, Juan Salazar and Mike Tolley, for all the support and encouragement. I value their friendship and camaraderie and hopefully will continue in touch as we all continue into our future endeavors in our professional lives.

I would also like to thank Marcia Sawyer, Cornell University's Mechanical and Aerospace Engineering Graduate Field Administrator. Marcia has been a joy to know, and is responsible for helping all graduate students go through a smooth graduate program process. She is always in top of everything that is required and it has made my graduate experience much easier.

Finally, last but not least, to my family, whose support has been the foundation of all of my successes. I thank my parents, Luis and Luz Cuji for all the support and for

always teaching me that hard work is key to success in life. Thank you for all the sacrifices that have made to help me get to this stage. Their attitude of always working hard has been my inspiration and guide for everything I have done. I thank my two brothers, Fabian and Jorge, for all the support and encouragement throughout my life.

TABLE OF CONTENTS

LIST OF FIGURES

CHAPTER 1

CHAPTER 2

CHAPTER 4

LIST OF TABLES

LIST OF SYMBOLS

CHAPTER 1

α	angle of attack
β	sideslip angle
D	aircraft drag
g	gravity
γ	flight path angle
Γ	vortex strength
L	wingspan length
L1	lift in section 1 of V-shape wing
L2	lift in section 2 of V-shape wing
L3	lift in section 3 of V-shape wing
L4	lift in section 4 of V-shape wing
L2h	horizontal force in section 2 of V-shape wing
L3h	horizontal force in section 3 of V-shape wing
n	load factor
R	turning radius
T	aircraft thrust
μ	bank angle
V	aircraft speed
$V\infty$	velocity of the freestream flow
W	aircraft weight
ω	turning rate

CHAPTER 2

α	angle of Attack
AR	aspect ratio
b	wing span
c	chord-length
Clift	coefficient of lift
Croll	coefficient of roll
Γ	vortex Strength
L	wing length
x	chord-wise coordinate
y	span-wise coordinate
z	vertical coordinate
dx	separation in the x direction
dy	separation in the y direction
dz	separation in the z direction
V	velocity of the freestream flow

CHAPTER 3

α	angle of Attack
AR	aspect ratio
b	wing span
c	chord-length
Γ	vortex Strength
L	wing length
x	chord-wise coordinate
y	span-wise coordinate

z	vertical coordinate

CHAPTER 4

AoA	angle of Attack
b	wing span
c	chord-length
L	wing length
x	chord-wise coordinate
y	span-wise coordinate
z	vertical coordinate
r_0	initial separation
r(t)	docking trajectory
dr	change in trajectory
J	total scalar cost function
Λ_F	force weighting matrix
Λ_M	moment weighting matrix
$F_{l(r)}$	close proximity forces of leader
$F_{f(r)}$	close proximity forces of follower
$M_{l(r)}$	close proximity moment of leader
$M_{f(r)}$	close proximity moment of follower

CHAPTER 1

ANALYSIS OF TURNING PERFORMANCE OF SYMMETRIC AND ASYMMETRIC V-SHAPE MORPHING WINGS*

1.1 Abstract

This paper present the effect of morphing on the aircraft turning dynamics for symmetric and asymmetric V-shape changing wings. The aerodynamic forces will be calculated using a 3D aerodynamic model developed that utilizes a modern adaptation of Prandtl's lifting-line method which can be used for wings of arbitrary camber, sweep and dihedral. The method will be applied to analyze symmetric and asymmetric V-shaped wing configurations of interest for morphing aircraft applications. The V-shaped wing has two panels, an out-of-plane dihedral panel and a horizontal panel. A study of the lift characteristics for symmetric and asymmetric configurations with and without flap deflection will be presented. An investigation as to how the partial dihedral affects the dynamics of the vehicle, in turning, for wings with asymmetric flap deflection is performed. A comparison of the different turning performance measurements, turning radius, bank angle, load factor, turning rate and roll moment coefficient will be presented.

*Reprinted with permission from Cuji, E. and Garcia E. "Analysis of Turning Performance of Symmetric and Asymmetric V-Shape Morphing Wings", *International Review of Aerospace Engineering Journal*, Vol 4, No 1, February, 2011.

1.2 Introduction

Presently, most aircraft are designed and optimized for a particular mission. Increasingly it has been considered desirable for an aircraft to perform multiple missions in different flight regimes [1]. For example, an aircraft that could fly efficiently and morph to be maneuverable would enable new missions. As seen in nature, birds morph their bodies in different flight regimes to increase performance [2], [3]. Using birds as an inspiration, research toward the development of a morphing aircraft has been suggested [1]. A morphing aircraft is defined as an aircraft vehicle that could perform gross shape changes in-flight to increasing efficiency, adaptability and/or mission performance [4], [5]. Recent advances in smart materials and actuators have enabled shape changing structures and, eventually, the development of a morphing aircraft structures without the addition of extra weight [6].

Morphing technologies are currently being studied to expand the range of missions that an aircraft can perform. There have been programs dedicated to study the feasibility of incorporating morphing technology to aircraft, especially for UAVs, like the DARPA Morphing Aircraft Structures program [7]. Herein Joshi, et al., have demonstrated the impact of morphing wings on aircraft performance and provided a method for performance metrics for a morphing aircraft [8]. The goal of a morphing aircraft is to impact the performance of different maneuvers and flight conditions for an array of different missions.

In this paper, we will investigate the impact of out-of-plane wing shape changes on different flight conditions like turning flight. The wing configuration that we will be studying is a wing configuration that has two panels, an out-of-plane dihedral section and a horizontal section, like a V shape wing configuration as it can be seen in Figures

1.2 and 1.3. Both symmetric and asymmetric dihedral angle changes will be performed. An investigation of the effects of flaps on the wings for both configurations will also be performed. We want to investigate how both symmetric and asymmetric wing shape changes affect the aircraft response for the different flight conditions. We want to see how we can take advantage of these properties by utilizing both symmetric and asymmetric wing shape changes to perform maneuvers that conventional aircraft cannot do.

Each of the different performance metrics will have a different importance depending on the aircraft mission. For example, for a fighter aircraft the ability for fast and sharp turns is desirable. But for surveillance missions having small bank angles during a turn to keep the surveillance equipment pointing at a certain direction is desirable. An application where small bank angles are desirable is for when the aircraft energy is beamed to the aircraft. For example, for a microwave powered airplane, power is beamed directly into rectennas located in the plane and controlling orientation is critical for minimizing power losses [9], [10].

In this paper we are going to explore the effects of the partial dihedral on the aircraft dynamics and performance, especially on turning, for wings with flaps deflections. An analysis for both symmetric and asymmetric V-shaped wings without flaps has previously been presented [11]. First, we will present the aerodynamics characteristics for both symmetric and asymmetric wings with and without flap deflections. The vertical and lateral lift force will be presented for wings with different partial dihedral angles. An analysis of the effect of the partial dihedral on different turning performance measurements (which are turning radius, turning rate, bank angle, load factor and roll moment) will be performed. For this wing configuration, since some of the lift force at the dihedral portion will have a horizontal component, it will

have an effect on the turning performance. We anticipate that the horizontal lift force will have a bigger impact on turning performance for the asymmetric wing. Also we will investigate the effects of these different configurations on roll and pitch.

1.3 Aerodynamic Model

1.3.1 Adaptation of lifting-line method

The new capabilities of a morphing aircraft can be reached by manipulating the aerodynamics forces and moments that act upon the aircraft. To determine the forces, an aerodynamic analysis for both varying geometries and flight condition are required. A computational fluid dynamics (CFD) package would not be efficient, since a new mesh would be needed for every shape and flow field configuration, resulting in high computational cost. Instead, we are utilizing an approach to 3D modeling which incorporates a modern adaptation of Prandtl's lifting-line method, based on a fully three-dimensional vortex lifting law that we have developed [12]. This method enables to analyze the aerodynamic properties of wings of arbitrary camber, sweep, and dihedral, with either symmetric or asymmetric planform.

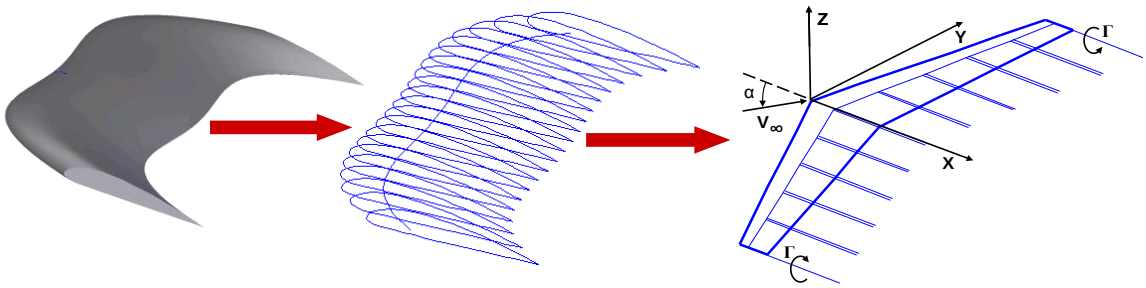

Figure. 1.1 A 3-D finite wing decoupled into a series of 2-D airfoils and into a series of horseshoe vortices

There are several variations of lifting-line method, for example the adaptation of the Weissinger's method present by Wickenheiser and Garcia, which can be used for wings with arbitrary planform, but cannot calculate fully 3D geometries [13]. The method that we have developed is based on the adaptation of Prandtl's lifting-line method developed by Phillips and Snyder [14]. This method is derived from the classical lifting-line method, but it is generalized to correct for the violations of the classical lifting-line theory for wings with sweep and dihedral. This method synthesizes the 3D finite wing into a series of 2D horseshoe vortices distributed at the quarter chord as seen in Figure 1.1. It uses Prandtl's theory [15] but instead of using the two dimensional Kutta-Joukowski law, this method is based on a fully three dimensional vortex lifting law. This modification allows it to be used for systems of arbitrary camber, sweep and dihedral. Furthermore with this method we can compute the aerodynamic forces for out-of-plane wing configurations which conventional lifting-line methods do not. This lifting method has been verified both by wind tunnel testing and CFD modeling, using Fluent, for other non-linear system of lifting surfaces [16].

A lifting-line approach is being used because it is a fast computational approach with a low order model compared to CFD for analysis of different morphing configurations. The wing configuration that will be analyzed in this paper is a wing configuration that has two panels, an out-of-plane dihedral section and a horizontal configuration, like a V shape wing configuration as seen in Figure 1.2. An analysis of both symmetric and asymmetric wing shapes, as seen in Figure 1.2 and 1.3 respectively, will be performed. All the wings analyzed have the same reference area and length, therefore foreshortening the effective span of the wing as the dihedral

angle increases. The lift characteristics for wings with and without flaps will be performed for both symmetric and asymmetric wing configurations.

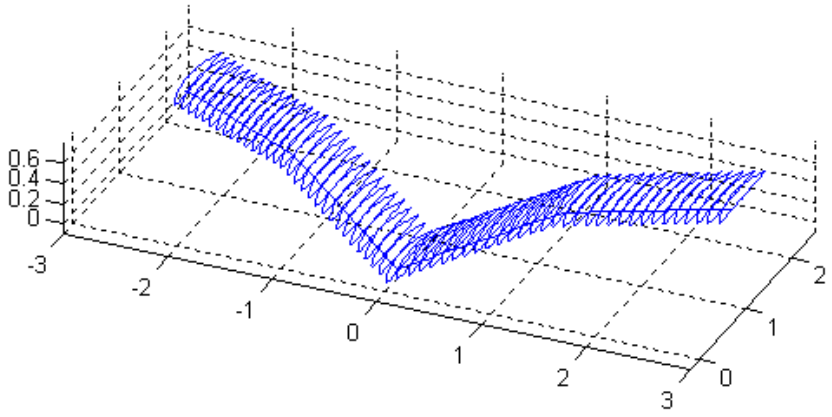

Figure. 1.2 Symmetric V Shaped Wing

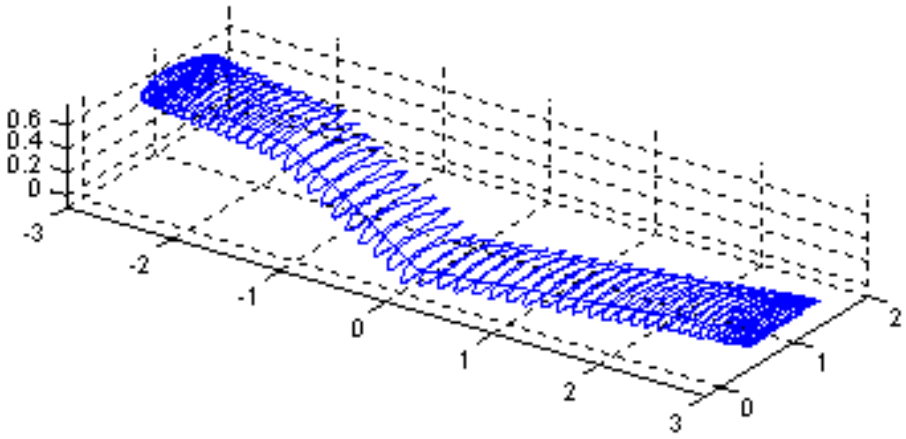

Figure. 1.3 Asymmetric V Shaped Wing

1.3.2 Lift characteristics for symmetric wings without flaps

The lift characteristics of the V shaped wings without flap deflection will vary as a function of the dihedral angle. The lift distribution is plotted in Figure 1.4 for a flat wing and two V shaped wings with dihedral angles of 25 and 45 degrees with the

same reference area. As it can be seen in Figure 1.4, the lift distribution decreases as the dihedral angle is increased. The decrease in lift is due to the lateral component of lift force the dihedral part has, therefore decreasing the vertical lift force. Another factor that had an effect on the decrease of lift is the foreshortening of the wing as the dihedral increases which decreases the effective planform area of the lifting surface. This explains why the lift decreases throughout the span instead of only where some dihedral is present. From Figure 1.4 we see that the dihedral effect, loss of lift due to dihedral, increases as dihedral angle increases as it was expected.

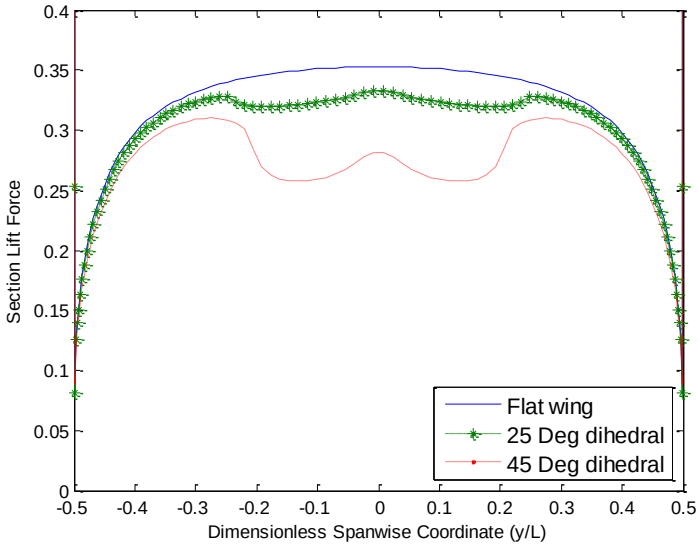

Figure. 1.4 Section lift distribution for symmetric wing

Figure 1.5 shows the plot of the lateral aerodynamic force. As mentioned before the dihedral component induces a lateral force. However, since the wing is symmetric the overall resultant force will be zero, since each dihedral part has an equal but opposite force as it can be seen in Figure 1.5. Even though the resultant lateral force is zero this characteristic could still be useful. For example, it could provide roll control. In addition, if flaps are located on the dihedral part of the wing it can provide yaw control

which can provide some interesting characteristics that can be applied to perform different maneuvers that conventional aircrafts cannot.

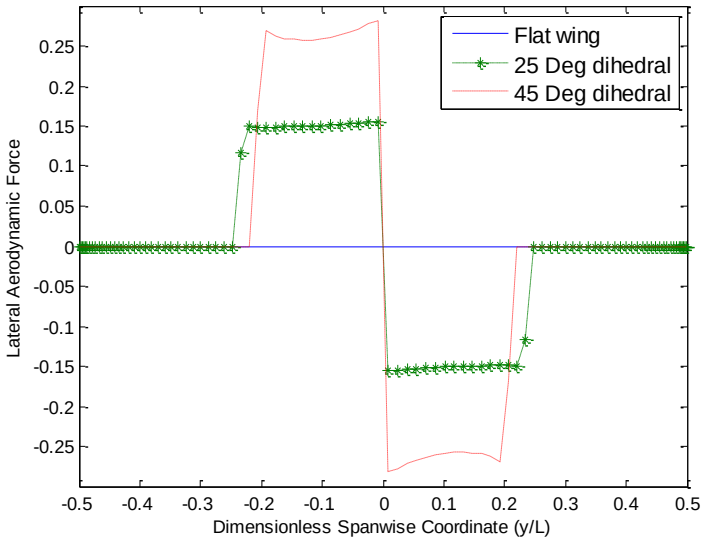

Figure. 1.5 Lateral aerodynamic force distribution for symmetric wing

1.3.3 Lift characteristics for an asymmetric wing without flaps

Another type of wing configuration of interests is an asymmetric wing as seen previously in Figure 1.3. Figure 1.6 shows the lift distribution for a flat wing and two asymmetric wings with dihedral angles of 25 and 45 degrees with a constant reference area and without flap deflections. Similar to the symmetric V shaped wings, we see a decrease in lift as the dihedral angle is increased. However, for the asymmetric the lift distribution is also asymmetric, as expected. Once again, the decrease in lift is due to the horizontal force induced by the dihedral component and the foreshortening of the wing which decreases the effective planform area of the overall lifting surface. Due to the asymmetric lift distribution there will be a roll moment induced on the wing.

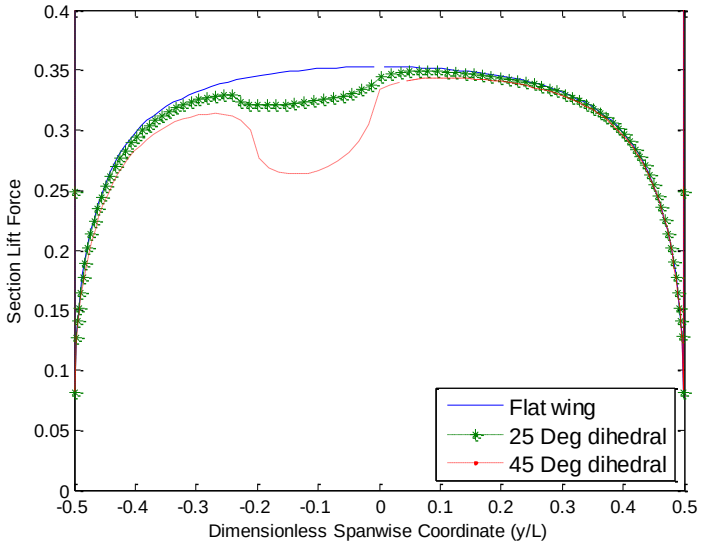

Figure. 1.6 Section lift distribution for asymmetric wing

Figure 1.7 shows the lateral aerodynamic section force for the asymmetric wings. Contrary to the symmetric wing, where the lateral resultant forces were zero, the asymmetric wing has a resultant lateral force from the asymmetric dihedral section. As expected, the lateral forces increases as the dihedral angle of the wing increases. In addition, from the plot it can be seen that the lateral force has a significant value of the total lift force. For example, the asymmetric wing with a 25 degree dihedral the lateral force is about 15% of the lift force. This lateral force can lead to significant applications to morphing aircraft. In addition, the resultant lateral force can allow an aircraft to perform maneuvers that conventional aircraft cannot.

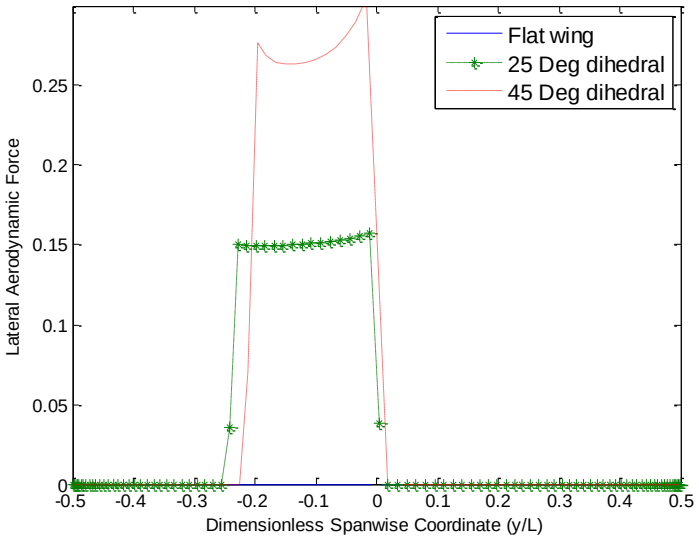

Figure. 1.7 Lateral aerodynamic force distribution for asymmetric wing

1.3.4 Lift characteristics for a symmetric wing with flaps

This section presents the lift characteristics for V-shaped wings with an asymmetric flap deflection as see in Figure 1.8. The length of each flap is 1/8 of the total length and with 40% of the chord length. The flaps will be located in the middle of the horizontal panels of the V-shape wings as it can be seen in Figure 1.8. The wings have been analyzed with an asymmetric flap deflection of 10 degrees.

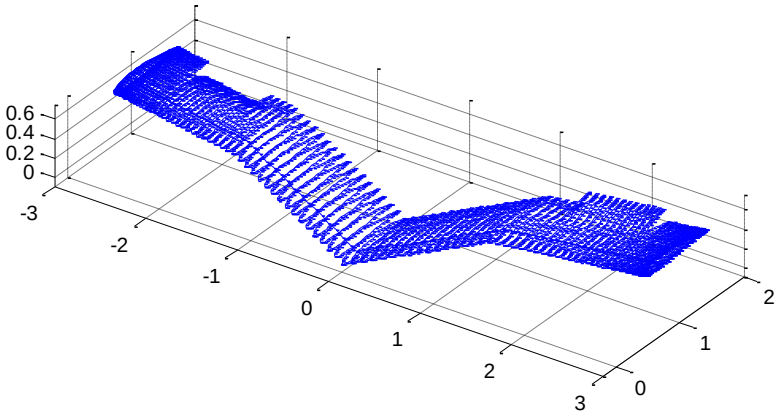

Figure. 1.8 Symmetric V Shaped Wing with asymmetric flap deflection

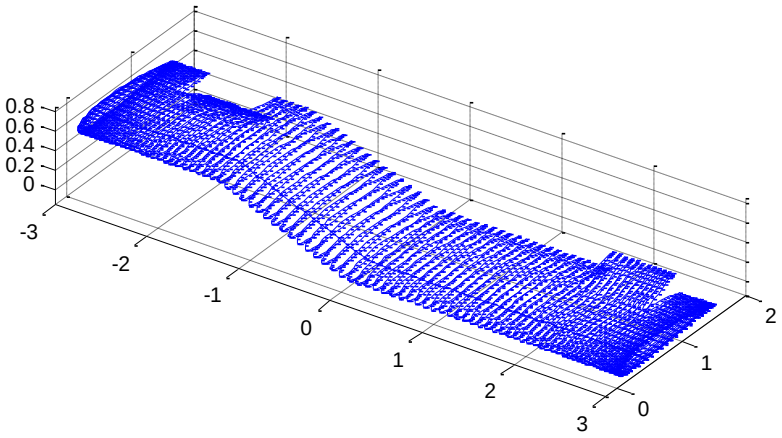

Figure. 1.9 Asymmetric V Shaped Wing with asymmetric flap deflection

The lift distribution is plotted in Figure 1.10 for a flat wing and two V shaped wings with dihedral angles of 25 and 45 degrees with the same reference area and an asymmetric flap deflection. As it can be seen in Figure 1.10, the lift distribution decreases as the dihedral angle increases similarly to the V shaped wings without flap seen in the previous section. Similarly to the symmetric wing without flaps, the decrease on lift is due to the lateral component of lift force the dihedral section of the wing has and the decrease of the effective planform area of the lifting surface. As expected, there is an increase in lift in the section where the positive flap deflection is present and a decrease in lift where there is a negative flap deflection. Since we are performing an asymmetric flap deflection the change in total lift compared to the symmetric V shape wing without flaps is negligible. However, due to asymmetry of the lift distribution it produces a roll moment which will help during a turning maneuver.

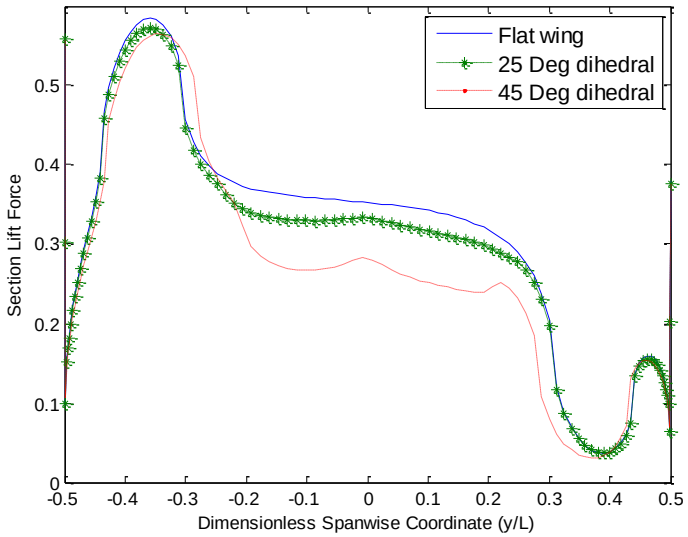

Figure. 1.10 Section lift distribution for symmetric wing with asymmetric flap deflection

The lateral aerodynamic force is plotted in Figure 1.11 for a symmetric V shape wing with asymmetric flap deflection. Similarly to symmetric wing in the previous section, the lateral force is symmetric and the resultant net force is negligible since each dihedral part has an equal but opposite force as it can be seen in Figure 1.11. However we do see that the lift distribution on each dihedral part is bigger than of the wing without flaps due to the flap interactions on the dihedral parts, but the resultant force is still negligible.

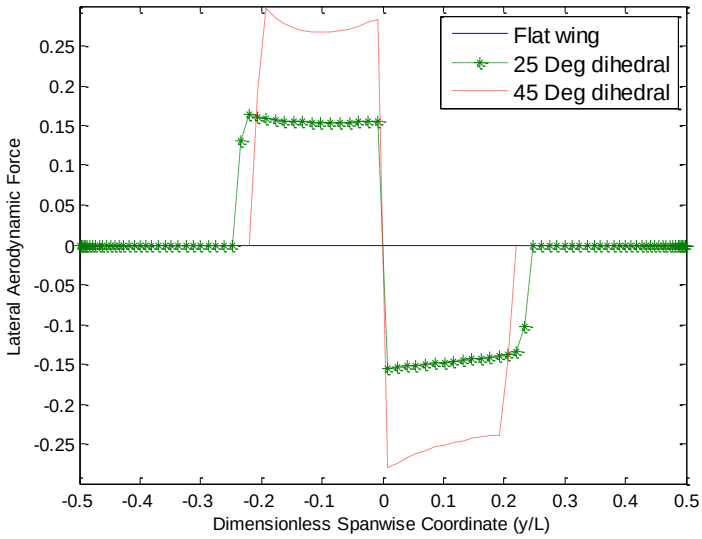

Figure. 1.11 Lateral aerodynamic force distribution for symmetric wing with asymmetric flap deflection

In this section we present the lift characteristics for asymmetric wing configuration with an asymmetric flap deflection as seen previously in Figure 1.9. The characteristics of the flaps are the same as for the symmetric wing. Figure 1.12 shows the lift distribution for a flat wing and two asymmetric wings with dihedral angles of 25 and 45 degrees with a constant reference area. Similar to the asymmetric V shaped wings without flap deflections, there is a decrease in lift as the dihedral angle is increased. As expected, due to asymmetric wing configuration and flap deflection the lift distribution is also asymmetric. However, for this case the asymmetry is even bigger due to flap deflections compared to the asymmetric wing without flaps as seen in Figure 1.6.

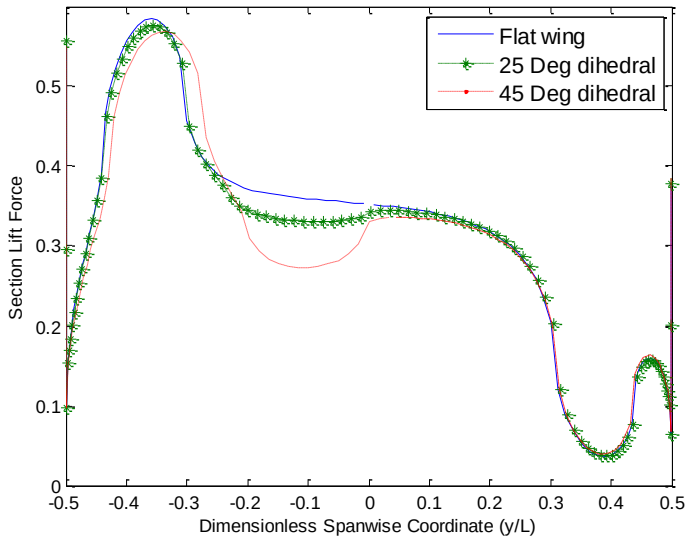

Figure. 1.12 Section lift distribution for asymmetric wing with asymmetric flap deflection

Figure 1.13 shows the plot for the lateral aerodynamic section force for the asymmetric wings with asymmetric flap deflection. Contrary to that of the symmetric wing, where the lateral resultant forces was zero, for the asymmetric wing there is a resultant lateral force from the asymmetric dihedral part. As expected, the lateral forces increases as the dihedral angle of the wing increases. Due to the flap interactions, the lateral force for these wings is higher than of the asymmetric wings without flap deflections, resulting in a higher overall lateral force. In addition, the lateral force has a significant value of the total lift force, for example for the 25 degree asymmetric dihedral wing the lateral force is about 18% of the total lift force. This lateral force can have significant applications to morphing aircraft. This resultant force can allow an aircraft to perform maneuvers that conventional aircraft cannot. For example, this force will have a significant effect in the turning capabilities of an aircraft, as it will be explore in the following section.

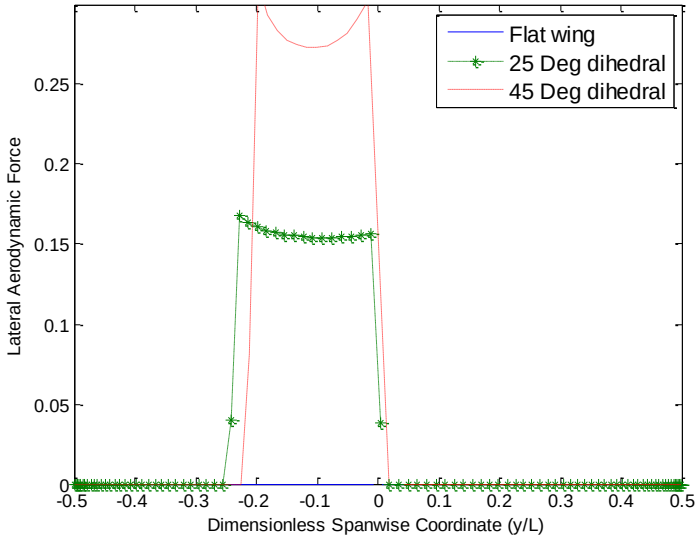

Figure. 1.13 Lateral aerodynamic force distribution for asymmetric wing with asymmetric flap deflection

1.4 Turning Flight Mechanics

The effects of the dihedral portions, for both symmetric and asymmetric wings, have on the aircraft turning capabilities will be investigated in this section. Turning capabilities is one measurement of overall performance, since turning flight is one of the most common routine maneuvers for all aircraft. Turning performance is one of the most important metrics of air superiority for fighter aircraft since it is a key tactical maneuver for a combat aircraft [17]. In addition, turning performance is important for aircraft maneuvering in urban environments, for example surveillance UAV, where the aircraft has to be able to maneuver through dense obstacles.

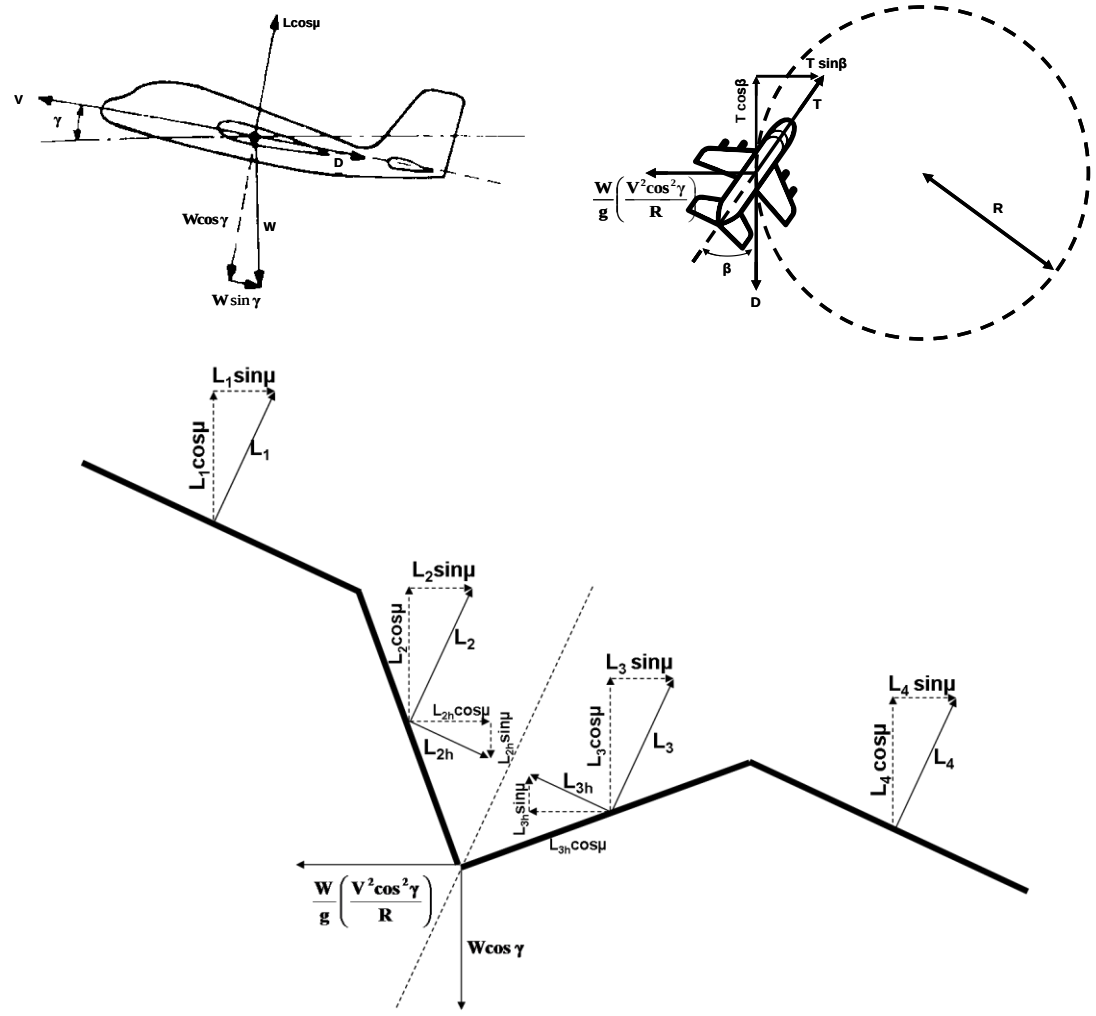

Figure 1.14. Aircraft in turning in a horizontal plane

Turning flight is usually characterized in two categories, a steady turning flight and general turning. In steady turning flight the aircraft stays at a constant altitude and velocity in a horizontal plane. In general turning, there may be a gain or loss of altitude [17]. In this study we are going to analyze the different wing configurations performing a steady turning flight. The forces acting on a V shape wing aircraft in steady turning with bank angle μ, sideslip β and flight path angle γ can be seen in Figure 1.14. To generate the necessary centripetal force to perform the turn the aircraft

has to bank or sideslip. The equations that govern the steady turning flight are the following.

The forces are summarized along the flight path as,

$$T\cos\beta - D - W\sin\gamma = 0 \tag{1.1}$$

and along the normal plane as,

$$\left(L_1 + L_2 + L_3 + L_4\right)\cos\mu + \left(L_{3h} - L_{2h}\right)\sin\mu - W\cos\gamma = 0 \tag{1.2}$$

and along the binormal as,

$$T\sin\beta + \left(L_1 + L_2 + L_3 + L_4\right)\sin\mu + \left(L_{2h} - L_{3h}\right)\cos\mu - \frac{WV^2\cos^2\gamma}{gR} = 0 \tag{1.3}$$

where T is the thrust, D is the drag, W is the weight, V is the velocity and R is the turning radius as defined in Figure 1.14.

1.4.1 Coordinated turning

To analyze the turning performance for the different symmetric V shaped wings and asymmetric wing, we are going to consider a steady coordinated turns. A coordinated turn is a turn with zero sideslip (β) and flight path angle (γ) and the aircraft is correctly banked so that the lift force component balances the weight so there is no loss of altitude. By examining at Equations 2 and 3, we can see that the lateral forces from the dihedral part of the wing will completely cancel if the wing is symmetric. However, if the wing is not symmetric, we can see that it will affect both the bank angle and the turning radius. The aerodynamic forces for all the four segments of the V-shaped wing are calculated using the numerical lifting-line method previously discussed. The turning radius (R) and bank angle (μ) are computed by solving Equations 1.1, 1.2 and 1.3 simultaneously using a numerical Newton method.

1.5 Effects of Morphing on Maneuverability

For the turning flight analysis, for both the symmetric and asymmetric wings with asymmetric flap deflections of 10 degrees, the dihedral angle where varied from 0 to 60 degrees with increments of 5 degrees. The wing was divided in four equal sections, as seen in Figure 1.8, with two horizontal and two dihedral parts for the symmetric wing and three horizontal and one dihedral for the asymmetric wing. The simulations where performed for a rectangular wing of aspect ratio of 10 with a NACA airfoil of 2412. The reference area was kept constant for all symmetric and asymmetric wings. As mentioned before, the velocity of 20 m/s was kept constant for the steady coordinated turn. The angle of attack of the aircraft is kept constant throughout the turning maneuver.

1.5.1 Turning radius

Figure 1.15 shows the plot of the turning radius as the dihedral changes from 0 to 60 degrees. As it can be seen in Figure 1.15 the turning radius increases as the dihedral angle increases for both the symmetric and asymmetric wing. The increase in turning radius is due to the decreases in the overall lift of the wing due to the dihedral portion as it was discussed in the previous sections. With the decrease in lift, the lift contribution to the centripetal force needed to perform the turning maneuver in equation 1.3 decreases and therefore resulting in an increase in turning radius. Comparing the symmetric and asymmetric wings, the turning radius for the asymmetric wing is smaller for all dihedral angles. For example, at a dihedral angle of 60 degrees, the turning radius for an asymmetric wing is 30% lower than of a symmetric wing. Therefore an asymmetric wing is able to perform sharper turns. A reason for a lower turning radius for an asymmetric wing is due to the net lateral force

component on the dihedral portion of the wing which contributes to the centripetal force needed to perform the turn. Also, the asymmetric wing has a higher overall lift compared to a symmetric wing at a given dihedral angle, as discussed in the previous section, resulting in a bigger contribution to the centripetal force to perform the turn.

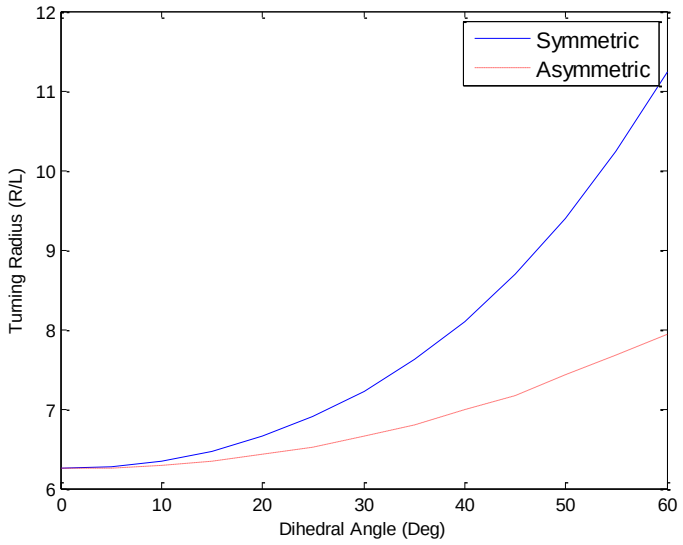

Figure. 1.15 Turning radius for symmetric and asymmetric wings with asymmetric flap deflection

1.5.2 Bank angle and load factor

The bank angle for a coordinated turn was calculated by equating the weight to the total vertical lift component contribution from all the wing sections. The bank angle is plotted in Figure 1.16 for both the symmetric and asymmetric wing as the dihedral angle is increased from 0 to 60 degrees. The bank angle needed to maintain a coordinated turn decreases as the dihedral angle is increased for both wings. Again this is due to the decrease in the total lift resulting in a smaller bank angle needed to balance the weight of the aircraft. The bank angles for the asymmetric wing are significantly smaller compared to both a flat and a symmetric wing. Again the

resultant lateral component of the lift for the asymmetric wing contributes to balance the total weight of the aircraft resulting in a smaller bank angle needed to maintain a coordinated turn. When performing a turn small bank angle are desirable because the lower the bank angle the smaller the loading that the aircraft experiences. Therefore we can see that the asymmetric wing performs better than the symmetric wing. Also, one may observe that for a turning radius of 8, the symmetric wings banks 78.9 degrees whereas the asymmetric wing banks 69.8 degrees.

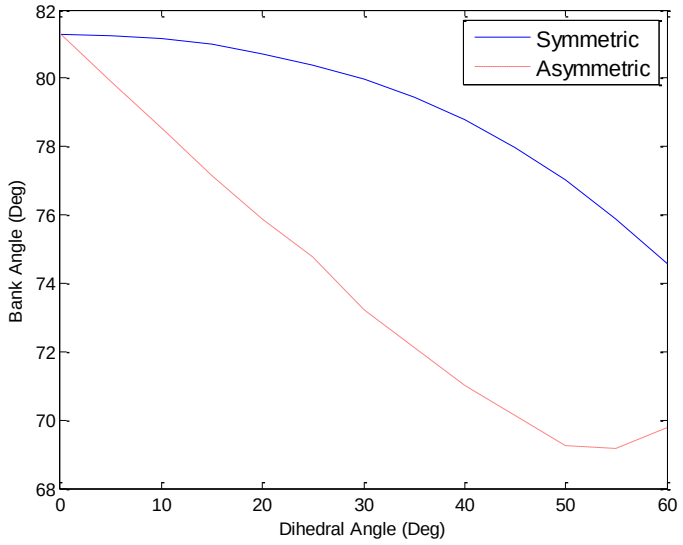

Figure. 1.16 Bank angle for symmetric and asymmetric wings with asymmetric flap deflection

The load factor is a measure of the stress to which the aircraft is subjected during turning flight [17]. The load factor is defined as the ratio of the lift generated during the turning maneuver to the weight of the aircraft and is given the following equation,

$$n = \frac{L}{W} \tag{1.4}$$

where, L is the overall lift of the aircraft and W is the weight.

For a coordinated turn the load factor is a function of only the bank angle and is given by the following equation,

$$n = \frac{1}{\cos(\mu)} \tag{1.5}$$

From Equation 1.5, we can see that load factor is inversely proportional to the cosine of the bank angle. The higher the bank angle the higher the load the aircraft will experience during a turn. Figure 1.17 shows the plot of the load factor experienced during the coordinated turn for the symmetric and asymmetric wings as the dihedral is changed. As the dihedral component of the wing increases the load factor decreases for both the symmetric and asymmetric wings. The addition of dihedral decreases the load on the aircraft during the coordinated turn compared to a wing with no dihedral i.e. a flat wing. Similarly to the bank angle we can see that the loads are much smaller for the asymmetric wing than the symmetric wings. Therefore the asymmetric wing experiences smaller loads than both symmetric and flat wings.

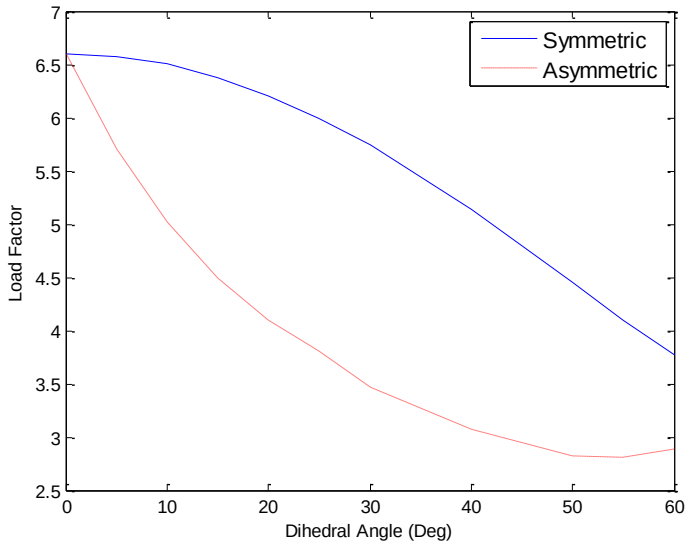

Figure. 1.17 Load factor for symmetric and asymmetric wings with asymmetric flap deflection

1.5.3 Rate of turn

Another important metric for turning performance is the turn rate which measures how fast the aircraft can perform the turning maneuver (Pamadi, 1998). The turning rate is given by the following equation,

$$\omega = \frac{V}{R} \tag{1.6}$$

Figure 1.18 shows the turning rate for both the symmetric and asymmetric wings. The turning rate decreases for both symmetric and asymmetric wing compared to a flat wing. Similar to the previews parameters discussed before we can see that the asymmetric wing performs better than the symmetric wing. Again the asymmetric wing performs better because it has a resultant lateral force and a higher overall lift compared to a symmetric wing which helps during the turning maneuver. The turning rate for the asymmetric wing are higher than of the symmetric wing, therefore combine with turning radius results, from Figure 1.15, the asymmetric wing can perform faster and tighter turns. For example, one can state that for a turning rate of 2.48, the turning radius for a symmetric wing is 8.1, whereas for an asymmetric wing, the turning radius is 7.9. So, an asymmetric wing performs a tighter turn at the same rate resulting in an improvement in turning ability.

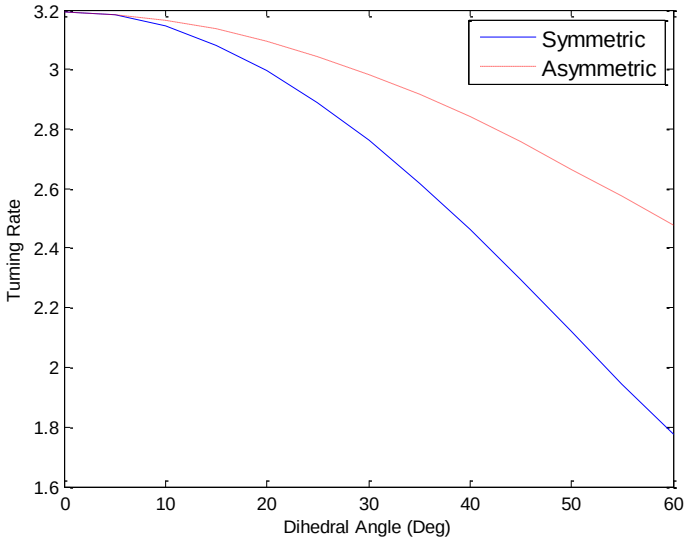

Figure. 1.18 Rate of turn for symmetric and asymmetric wings with asymmetric flap deflection

1.5.4 Roll and pitch moment coefficient

The roll moment coefficient is plotted in Figure 1.19 for both symmetric and asymmetric V shaped wing. A roll moment is produced for both symmetric and asymmetric wings due to the asymmetric flap deflection, which produced an asymmetric lift distribution resulting in a moment force. For the symmetric wing the roll moment coefficient decreases as the partial dihedral is increased. One of the factors that contributed to the decrease in the roll moment coefficient is due to the decrease in lift distribution as the dihedral angle is increased, as seen in Figure 1.10. Also, the roll moment coefficient decreases because as the dihedral angle increases the position of flaps gets closer to the center resulting on a decrease in the effective moment arm due to the asymmetric lift distribution from the flap deflections. The roll moment coefficient for the asymmetric wing does not decrease as the dihedral angle increases. There is even an small increase for some dihedral angles. Even though there is a decrease in the lift distribution and in the moment arm, the roll moment does

not decrease because there is also a roll moment produced by the spanwise force on the asymmetric dihedral portion of the wing. This results in roll coefficient staying constant and even increasing when the lateral force contributions are bigger than the losses due to smaller moment arm and decrease in lift.

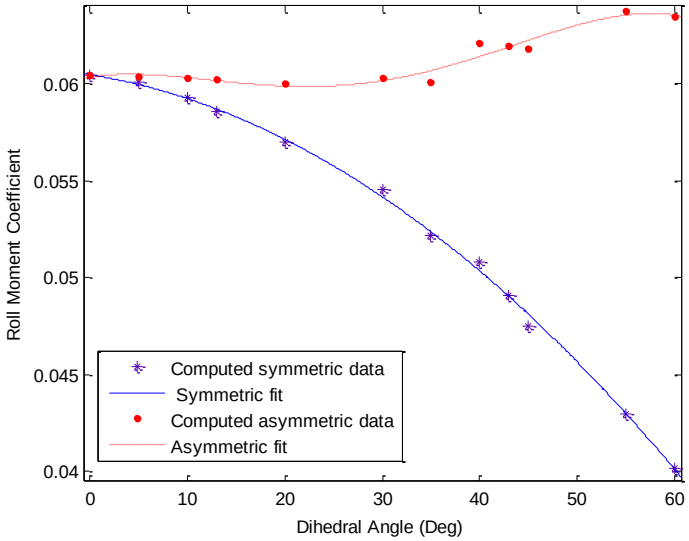

Figure. 1.19 Roll moment coefficient for symmetric and asymmetric wing with asymmetric flap deflection

Figure 1.20 shows the plot of the pitch moment coefficient for the symmetric and asymmetric wings. We can see that the pitch moment magnitude also decreases as the dihedral angle is increased for both symmetric and asymmetric wings. The magnitude of the pitch moment is also larger for the asymmetric wing as the dihedral angle is changed. If we recall from Figures 1.10 and 1.12, the overall lift for an asymmetric wing were higher than a symmetric wing, therefore the higher lift forces results in higher pitch moments for the asymmetric wing.

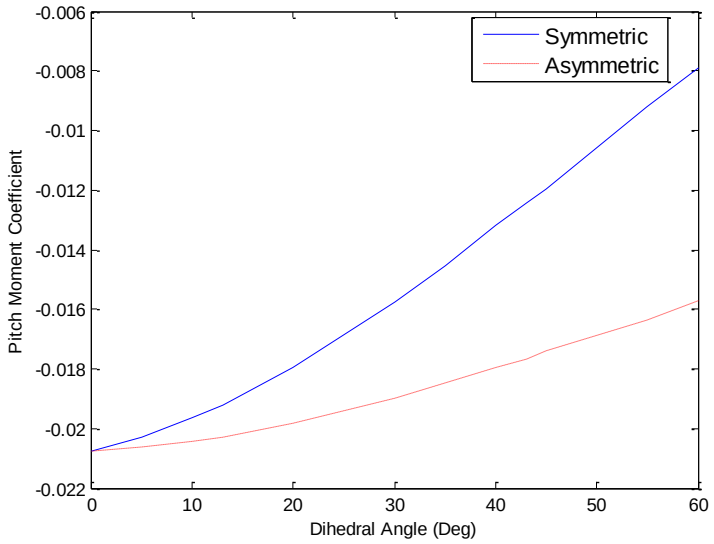

Figure. 1.20 Pitch moment coefficient for both symmetric and asymmetric wings with asymmetric flap deflection

In this section we have shown how the turning performance is affected by the addition of symmetric and asymmetric dihedral angles to a wing. The addition of the dihedral impacts all the turning metrics addressed previously. The dihedral part of the wing impacts both positively and negatively on the different turning metrics. A summary of the effects of the dihedral on the turning performance for the different turning metrics can be seen in Table 1.1. Table 1.1 compares the effects on the different turning measurements for a flat wing, with no dihedral, a symmetric wing and an asymmetric wing.

Table 1.1 Summary of the Effect of Different Turning Performance Metrics for the Wings Analyzed

Wing Type	Summary of the effects on turning performance
Flat (No dihedral)	• Smallest turning radius • Larger bank angle • Highest load factor • Higher turning rate • Roll moment is larger than a symmetric wing but smaller than an asymmetric wing with large dihedral angles
Symmetric dihedral deflections	• Turning radius increases with dihedral angle • Bank angle decreases with dihedral angle • Load factor decreases with dihedral angle • Turning rate decreases with dihedral angle • Roll moment decreases with dihedral angle
Asymmetric dihedral deflections	• The increase in turning radius is smaller than for a symmetric wing • Smaller bank angles compared to flat and symmetric wings • Lower load factors than for flat and symmetric wings • The decrease in turning rate is smaller than for a symmetric wing • Roll moments stay nearly constant for small dihedral angles and increases for large dihedral angles

1.6 Conclusion

For turning flight, we have shown that the asymmetric wing performs better than a similar symmetric wing for the following turning performance metrics, turning radius, bank angle, loading factor, turning rate and roll moment coefficient. Even though the turning radius and turning rate performances decreases as the dihedral is added to the wing, there are some large improvements due to decrease of both the bank angle and load factors compared to a flat wing. For the asymmetric wing at dihedral angles between 0 to 30 degrees we can see that there is no significant increase in turning radius, of about 6%, and a decrease of 6.5% in turning rate compared to a flat wing

with no dihedral, but there are significant improvements with a decrease of 11% in bank angle and a decrease of 50% in the loading factor. At this range the addition of dihedral makes the wing perform much better than a flat wing. For missions where the turning radius and turning rate are important, we can get significant improvements by asymmetrically changing the dihedral angle from 0 and 30 degrees, where we get a decrease in both the bank angle and load factor with just a small decrease of performance in turning radius and turning rate. Shape changes of dihedral angles higher than 30 degrees are good for missions where small bank angles are important and the ability of make sharp and fast turns are not as important. For example a surveillance missions where you want to keep your sensors pointing in a certain direction, therefore large changes in the aircraft orientations, like in the bank angle, are not desirable.

We have shown that the asymmetric wing have higher roll moment control compared to a symmetric wing. Asymmetric wing changes can produce big improvements in turning performance, for example by reducing the bank angles and loading factor, without a loss of roll control authority. Manipulating the dihedral angles, either by symmetric or asymmetric wing shape changes, we can affect the turning capabilities of an aircraft to perform a variety of different missions depending on the importance of each of the turning performance measurement discussed.

REFERENCES

1. Sanders, B., Crowe, R. and Garcia, E., "Defense Advanced Research Projects Agency - Smart Materials and Structures," *Journal of Intelligent Material Systems and Structures*, Vol. 15: 227-233, 2004.
2. Tucker, V.A. and G.C. Parrott, "Aerodynamics of gliding flight in a falcon and other birds", *Journal of Experimental Biology*, Vol. 52: 346-67, 1970.
3. Wickenheiser, A., Garcia, E., and Waszak, M., "Evaluation of Bio-Inspired Morphing Concepts with Regard to Aircraft Dynamics and Performance," *Proceedings of SPIE: International Society for Optical Engineering*, Vol. 5390, 2004, pp. 202–211.
4. Bowman, J., Sanders, B. and Weisshaar, T., "Evaluating the Impact of Morphing Technologies on Aircraft Performance," AIAA-2002-1631.
5. Wickenheiser, A. and Garcia, E. "Longitudinal Dynamics of a Perching Aircraft", *Journal of Aircraft*, Vol. 43, No. 5, 2006, pp. 1386-1392.
6. McGowan, A. R., "AVST Morphing Project Research Summaries in FY 2001," NASA TM-211769-2002, 2002.
7. Weisshaar, T.A. "DARPA Morphing Aircraft Structures (MAS)" http://www.darpa.mil/dso/thrust/matdev/mas.htm
8. Joshi, S.P., Z. Tidwell, W.A. Crossley and S. Ramikrashnan, (2004) "Comparison of Morphing Wing Strategies Based Upon Aircraft Performance Impacts" AIAA/ASME/ASCE/AHS/ASC Structures, Structural Dynamics, and Materials Conference, AIAA-2004-1722, April 2004, Palm Springs, CA

9. DeLaurier, J., Gagnon, B. Wong, J. Williams, R. Hayball, C. and Advani, S. (1987) “Flying High with Hale” *Unmanned Systemst*, **5** no.3, pp. 26-46, 1987.

10. Wickenheiser, A. M. and Garcia, E. "Mission Performance of a Solar- and Microwave-Powered Aircraft", Smart Structures and Materials 2008: Active and Passive Smart Structures and Integrated Systems II, March 10-13, San Diego, CA. published in: *Proc. SPIE* Vol. 6928, 2008.

11. Cuji, E. A. and Garcia, E. "Prediction of Aircraft Dynamics with Shape Changing Wings", Smart Structures and Materials 2008: Active and Passive Smart Structures and Integrated Systems II, March 10-13, San Diego, CA. published in: *Proc. SPIE* Vol. 6928, 2008.

12. Cuji, E., Garcia, E. “Analytic Modeling of the Aerodynamics of Shape Changing Wings”, *Proc. 18th International Conference on Adaptive Structures and Technologies* 127, 2007.

13. Wickenheiser, A. M., and Garcia, E., “Aerodynamic Modeling of Morphing Wings Using an Extended Lifting-Line Analysis,” *Journal of Aircraft*, **44** no.1, pp. 10-16, 2007.

14. Phillips, W. F., Snyder, D. O. “Modern Adaptation of Prandtl’s Classic Lifting-Line Theory”, *Journal of Aircraft* , Vol. 37, No. 4, 2000, pp. 662-670.

15. Prandtl, L., “Aerofoil Theory, I and II Communications”, *Nachr. Kgl. Gesellschaft der Wissenachaft, Math-phys. Classes*, Göttingen, 1918-19.

16. Cuji, E., Lukaczyk, T., and Garcia, E., “Aircraft Dynamics, Wind Tunnel Testing and CFD Flow Visualization of Two Linked UAVs Flying at Close Proximity”, Proceedings of the Smart Structures and Materials 2008: Active

and Passive Smart Structures and Integrated Systems, Vol. 7645, SPIE, San Diego, CA, March, 2010.

17. Pamadi, B. *Performance, Stability, Dynamics, and Control of Airplanes*, American Institute of Aeronautics and Astronautics, 1998, pp. 122–146

CHAPTER 2

AERODYNAMIC SIMULATION, WIND TUNNEL TESTING AND CFD FLOW VISUALIZATION OF CLOSE PROXIMITY AERODYNAMICS OF TWO LINKED UAVS[*]

2.1 Abstract

This paper presents an analysis of close proximity aerodynamics of two UAVs attempting to link in mid-air. As the UAV approach each other for this wingtip docking maneuver there will be strong aerodynamic coupling between the UAV wings tips. Modeling the aerodynamic coupling effects on all the forces and moments is essential to determine a trajectory and controls for each UAV to perform the docking maneuver. Lifting line simulations and Computational Fluid Dynamics (CFD) simulation as well as wind tunnel testing of the close proximity effects on lift, drag, roll, pitch and yaw moments for two UAV wings has been performed. The computational aerodynamics simulations are done utilizing a modern adaptation of lifting-line method, which is based on a fully three-dimensional vortex lifting law. The proximity aerodynamics effects between the UAVs wings are analyzed as a function of its relative position in all three directions: chord-wise (x – direction), span-wise (y – direction), and vertical direction (z – direction). An aerodynamic disturbance intensity field is generated, utilizing both simulation and wind tunnel data, to determine the

[*] Submitted for publication to *Journal of Aircraft* by Cuji, E., Lukaczyk, T. and Garcia E. "Aerodynamic Simulation, Wind Tunnel Testing and CFD Flow Visualization of Close Proximity Aerodynamics of Two Linked UAVs"

forces acting on the aircraft in 3-D space. CFD flow visualization has also been performed to gain insight into the flow physics.

2.2 Introduction

Currently, UAVs are heavily used for Intelligence, Surveillance and Reconnaissance (ISR) missions. One advantage of using UAVs for ISR missions is that they can be rapidly deployed from any airfields due to their small wingspan. However, having a small aspect ratio wing also limits its range and endurance [1]. An effective ISR platform requires its units to be rapidly deployable, have long range and endurance capabilities. It is known that large aspect ratio wings aircraft has better aerodynamic efficiency due to the reduction of induce drag for the given lift [1, 2] . Wingtip docking UAVs in midair to form a linked UAV system will increases the effective aspect ratio of the linked aircraft. The larger aspect ratio of the linked UAV leads to an improvement in overall aerodynamic efficiency due to the decrease of the induce drag as previously mentioned. The improvements in aerodynamic efficiency are similar to the improvements seen in formation flight [3, 4], but without having the trailing aircraft fly in the vortex wake of the leading aircraft which can lead to both stability and control problems [5, 6]. The linked UAV concept allows for rapidly deployable ISR platform using individual UAVs with wingspans small enough to be deployed from small aviation airfields. Individual UAVs will link at high altitude to create an aerodynamically efficient aircraft which has long endurance capabilities and can be able to cruise for extended periods significantly reducing their power loads. One might even consider scenario where some aircraft in the linked formation might reduce thrust or shutdown to radically increase endurance of the formation.

This paper presents an analysis of close proximity aerodynamics of two UAVs linked at their wing tips. As the UAV approach each other for wingtip docking there are strong aerodynamic coupling between the UAV wings tips [7, 8]. Determining the aerodynamic coupling effects on all the forces and moments on each vehicle is essential to determine a trajectory and controls for each UAV to perform the docking maneuver. Lifting-line simulation, Computational Fluid Dynamics (CFD) simulation and wind tunnel testing of the close proximity effects on all the aerodynamic forces and moments for two UAV wings will be performed. The aerodynamic simulations are performed utilizing a modern adaptation of Prandtl's lifting-line method, which is based on a fully three-dimensional vortex lifting law. The proximity aerodynamics effects between the UAVs wings will be analyzed as a function of its relative position in all three directions: chord-wise (x – direction), span-wise (y – direction), and vertical direction (z – direction). An aerodynamic disturbance intensity field is generated, utilizing both simulation and wind tunnel data. In turn this forces and moments from this field are employed to determine an optimal trajectory for the two UAVs to approach each other for docking. CFD flow visualization of the vortex interaction between the two wings will also be presented.

2.3 Aerodynamic Model

2.3.1 Adaptation of lifting-line method

As the UAVs fly in close proximity to each other there will be strong aerodynamic coupling between them. As the UAVs approach each other, to link in midair, it will experience different aerodynamic forces and moments depending on its relative

position and flight condition. To determine trajectories for docking and analyze the aircraft dynamics, an understanding of the close proximity aerodynamic forces and moments that act upon the UAV wings are needed. An aerodynamic analysis for both varying relative positions between the UAVs and flight condition are required. A computational fluid dynamics (CFD) package would not be efficient, since a new mesh would be needed for every relative position and flow field configuration, resulting in high computational cost. Instead, we are utilizing an approach to 3D modeling which incorporates a modern adaptation of Prandtl's lifting-line method, based on a fully three-dimensional vortex lifting law that we have developed [9, 10].

There are several variations of lifting-line method, for example the adaptation of the Weissinger's method present by Wickenheiser and Garcia, which can be use for wings with arbitrary planform, but cannot calculate fully 3D geometries [11]. The method that we have employed is based on the adaptation of the Prandtl's lifting-line method developed by Phillips and Snyder [12]. This method is derived from the classical lifting-line method, but it's generalized to correct for the violations of the classical lifting-line theory for wings with sweep and dihedral. This method synthesizes the 3D finite wing into a series of horseshoe vortices distributed at the quarter chord as seen in Figure 2.1. It uses the Prandtl's theory [13] but instead of using the two dimensional Kutta-Joukowski law, this method is based on a fully three dimensional vortex lifting law. This modification allows it to be used for systems surfaces of arbitrary camber, sweep and dihedral. Furthermore, with this method we can compute the aerodynamic forces for a system of lifting surfaces with arbitrary position and orientation which conventional lifting-line methods do not.

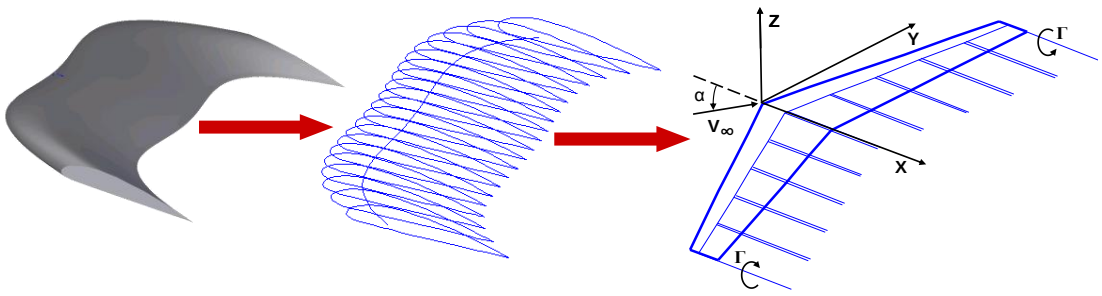

Figure. 2.1 A 3-D finite wing decoupled into a series of 2-D airfoils and into a series of horseshoe vortices.

A lifting-line approach is being used because it is a fast computational approach with a low order model compared to CFD for aerodynamic analysis of different relative separations. The speed of this method allows to determine the aerodynamic forces and moments acting on each UAV wing as a function of its relative separation in all directions and its corresponding angle of attacks. An aerodynamic intensity field between two UAVs wings will be performed as a function of its relative position in all three directions: chord-wise (x – direction), span-wise (y – direction), and vertical direction (z – direction) as seen in Figure 2.2.

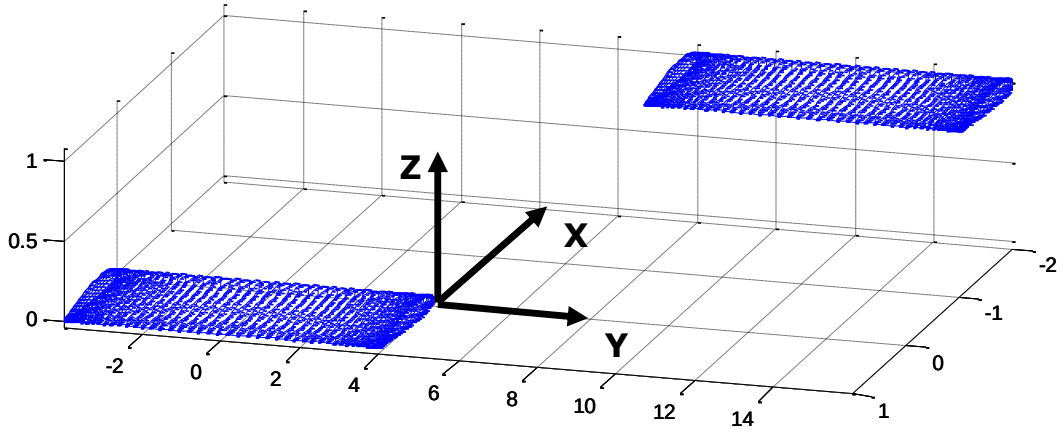

Figure. 2.2 Coordinate frame for the relative separation between the two UAV wings.

2.3.2 Close proximity aerodynamic analysis

The lift characteristics of the UAV wings will vary as a function of its relative separation and orientation. The behavior of the lift characteristic will vary depending on the direction the UAV wings approach each other. In addition, it is expected, for wings in formation, the wing flying in front to have different lift characteristic than a wing flying behind in the vortex wake of the leading wing. In this section we are going to examine how the lift distribution, lift, drag, roll, pitch and roll moments coefficients changes for two UAV wings separated in the following scenarios: only in the chord-wise, span-wise and vertical direction as shown schematically in Figure 2.3. The wings studied in this section have a rectangular planform area. It has a LA2573A airfoil and an aspect ratio of 8.

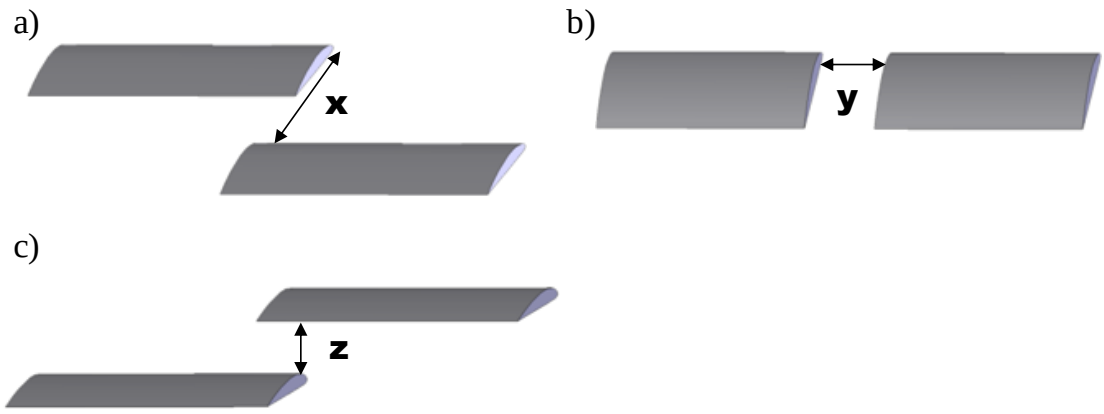

Figure. 2.3 a) UAV wings separated only in the chord-wise direction. b) UAV wings separated only in the span-wise direction. c) UAV wings separated only in the vertical direction.

The lift distribution of two UAV wings for different separation only in the chord-wise direction and for wing with double the aspect ratio as of a single UAV wings are plotted as a function of position along the span for an angle of attack of 6 degrees in Figure 2.4. For this case, where the wings are separated only in the chord-wise direction, the two wings are in the same vertical position and the wing tips of the left-hand side and the right-hand side wings are aligned as seen in Figure 2.3a. Figure 2.4 plotted data correspond to the scenario seen in Figure 2.3a, where the left data corresponds for wing in the front and the right data corresponds to the trailing wing. When the two UAVs are far away from each other, i.e. infinite separation, the lift distributions for each individual wing correspond to that of a single wing by itself, as expected.

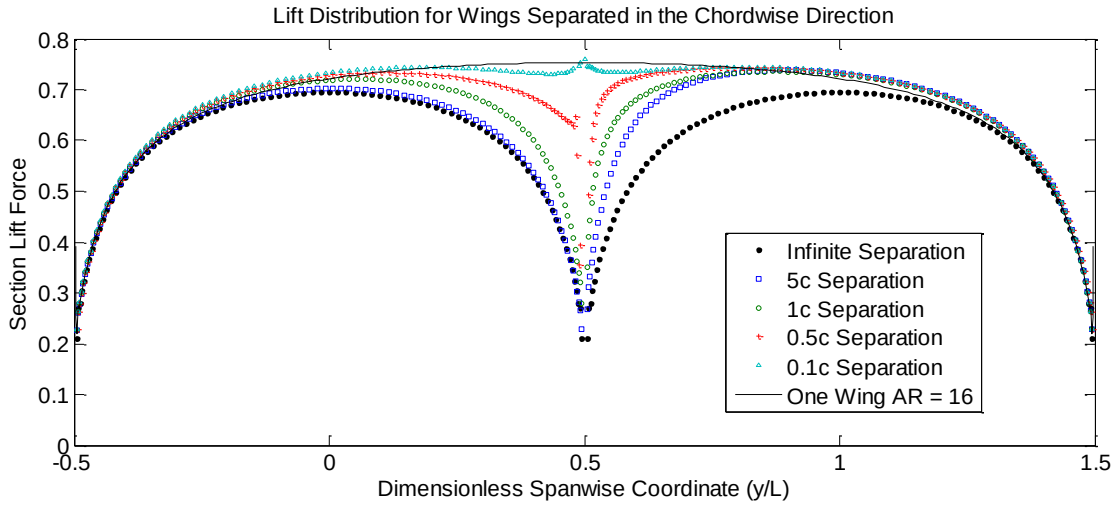

Figure. 2.4 Lift distribution for two UAV wings separated only in the chord-wise direction at different separations.

As the UAVs start getting closer to each other, we see the aerodynamic coupling between the two wings increases. These effects can be seen in Figure 2.4, where the lift distribution around the wing tips at y/L = 0.5, as the value for x separation varies.

Most of the aerodynamic coupling occurs around the wing tips due to the vortex interactions and to the change in flow condition around that section due to the presence of the other wing. The lack of symmetry in the lift distributions indicates that there is a roll moment about the mid-span axis for each wing, but stronger for the right wing. From the results in Figure 2.4, it is clear that the total lift, which is proportional to the area under the section lift distribution curve, increases as the separation decreases for both wings. As the separation decreases to zero, where the two wings are linked, the lift distribution of the two UAV wings will approach the lift distribution of a single wing with double its aspect ratio, represented by the solid line.

Comparing the lift distributions of the left and right wings at given separation, we can see that they are not symmetric. For example, for a 5 chord-lengths separation we see that the lift distribution for the left wing is about the same as of a single wing, but for the right wing, which is flying behind the left wing, we see that there is a significant increase in the section lift distribution. The increase in aerodynamic disturbance for the UAV wing flying behind is due to the wing tip trailing vortex shedding from the front UAV wing. This phenomenon is similar to what is seen in formation flying where the trailing aircrafts benefits from the trailing vortex shedding of the lead aircraft [3, 4, 14]. However, as the separation between the UAVs wings gets small, the front UAV wing is also subjected to the flow field interactions that the back UAV induces upstream with its bound and trailing wing vortex [15]. The asymmetry in the section lift distributions between each wing disappears as the separation gets close to zero. As seen in Figure 2.4, the lift distribution for a separation of 0.1 chord lengths is symmetric.

The lift distribution of two UAV wings for different separation only in the span-wise direction and for wing with double the aspect ratio as of a single UAV wings are

plotted as a function of position along the span for an angle of attack of 6 degrees in Figure 2.5. For this case, the wings are separated only in the span-wise direction and the two wings are in the same vertical position. The leading edges of both wings are aligned as seen in Figure 2.3b. Figure 2.5 plotted data correspond to the scenario seen in Figure 2.3b, where the left data corresponds for wing on the left and the right data corresponds to the wing on the right. When the two UAVs are far away from each other, 5 chord-length or higher, the lift distributions for each individual wing correspond nearly to that of a single wing by itself as it can be seen in Figure 2.5.

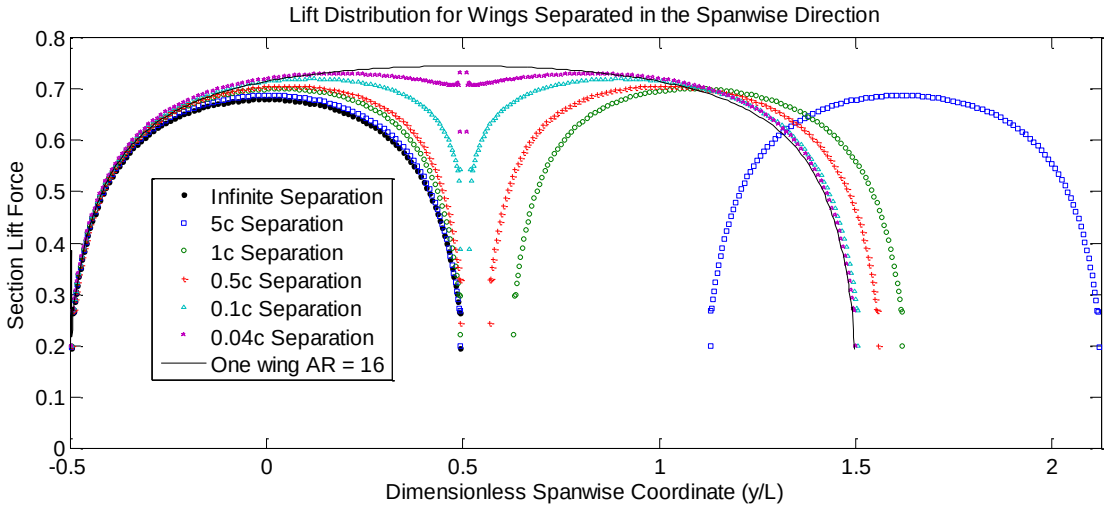

Figure. 2.5 Lift distribution for two UAV wings separated only in the span-wise direction at different separation values

As the wings approach each other, we start seeing the aerodynamic coupling begin to distort the lift distribution as in the previous case. Again, most of the aerodynamic coupling occurs around the wing tips due to the change in flow condition around the wing tip. The lack of symmetry in the lift distributions when the wings fly in close proximity indicates that there is a roll moment about the mid-span axis, opposite to each other, thus repelling any attempt to dock. Contrary to the results for the chord-

wise separation, the lift distributions of the left and right wings at given span-wise separation are symmetric. In this case since both the leading and trailing edges for both wings are aligned, as the wings get closer, both will experience the same change in flow conditions and vortex interaction around the wing tips. As the separation decreases to zero, where the two wings are linked, the lift distribution of the two UAV wings will approach the lift distribution of a single wing with double its aspect ratio.

The section lift distribution of two UAV wings for separation only in the vertical direction, as seen in Figure 2.3c, behaves similar to the section lift distribution for separation in the span-wise separation. For this case the lift distribution for both wings have a small asymmetric at the given separations. However, the asymmetry is not as big as what was seen for the chord-wise separation. Even though both wings will experience the same flow conditions because the leading and trailing edges for both wings are aligned with each other, the small asymmetry in lift distribution occurs because the wings that are positioned above and below will experience different wing tip vortex interaction due to the directions of the vortices. The asymmetric in the lift distribution gets stronger at small separation because the vortex interaction also gets stronger at small separations.

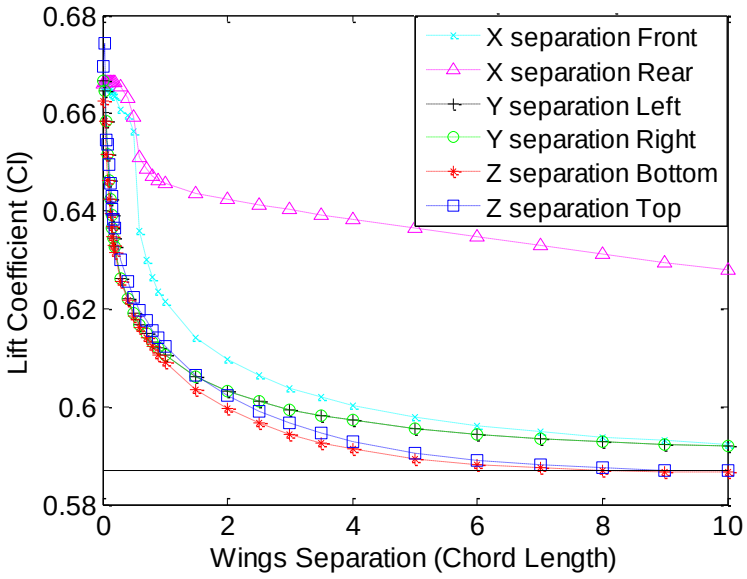

Figure. 2.6 Close proximity lift coefficient effects as a function of separation

The lift distributions generated in Figures 2.4 & 2.5 are plotted as coefficients of lift and drag in Figure 2.6 and 2.7. The drag is, of course, the induced drag. The total lift and drag coefficients for two UAV wings for the chord-wise, span-wise and vertical separation are plotted as a function of separation for an angle of attack of 6 degrees in Figure 2.6 & 2.7 respectively. The lift and drag coefficient increases as the wing separation decreases. The increase of both forces is especially strong after the separation is below 1 chord length, and the maximum lift occurs when then the two wings are joined. As previously mentioned, we can see that lift and drag coefficients for chord-wise separation are different for the front and back wings. The front wing starts behaving as a single wing for separation above 8 chord lengths. However, the back wing has higher lift coefficient for a larger range of separation. From Figure 2.6 & 2.7, we can see that the proximity effects for the back wing extend pass the 10 chord length. The effects for the back wing extend for larger range because the wing is affected by the vortex shedding from the front wing. Also our analysis is inviscid, so the vortex effects can be propagated in the simulation.

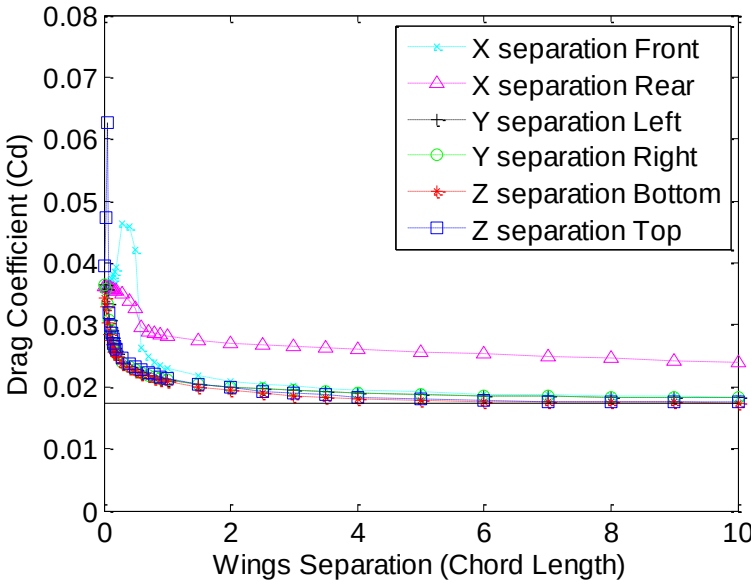

Figure. 2.7 Close proximity drag coefficient effects as a function of separation

For the span-wise and vertical separations the close proximity effects on the lift and drag coefficient dies out quicker than the chord-wise separation. From Figure 2.6 & 2.7, the close proximity effects for both the span-wise and vertical separations are negligible for separation above 4 chord lengths. Comparing the lift coefficient for a single UAV wing and two linked UAVs wings there is an increase of about 15%. Comparing the induced drag coefficient for a single UAV wing and the maximum induced drag between two UAVs wings there is an increase of about 50%. Contrary to the lift coefficient, the maximum drag does not occur when the two UAV wings are linked. From Figure 2.7, we can see that the maximum induced drag occurs around 0.5 chord lengths for the front wing separated in the chord-wise direction.

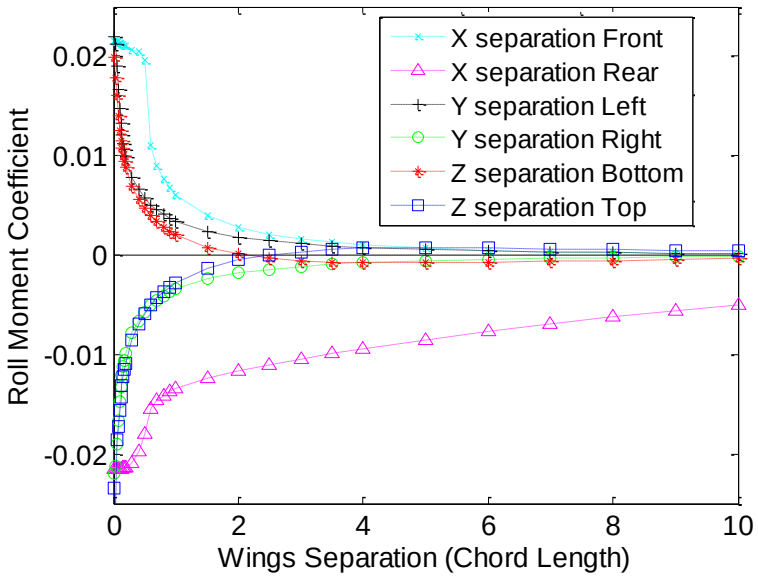

Figure. 2.8 Close proximity roll moment coefficient effects as a function of separation

As seen in Figure 2.4 and 2.5, the close proximity aerodynamic effects induces an asymmetric lift distribution around the UAV wings. The asymmetry in the lift distributions will yield a roll moment about the semi axis span. The roll and pitch moment coefficients for two UAV wings for the chord-wise, span-wise and vertical separation are plotted as a function of separation in Figure 2.8 and 2.9, respectively (AoA = 6°). As the UAV wings are far away from any aerodynamic interactions the roll moment is zero. Similar to the other aerodynamic coefficients, the roll moment coefficient magnitude increases as the wing separation decreases. As the UAV wings get closer, each will induce an opposite roll moment on each other as seen in Figure 2.8. The magnitude of roll moment coefficient for chord-wise separation are also different for the front and back wings as seen in Figure 2.8. The range of the close proximity effects on roll moment are the same as for the lift coefficient, for the chord-wise separation it extends pass 10 chord-length and for the span-wise and vertical separation extends until about 4 chord lengths.

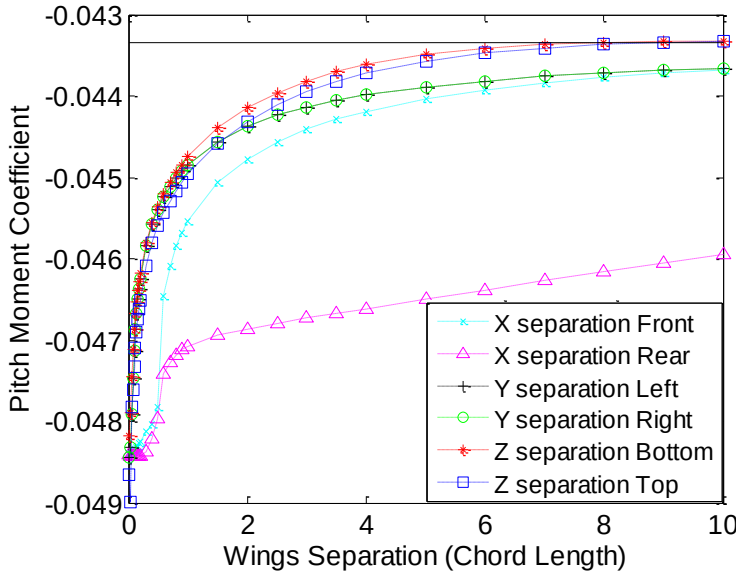

Figure. 2.9 Close proximity pitch moment coefficient effects as a function of separation

The pitch moment coefficient magnitude increases as the wing separation decreases. The increase in pitch moment is especially strong after the separation is below 1 chord length. The pitch moment coefficients for chord-wise separation are also different for the front and back wings as seen in Figure 2.9. The range of the close proximity effects on pitch moment are the same as for the lift coefficient, for the chord-wise separation it extends pass 10 chord-length and for the span-wise and vertical separation extends until about 4 chord lengths.

Due to the asymmetry in the lift distributions seen in Figures 2.4 and 2.5 it will also induce a yaw moment as the wings approach each other, as seen in Figure 2.10. As the UAV wings are far away from any aerodynamic interactions the yaw moment is zero. Similar to the other aerodynamic coefficients, the yaw moment increases, and are opposite to each other, as the wing separation decreases. The magnitude of yaw moment coefficient for chord-wise separation are also different for the front and back wings as seen in Figure 2.10. A difference for the yaw moment compared to the other

aerodynamic coefficients is that the yaw moment we can see a more nonlinear behavior.

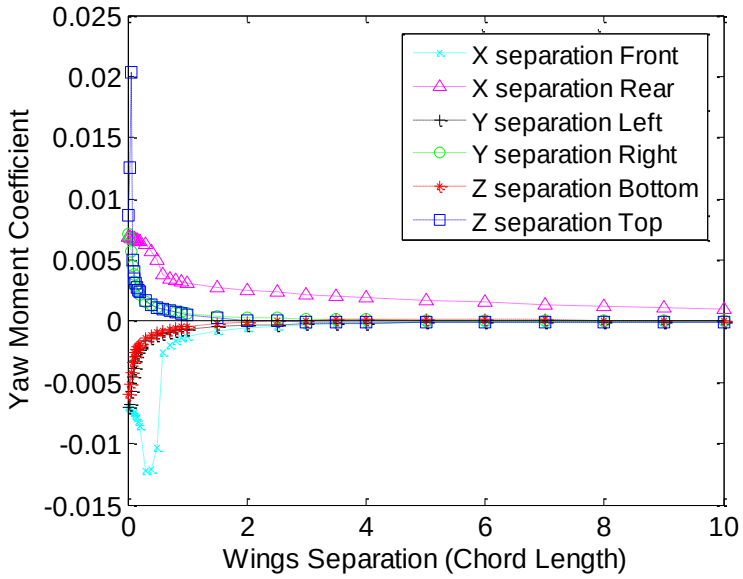

Figure. 2.10 Close proximity yaw moment coefficient effects as a function of separation

2.3.3 Close proximity aerodynamic intensity field

The objective of the close proximity aerodynamic analysis between two UAV wings is to generate an aerodynamic intensity field which will be used to determine forces acting between the approaching aircraft. Utilizing the lifting line method presented in the previous section we will compute all the aerodynamic forces and moments, lift, drag, roll, pitch and yaw, for the two wings for different separations in all three directions and different angles of attack for each wing. In Table 2.1, contains the wing and simulation parameters used to develop the aerodynamic intensity field. The nominal angle of attack that the UAVs will fly is around 6 to 8 degrees, therefore a computing range from 2 to 12 degrees angle of attack for each wing has been

chosen. For the x separation a range between 0 to 40 chord lengths has been chosen. As we can recall from the previous section, the close proximity effects for all forces and moments for a chord-wise separation extended pass 10 chord lengths. It was determined that most of the aerodynamic coupling between the two wings dies out by 40 chord lengths. For the y and z separation the range computed is from 0 to 10 chord lengths. From the previous section we notice that in these two directions there is no aerodynamic coupling beyond 10 chord lengths. Table 2.1 also presents the data points computed for each of the simulation parameters. A total of 97,344 simulations were run to compile the aerodynamic intensity field.

Table 2.1 Wing and simulation parameters for the aerodynamic intensity field computed

Wing and simulation parameters		**Data points Computed**
Airfoil	LA2573A	
Planform	Rectangular	
Aspect ratio	4.5	
Angle of attack W1	2° to 12°	2, 4, 6, 8, 10, 12
Angle of attack W2	2° to 12°	2, 4, 6, 8, 10, 12
X separation	0 to 40c	0, 0.05, 0.1, 0.2, 0.4, 0.6, 1, 1.5, 2, 3, 4, 5, 10, 20, 30, 40
Y separation	0 to 10c	0, 0.05, 0.1,0 .2, 0.4, 0.6, 1, 1.5, 2, 3, 4, 5, 10
Z separation	0 to 10c	0, 0.05, 0.1, 0.2, 0.4, 0.6, 1, 1.5, 2, 3, 4, 5, 10

2.4 Wind Tunnel Testing

Wind tunnel tests for close proximity aerodynamic effects of two wings were performed to compare with the prediction from the lifting-line method. The wind tunnel setup consists of a complete (full) wing and a half wing with a rectangular

planform and an aspect ratio of 4.5 as seen in Figure 2.11. The wings have a chord of 3 inches and a span of 13.5 and 6.75 inches for the full and half wing, respectively. The full wing was used to measure the aerodynamic forces and moments using a 6 degree-of-freedom JR3 load cell, which measures lift to 25 lb with a resolution of less than 0.01 lb. Tests use the Cornell University environmental wind tunnel facility, an open return wind tunnel with a 48" x 43" test section. A splitter plate was attached to the half wing to emulate a full wing. The full wing remained stationary and the half wing was able to move in all three directions chord-wise (x – direction), span-wise (y – direction), and vertical direction (z – direction).

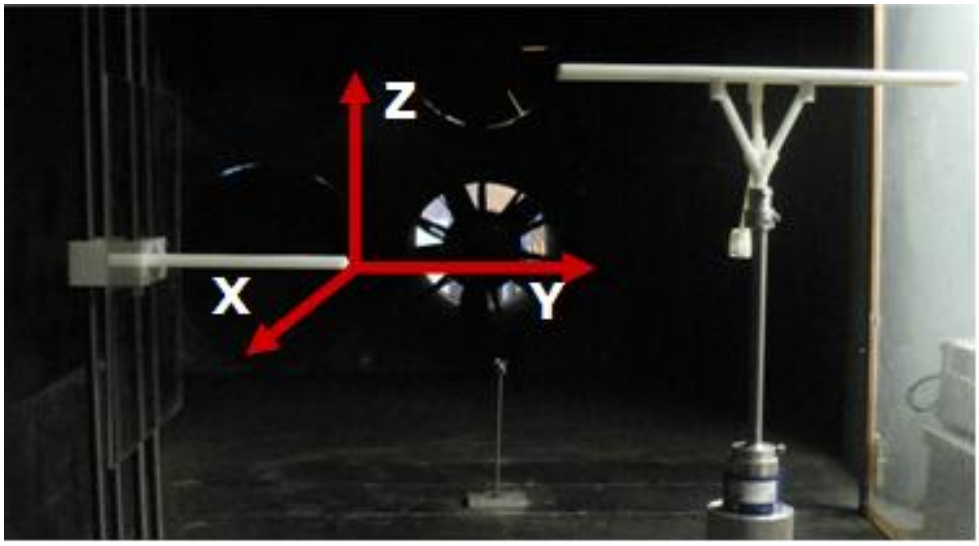

Figure. 2.1 Wind tunnel setup of the two UAV wings.

2.4.1 Chord-wise separation tests

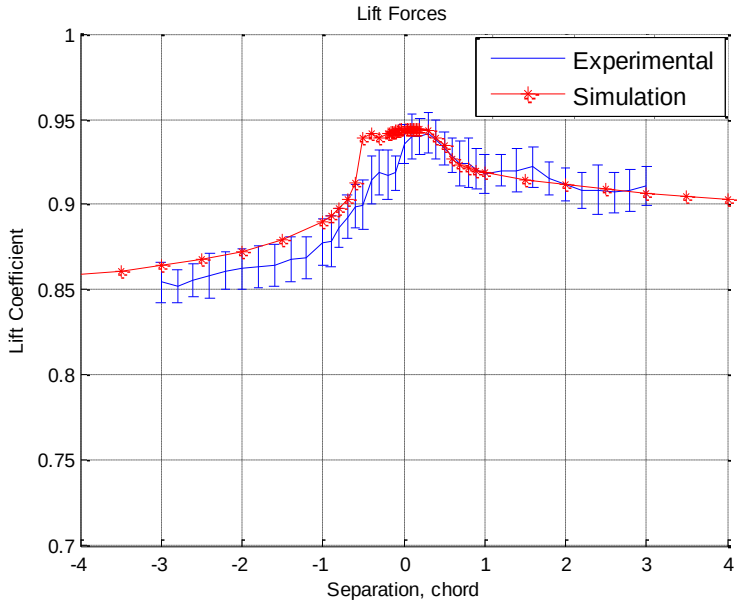

Figure. 2.12 Predicted and measured lift coefficient for two UAV wings separated in the chord-wise direction

The lift coefficient for two UAV wings separated in the chord-wise direction for both predicted and measured are plotted as a function of separation for an angle of attack of 9 degrees in Figure 2.12. Since only the full wing is attached to a load cell, we tested both positive and negative separation values. In Figure 2.12, the positive separations corresponds for when the full wing is behind the half wing and negative separations for when the full wing is in front of the half wing. Due to limited space in the wind tunnel testing area, tests will be performed for a range of separations between -3 and 3 chord lengths. We can see that the measured values for the lift coefficients have a good agreement with the predicted values from the lifting-line method. In addition, for chord-wise separation, the measured results verifies that there is higher lift coefficient for the rear wing is behind (positive separation) than for the front wing.

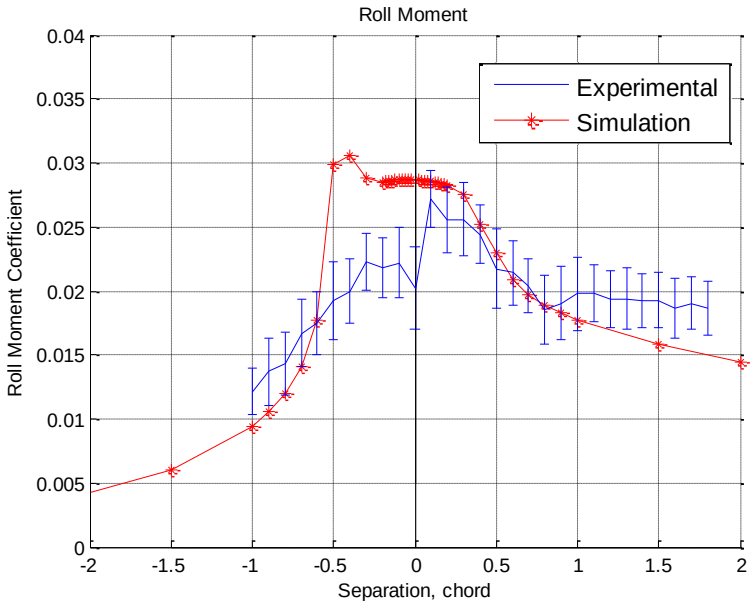

Figure. 2.13 Predicted and measured lift coefficient and roll moment coefficient for two UAV wings separated in the chord-wise direction

The roll moment coefficient for two UAV wings separated in the chord-wise direction for both predicted and measured are plotted as a function of separation Figure 2.13. Figure 2.13 shows the results for both positive and negative separations, where positive separations corresponds to the full wing in the rear of the half wing and the negative separations corresponds to the fill wing in front of the half wing. For the roll moment coefficient we can see that there is a good agreement between the measured and predicted values from the lifting-line method. The agreement is not as good as for the lift coefficient but we can see that both the measured and predicted values have the same trends. The roll moment coefficient increases as the separation decreases. For chord-wise separation, the measured results verify that there is higher roll moment coefficient for the rear wing (positive separation) than for the front wing.

2.4.2 Vertical separation tests

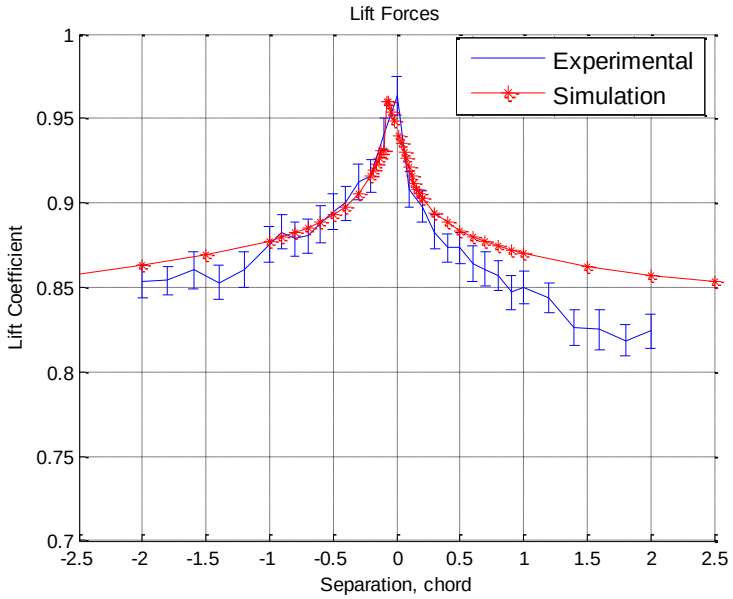

Figure. 2.14 Predicted and measured lift coefficient for two UAV wings separated in the vertical direction

The lift coefficient for two UAV wings separated in the vertical direction for both predicted and measured are plotted as a function of separation for an angle of attack of 9 degrees in Figure 2.14. Since only the full wing is attached to a load cell, we tested both positive and negative separation values. In Figure 2.14, positive separations correspond to the full wing below the half wing, and negative separations correspond to the full wing above the half wing. Due to limited space in the wind tunnel testing area, tests will be performed for a range of separations between -2 and 2 chord lengths. We can see that the measured values for the lift coefficients have good agreement with the predicted values from the lifting-line method. As expected, the lift coefficient increases as the separation decreases, as mentioned in the previous sections. In addition, for vertical separation, the measured results verify that there is a small

asymmetry in the lift coefficient between the wings that are above and below. Comparing Figure 2.12 and 2.14, the differences between the lift coefficient values are not as big as it was seen for chord-wise separation. For the roll moment coefficient, similar to the lift coefficient, there is a good agreement between the measured and predicted values from the lifting-line method as seen in Figure 2.15. The roll moment coefficient increases as the separation decreases.

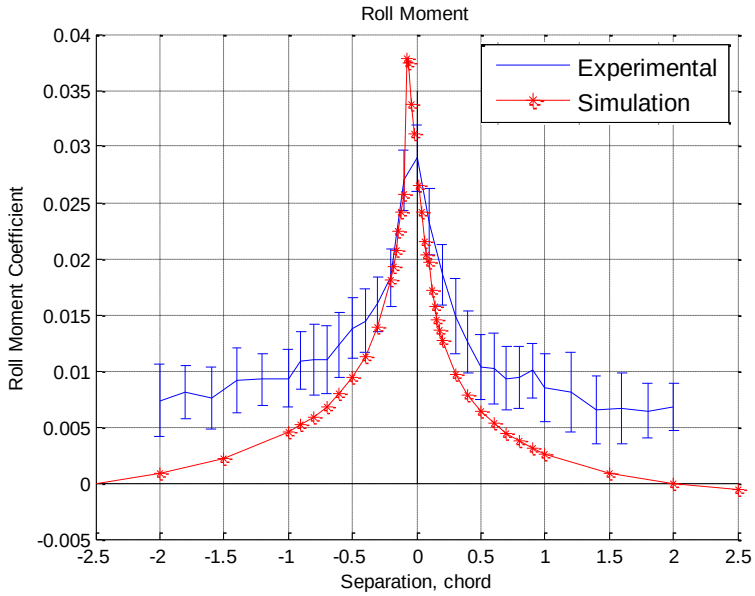

Figure. 2.15 Predicted and measured lift coefficient and roll moment coefficient for two UAV wings separated in the vertical direction

2.4.3 Span-wise separation tests

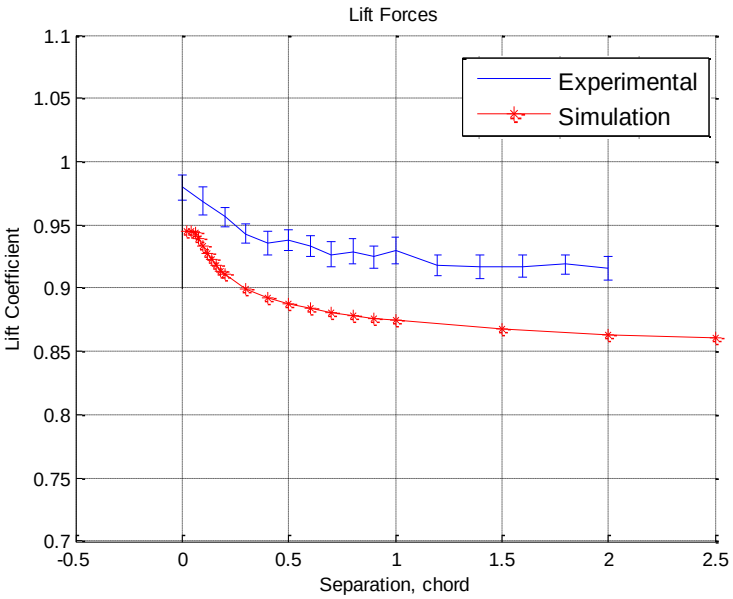

Figure. 2.16 Predicted and measured lift coefficient for two UAV wings separated in the span-wise direction

The lift and roll moment coefficient for two UAV wings separated in the span-wise direction for both predicted and measured are plotted as a function of separation in Figure 2.16 and 2.17 respectively. For span-wise separation since both wings will experience the same close proximity aerodynamic effects, as discussed in the previous section, we tested only for positive separation values. Due to limited space in the wind tunnel testing area, tests were performed for only up to 2 chords separation. We can see that the measured values for the lift coefficients have a good agreement with the predicted values from the lifting-line method. The agreement is not as good as for the lift coefficient for the other two cases but we can see that both the measured and predicted values have the same trends. The maximum difference between measured and predicted values is of about 5%. A source for the discrepancy between the

measured values of lift for the span-wise separation and the other two cases is that for this case the wings are moving closer to the wind tunnel walls, which could increase the wall effects. The lift coefficient increases as the separation decreases, as mentioned in the previous sections. For the roll moment coefficient, once again there is good agreement between the measured and predicted values. The agreement is not as good as for the lift coefficient but we can see that both the measured and predicted values have the same trends. As expected, the roll moment coefficient increases as the separation decreases.

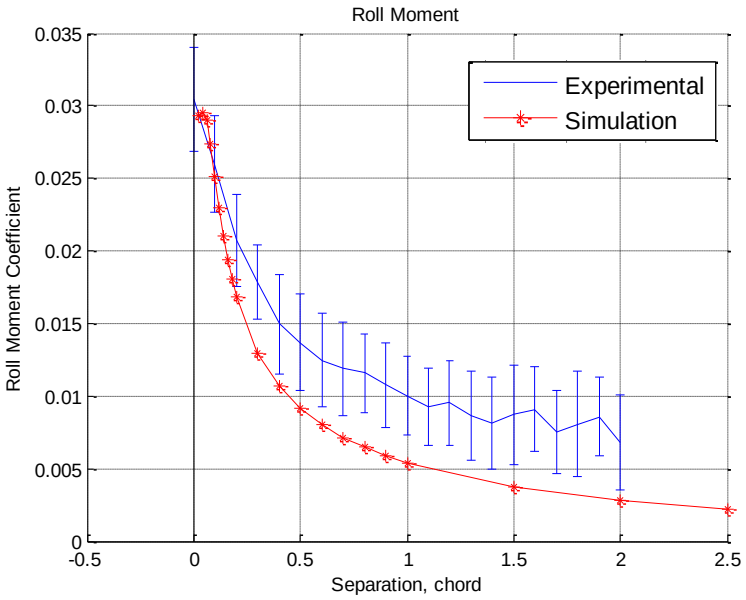

Figure. 2.17 Predicted and measured roll moment coefficient for two UAV wings separated in the span-wise direction

2.5 CFD Flow Visualization

The objective of this study was to investigate the proximity aerodynamics effects of rectangular wings with Computational Fluid Dynamics (CFD) methods. When

coupled with experimental data, CFD flow visualization techniques can enable a better understanding of the aerodynamics that will affect a docking UAV. The problem was simulated using ANSYS 12.0 Workbench, a finite element solution software package, and Fluent, a CFD solver. A single wing simulated at varying angles of attack was used to validate the simulation method against previous wind tunnel and lifting line data. Two docking wings were then simulated for chord-wise, span-wise, and vertical approaches. Force and moment coefficient data was compared to lifting line predictions. Streamline visualization plots were also used to analyze the qualitative behavior of the system's aerodynamics. The streamlines indicated a potential for wingtip vortex mixing, a source for buffeting that could negatively affect the two UAVs flying at close proximity.

2.5.1 Methods

A full body simulation of two docking wings in all three directions, as shown in Figure 2.18, was conducted using ANSYS 12.0 with Fluent. In all simulations, a rectangular plan-form wing with an aspect ratio of 4.5 was used. Angles of attack and velocities were chosen to match experimental data [7]. The Reynolds number of the simulations was 98,000, similar to that of the wind tunnel data. The K-Omega two-equation turbulence model with standard wall functions was implemented for all simulations. All simulations in this study were performed using the k-omega Reynolds Averaged Navier Stokes (RANS) model [16]. This two-equation turbulence model was chosen for its ability to adequately resolve turbulent flows at relatively low computational cost [17]. Work by Ahmad, et al suggests that qualitative characteristics of wingtip vortex formations are adequately modeled by unstructured RANS methods [18]. The present work similarly assumes that the solver is adequately capable of

resolving qualitative behaviors in order to evaluate the relative merits of different docking approach paths.

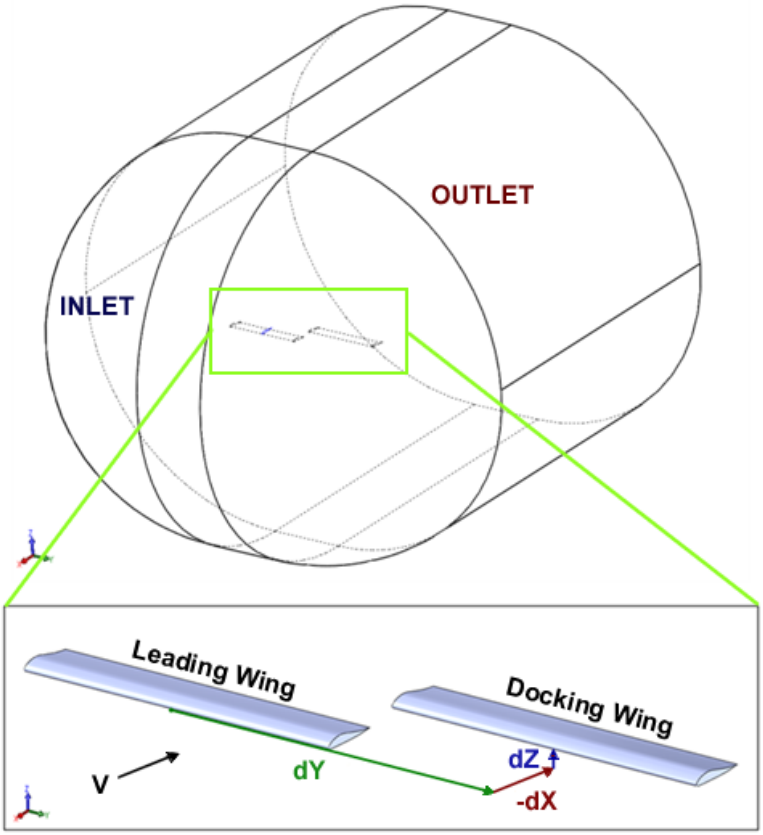

Figure. 2.18 Two full-body docking wing geometry and flow domain

2.5.2 Two wing docking

The flow domain and geometry of the two docking wings used for meshing is shown in Figure 2.18. The mesh strategy was adapted from methods used by Ahmad [18] and Alley [19]. A far-field inlet was created 12.5 chord-lengths in front, top and to the side of the wing, and 20 chord-lengths behind the wing. The geometry was meshed with the ANSYS 12.0 Workbench Mesher. A hybrid grid was implemented. A structured mesh was used near the wing surface to capture boundary layer effects and

in the wake region to capture wake and vortex effects. The remaining volume was meshed with tetrahedrons. The smallest elements were placed near regions where vortices were expected to form. The typical mesh size was 1.3 million cells. An overall view of the meshed geometry is provided in Figure 2.19a. A close-up view of the structured mesh around the wing is provided in Figure 2.19b.

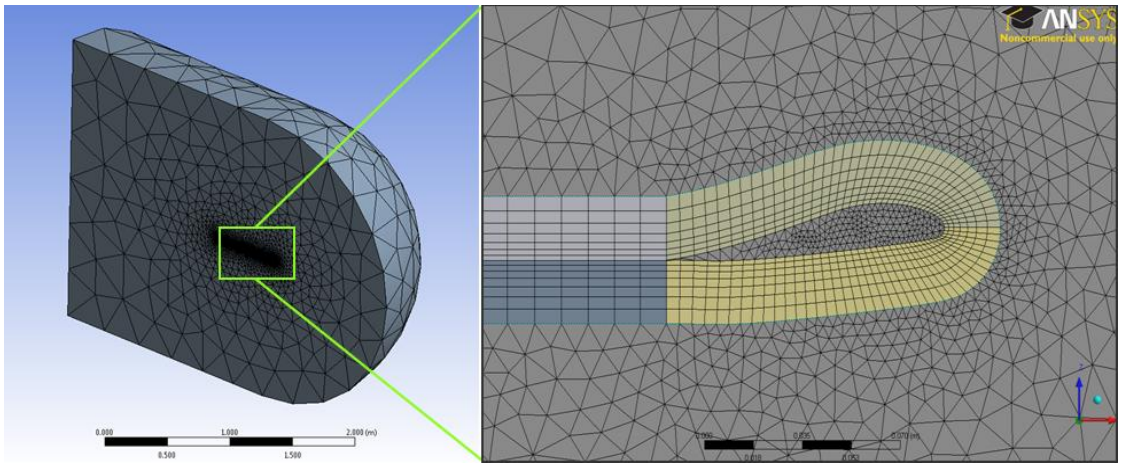

Figure. 2.19 Typical wing geometry and mesh. a) Overall view of mesh. b) Wing boundary layer and wake mesh

The wings were modeled at an angle of attack of 6º, and a velocity of 14.30m/s (32 MPH). The leading wing was held stationary in the flow domain while the docking wing's position was varied. The wing's position was varied in three uncoupled directions – chord-wise (x), span-wise (y) and vertically (z). To avoid skewed elements, the wings were separated span-wise such that there was a small gap between their wingtips. Each position was simulated individually as a static solution. Transient effects were not considered for this study. The residual convergence criterion was 1x10-6. A total of 33 simulations were run in Fluent for this study.

2.5.3 CFD results and discussion

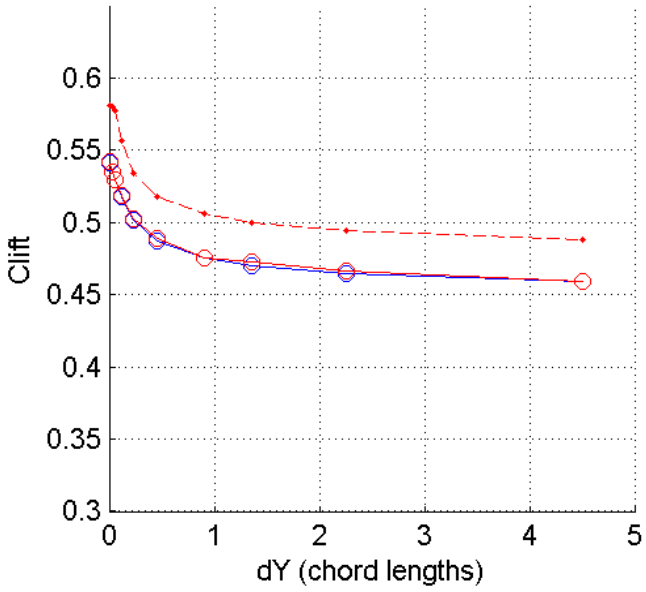

Figure. 2.20 Comparison of the lift coefficient between the CFD and lifting-line data for span-wise separation.

Comparisons of force and moment coefficient data between the CFD and Lifting Line methods for chord-wise, span-wise and vertical docking separation have been performed. A sample comparison of the lift and roll coefficient for span-wise separation is presented in Figure 2.20 and 2.21. The lifting line and CFD lift coefficient data match trends, but the magnitude is off by 5%. The difference in magnitude is within the range of accuracy of the lifting-line method. Roll data matches trends and magnitude within 1%. These are important force and moments to model correctly because they will require the most control authority from the UAV, and will also have the biggest impact on its position.

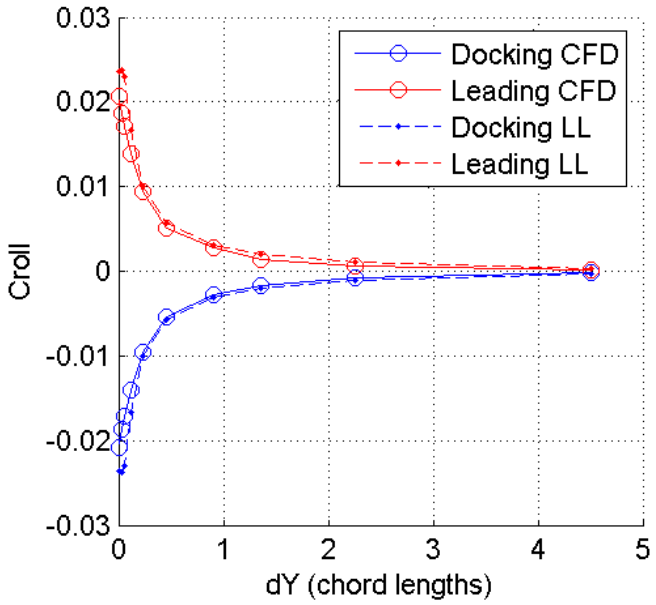

Figure. 2.21 Comparison of the roll moment coefficient between the CFD and lifting-line data for span-wise separation.

Visualization plots of streamlines from two views are presented in Figure 2.22, in the appendix, for select chord-wise displacements. The plots help characterize wingtip flow interactions. When the two wings are docked, the wingtip vortex of each wing is separate and rotating in opposite directions. As one wing moves backwards, the path-lines originating from the trailing wing mix with the leading wing vortex. They are pulled into the wake of the trailing wing. By x separation of 1.0c, the two vortices are shown to stop mixing, and the leading wing vortex bends around the wing tip of the trailing wing. The vortex mixing is a potential source of buffeting as the transition between separate and mixed vortices will likely be unstable. A transient CFD study would better explore this behavior.

Visualizations that characterize the behavior of the wingtip vortex interactions of the three docking approaches are presented in Figure 2.23 in the appendix. As mentioned above, the chord-wise approach displays flow mixing between x separation

of 0.1c and 0.5c. The vertical approach shows separate and counter-rotating wingtip vortices, but they are pulled into the wake of leading wing. The span-wise approach is characterized by separate and counter-rotating wingtip vortices through the entire approach path. The symmetry of the streamlines is consistent with the symmetry of the coefficient data in Figure 2.20 and 2.22.

The flow visualizations reveal that the span-wise approach offers a potential advantage over other approaches such as the wing approaching each other from the vertical or chord-wise direction. The symmetry displayed in the streamline plots suggests that flow around the wings would be simpler. Independent counter-rotating vortices would reduce the amplitude of time variant loading in the wing's lift distribution. Similarly, they would be less likely to decompose into large scale turbulent structures that would buffet the wing. Avoiding these turbulent interactions would reduce the complexity of the docking control strategies.

2.6 Conclusions

Close proximity aerodynamic analysis for two UAV wings at close proximity has been presented. A verification of the predicted aerodynamic data with both wind tunnel and CFD data for aerodynamic forces and moments have been presented. There is a reasonably good agreement between the predicted values calculated using the modified lifting-line method, CFD and the measured values from the wind tunnel tests. For all cases, as the separation between the two UAV wings decreases, there is an increase in lift, drag, roll, pitch and yaw moment magnitudes. Close proximity induced effects on lift were significant and there was an increase of around 15% from the nominal value of a wing by itself. The close proximity effects on induced drag

were also significant, there was as much as 50% increase on induced drag throughout the different separations. Both the roll and pitch moments where also significantly affected. As the wings get closer to each other, they will induce an opposite roll moment on each other. This means that as the wing approaches for docking it will tend to roll away from each other. Also at close proximity, the aerodynamic forces and moments demonstrate nonlinear behavior. This nonlinear behavior will have to be taken in to account when determining trajectories and control strategies for the UAV to link in midair. From the CFD simulation, we noticed that the presence of wing vortex mixing identifies potential negative effects of the chord-wise approach. A span-wise separation avoids this mixing because it exhibits symmetrical flow structures.

2.7 Appendix

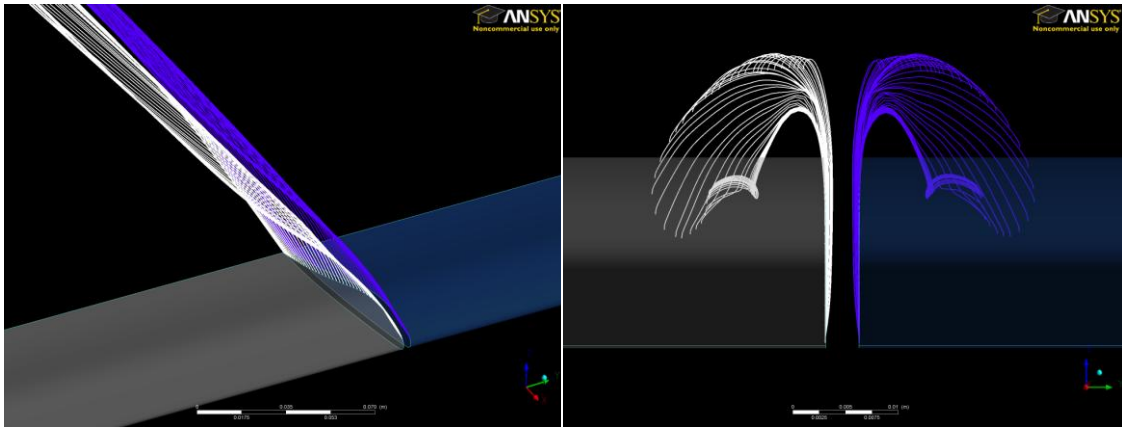

a) Isometric View, x separation = 0.00 b) Front View, x separation = 0.00

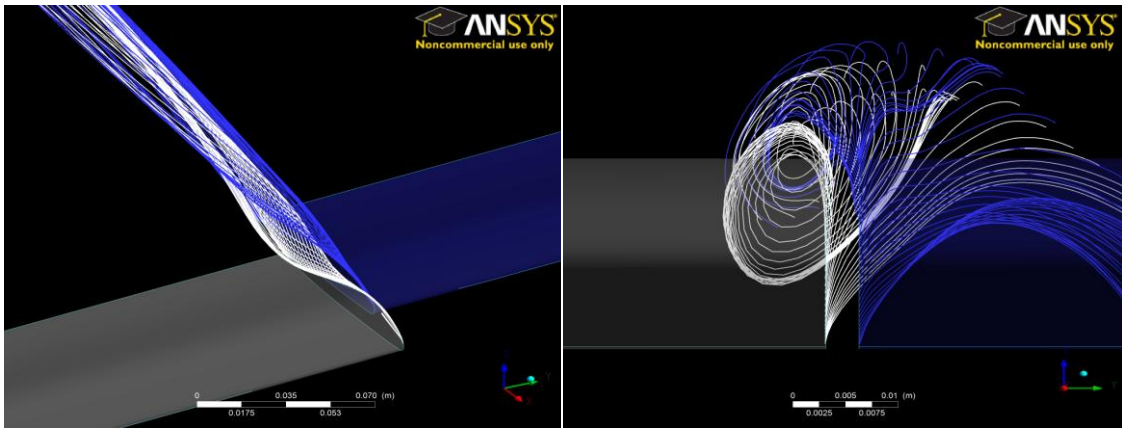

c) Isometric View, x separation = -0.30 d) Front View, x separation = -0.30

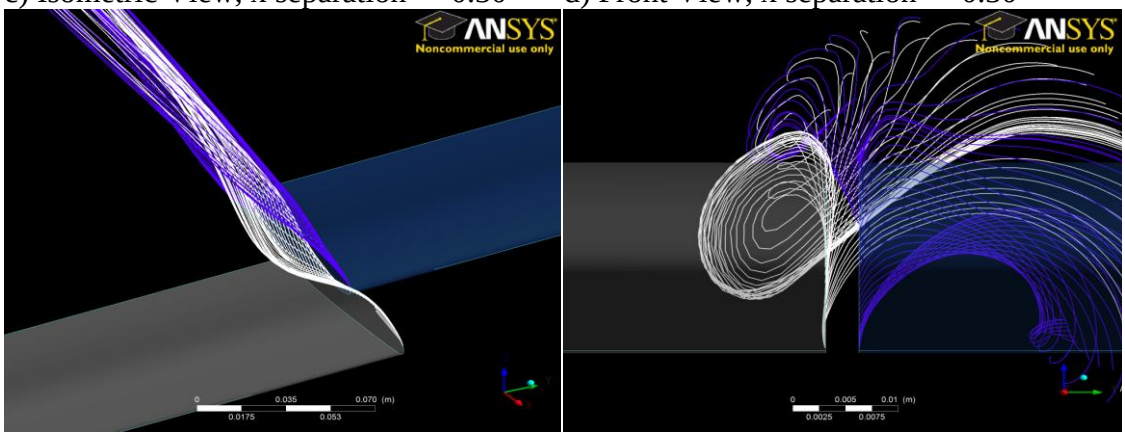

e) Isometric View, x separation = -0.50 f) Front View, x separation = -0.50

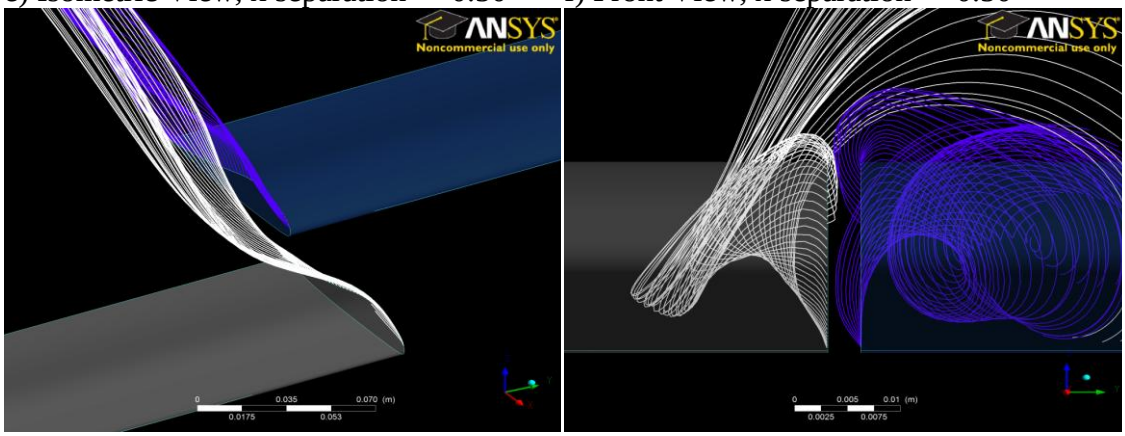

g) Isometric View, x separation = -1.00 h) Front View, x separation = -1.00

Figure. 2.22 Wingtip Particle Path-line Plots, Chord-wise Approach

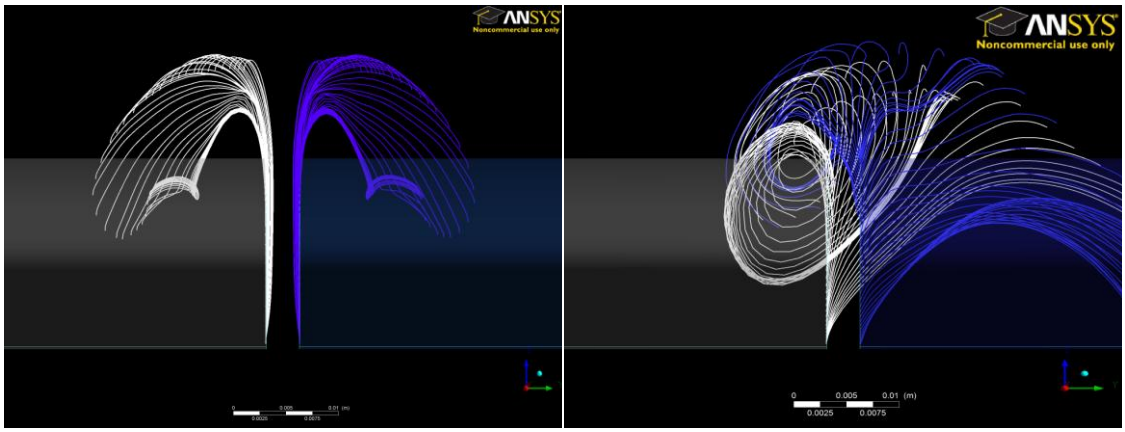

a) Chord-wise, x separation = 0.00 b) Chord-wise, x separation = -0.30

c) Span-wise, y separation = 0.03 d) Span-wise, y separation = 0.23

e) Span-wise, z separation = 0.00 f) Span-wise, z separation = 0.20

Figure. 2.23 Characteristic Wingtip Particle Path-lines

REFERENCES

1. Pamadi, B. *Performance, Stability, Dynamics, and Control of Airplanes,* American Institute of Aeronautics and Astronautics, 1998, pp. 106–119
2. Schumacher, C., Singh, S., “Nonlinear Control of Multiple UAVS in Close-Couple Formation Flight”, AIAA Guidance, Navigation, and Control Conference 14-17 August 2000, Denver, CO
3. Blake, W., and Multhopp, D., “Design, Performance and Modeling Considerations For Close Formation Flight,” AIAA Guidance, Navigation, and Control Conference, AIAA, Reston, VA, July 1998.
4. Pachter, M., D’Azzo, J., Proud, A., “Tight Formation Flight Control”, *Journal of Guidance, Control, and Dynamics,* Vol. 24, No. 2, March–April 2001.
5. Rossow, V.J., Sacco, J.N., Askins, P.A., Bisbee, L.S., and Smith, S.M., "Measurements in 80 by 120 Foot Wind Tunnel of Hazard Posed by Lift-Generated Wakes," *Journal of Aircraft*, Vol. 32, No. 2, pp. 278-284, August 1993.
6. Pete, K.R., Smith, S.T., and Vicroy, D.D., "Model Validation of Wake-Vortex/Aircraft Encounters," AIAA paper 2000-3979, presented at the AIAA Atmospheric Flight Mechanics Conference, Denver CO, August 2000.
7. Cuji, E., Garcia, E. “Simulation and Wind Tunnel Testing of Close Proximity Aerodynamics of Two Linked UAVs”, Proc. 20th International Conference on Adaptive Structures and Technologies, Hong Kong, 2009.

8. Cuji, E., Lukaczyk, T., and Garcia, E., “Aircraft Dynamics, Wind Tunnel Testing and CFD Flow Visualization of Two Linked UAVs Flying at Close Proximity”, Proceedings of the Smart Structures and Materials 2008: Active and Passive Smart Structures and Integrated Systems, Vol. 7645, SPIE, San Diego, CA, March, 2010. 1.

9. Cuji, E., Garcia, E.“Analytic Modeling of the Aerodynamics of Shape Changing Wings”, Proc. 18th International Conference on Adaptive Structures and Technologies 127, 2007.

10. Cuji, E. and Garcia E. "Analysis of Turning Performance of Symmetric and Asymmetric V-Shape Morphing Wings", *International Review of Aerospace Engineering Journal*, Vol 4, No 1, February, 2011.

11. Wickenheiser, A. M., and Garcia, E., (2007) “Aerodynamic Modeling of Morphing Wings Using an Extended Lifting-Line Analysis,” *Journal of Aircraft*, 44 no.1, pp. 10-16, 2007.

12. Phillips, W. F., Snyder, D. O. (2000) “Modern Adaptation of Prandtl’s Classic Lifting-Line Theory”, *Journal of Aircraft ,* Vol. 37, No. 4, 2000, pp. 662-670.

13. Prandtl, L., (1918) “Aerofoil Theory, I and II Communications”, *Nachr. Kgl. Gesellschaft der Wissenachaft, Math-phys. Classes*, Göttingen, 1918-19.

14. Wang, Z., Mook, D., “Numerical Aerodynamic Analysis of Formation Flight”, 41st Aerospace Sciences Meeting and Exhibit 6-9 January 2003, Reno, Nevada.

15. Bramesfeld, G., Maughmer, M., “Effects of Wake Rollup on Formation-Flight Aerodynamics”, *Journal of Aircraft,* Vol. 45, No. 4, July–August 2008.

16. Menter, F. R., “Two-Equation Eddy-Viscosity Turbulence Models for Engineering Applications”, *AIAA Journal*, Vol. 32, No. 8, August, 1994, pp. 1598-1605.

17. D.C. Wilcox. “Turbulence Modeling for CFD.” DCW Industries, Inc., La Canada, California, 1998.

18. Ahmad, S., Brewer, W., Pasqualle, C., “An Accurate Unstructured Simulation of Wingtip Vortex”, AIAA Aerospace Sciences Meeting, AIAA, Orlando, Florida, January 2009.

19. Alley, N.R., Phillips, W.F., Spall, R.E., “Predicting Maximum Lift Coefficient for Twisted Wings Using Computational Fluid Dynamics”, *Journal of Aircraft*, Vol 44, No3, pp. 911-917, June, 2007.

CHAPTER 3

AERODYNAMIC ANALYSIS AND AIRCRAFT DYNAMICS OF TWO LINKED UAVS FLYING AT CLOSE PROXIMITY[*]

3.1 Abstract

Unmanned aerial vehicles (UAVs) typically have small wingspans so it can be rapidly deployed from any airfield. However, having a small aspect ratio wing also limits its range and endurance. It is known that an aircraft with large aspect ratio wings have better aerodynamic efficiency due to the reduction of induce drag for the given lift. A linked UAV concept, where individual UAVs link at high altitude creates an aerodynamically efficient system of aircraft which has long endurance capabilities and can cruise for extended periods with significantly reduced power loads. The current research presents an analysis of close proximity aerodynamics and aircraft dynamics of two Linked UAVs. As the UAVs approach each other for wingtip docking there will be strong aerodynamic coupling between their wings tips. Lifting line and wind tunnel testing of two UAV wings shows significant close proximity effects on lift, drag, roll, pitch and yaw moments on each UAV. The dynamics and stability of the UAVs are also affected by the close proximity aerodynamic effects. For example, the UAVs roll away from each other in the close proximity presence of another UAV. An aerodynamic disturbance intensity field has been generated, utilizing both simulation and wind tunnel data, to determine a trajectory for the two UAVs to approach each other for midair docking. A span-wise trajectory experiences

[*] Submitted for publication to *Journal of Aircraft* by Cuji, E. Joshi, S. and Garcia E. "Aerodynamic Analysis and Aircraft Dynamics of Two Linked UAVs Flying at Close Proximity"

less overall aerodynamic disturbances for both the leader and follower UAVs, which makes this trajectory more desirable for midair docking.

3.2 Introduction

Currently, unmanned aerial vehicles (UAVs) are used mainly for Intelligence, Surveillance and Reconnaissance (ISR) missions. One advantage of using UAVs for ISR missions is that they can be rapidly deployed from any airfield due to their small wingspan. However, having a small aspect ratio wing also limits its range and endurance [1]. An effective ISR platform requires that it be rapidly deployable, have long range and endurance. It is known that an aircraft with large aspect ratio wings have better aerodynamic efficiency due to the reduction of induce drag for the given lift [1, 2]. Wingtip docking UAVs will increase the effective aspect ratio of a system of aircrafts. The larger aspect ratio of the linked UAV leads to an improvement in overall aerodynamic efficiency due to the decrease of the induce drag as previously mentioned. The improvements in aerodynamic efficiency are similar to the improvements seen in formation flight [3, 4], but without having the trailing aircraft fly in the vortex wake of the leading aircraft which can lead to both stability and control problems [5, 6]. The linked UAV concept allows for a rapidly deployable ISR platform using individual UAVs with wingspans small enough to be deployed from small aviation airfields or even being hand launched. Individual UAVs will link at high altitude to create an aerodynamically efficient system of aircraft which has long endurance capabilities and can cruise for extended periods with significantly reduced power loads.

This paper presents an analysis of close proximity aerodynamics and aircraft dynamics of two UAVs linked at their wing tips. As the UAV approach each other for wingtip docking there will be strong aerodynamic coupling between the UAV wings tips. Determining the aerodynamic coupling effects on all the forces and moments is essential to determine a trajectory and controls for each UAV to perform the docking maneuver. Simulation and wind tunnel testing of the close proximity effects on all the aerodynamic forces and moments for two UAV wings has been performed. The computational aerodynamics simulations are performed utilizing a modern adaptation of Prandtl's lifting-line method [7], which is based on a fully three-dimensional vortex lifting law. The proximity aerodynamics effects between the UAVs wings will be analyzed as a function of its relative position in all three directions: chord-wise, span-wise and vertical direction. A look-up table of aerodynamic forces and moments for all relative positions and angles of attack between the two UAVs has been developed. An aerodynamic disturbance intensity field is generated, utilizing both simulation and wind tunnel data. This was used to determine an optimal trajectory for the two UAVs to approach each other for docking. In this paper we will examine how the close proximity aerodynamics affects the dynamics and stability of the UAVs. The aircraft dynamics analysis will be done in Simulink, which will include the close proximity aerodynamic look-up library. A comparison of two docking trajectories paths will be presented.

3.3 Aerodynamic Model

3.3.1 Adaptation of lifting-line method

As the UAVs fly in close proximity to each other there is strong aerodynamic coupling between them. As the UAVs approach each other, to link in midair, it experiences different aerodynamic forces and moments depending on relative position and flight condition. To determine docking trajectories and analyze the aircraft dynamics an understanding of the close proximity aerodynamic forces and moments that act upon the UAV wings are needed. An aerodynamic analysis for both varying relative positions between the UAVs and flight condition is needed. A computational fluid dynamics package would not be efficient, since a new mesh would be needed for every relative position and flow field configuration, resulting in high computational cost. Instead, we utilized an approach to 3D modeling which incorporates a modern adaptation of Prandtl's lifting-line method, based on a fully three-dimensional vortex lifting law that we have developed [7, 8]. The method enables to analyze the aerodynamic properties of a system of lifting surfaces of arbitrary camber, sweep, and dihedral.

There are several variations of lifting-line method, for example the adaptation of the Weissinger's method present by Wickenheiser and Garcia, which can be use for wings with arbitrary planform, but cannot calculate fully 3D geometries [9]. The method that we have developed is based on the adaptation of the Prandtl's lifting-line method developed by Phillips and Snyder [10]. This method is derived from the classical lifting-line method, but it's generalized to correct for the violations of the classical lifting-line theory for wings with sweep and dihedral. This method

synthesizes the 3D finite wing into a series of horseshoe vortices distributed at the quarter chord as seen in Figure 3.1. It uses the Prandtl's theory [11] but instead of using the two dimensional Kutta-Joukowski law, this method is based on a fully three dimensional vortex lifting law. This modification allows it to be used for systems surfaces of arbitrary camber, sweep and dihedral. Furthermore, with this method we can compute the aerodynamic forces for a system of lifting surfaces with arbitrary position and orientation which conventional lifting-line methods do not.

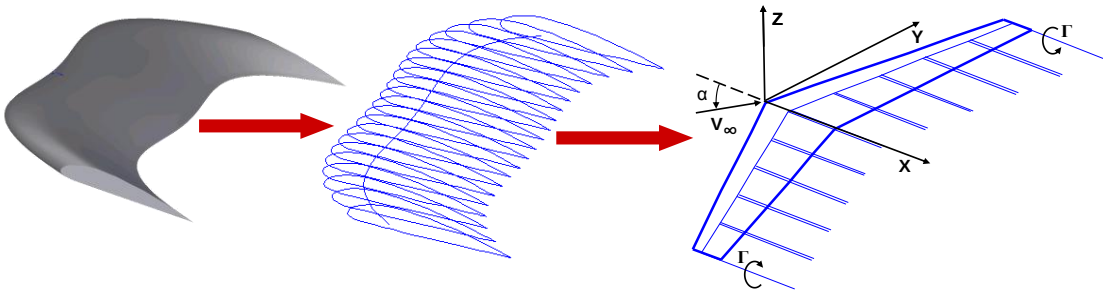

Figure. 3.1 A 3-D finite wing decoupled into a series of 2-D airfoils and into a series of horseshoe vortices.

A lifting-line approach was used to generate the aerodynamic database because it is a fast computational approach with a low order model compared to CFD for aerodynamic analysis of different relative separations. The speed of this method allows to determine the aerodynamic forces and moments acting on each UAV wing as a function of its relative separation in all directions and its corresponding angle of attacks. An aerodynamic intensity field between two UAVs wings will be generated as a function of its relative position in all three directions: chord-wise (x – direction), span-wise (y – direction), and vertical direction (z – direction) as seen in Figure 3.2.

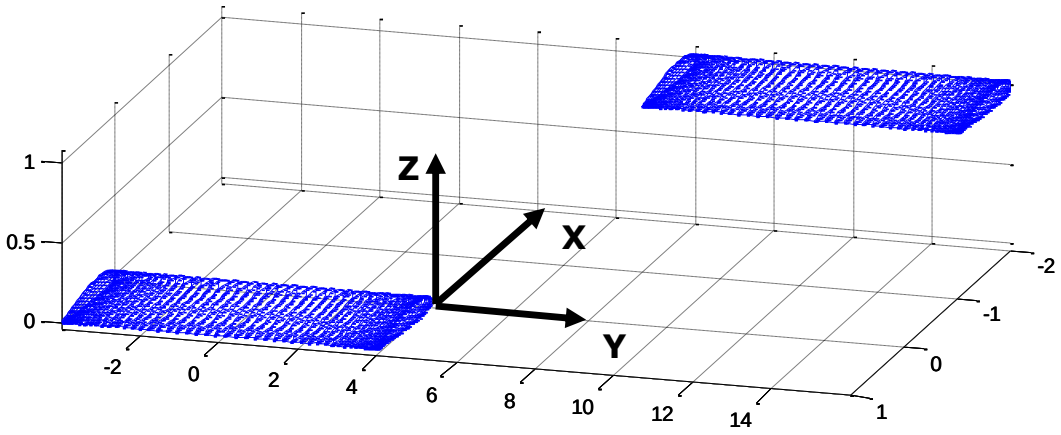

Figure. 3.2 Coordinate frame for the relative separation between the two UAV wings.

3.3.2 Close proximity aerodynamic analysis

The lift characteristics of the UAV wings will vary as a function of its relative separation and orientation. In addition, the lift characteristic acting on each UAV wing will be different depending on the wing position. For example, we expect a leading wing to have a different lift distribution than the wing in its wake. In this section we are going to examine how the lift distribution, total lift, drag and roll, as well as pitch and roll moments coefficients changes for two UAV wings separated in the chord-wise, span-wise and vertical directions, as shown schematically in Figure 3.3. A sample data of aerodynamic database analysis is presented in the following sections. A complete analysis has been previously presented [12, 13] and can be found in reference 12.

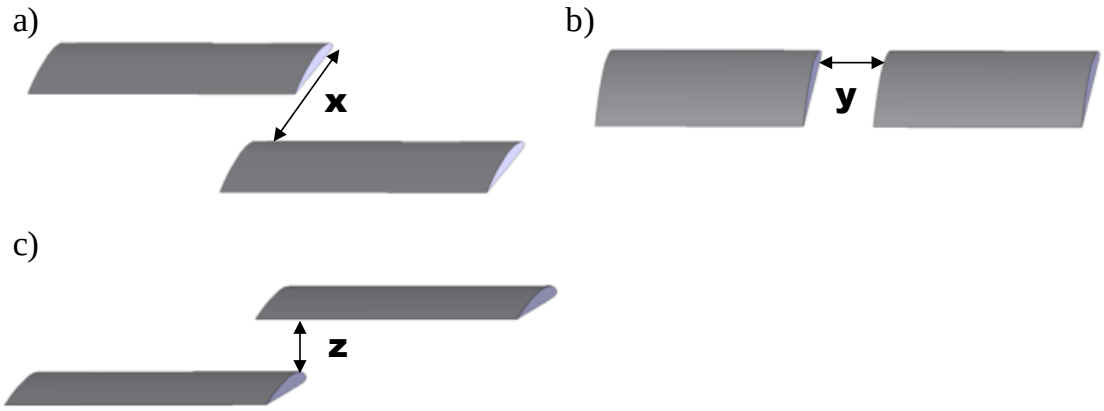

Figure. 3.3 a) UAV wings separated only in the chord-wise direction. b) UAV wings separated only in the span-wise direction. c) UAV wings separated only in the vertical direction.

The lift distribution of two UAV wings for different chord-wise separations from 0c (zero chord separation) to 5c are plotted as a function of position along the span for an angle of attack of 6 degrees in Figure 3.4. For this case, the two wings are in the same vertical position and wing tips of the left-hand side and the right-hand side wings are aligned as seen in Figure 3.3a. The left data corresponds for wing in the front and the right data corresponds to the wing behind. When the two UAVs are far away from each other, the lift distributions for each individual wing correspond to that of a single wing by itself, as expected. In addition the lift distributions are identical to each other since there is no aerodynamic coupling between each the wings as it can be seen in Figure 3.4 when there is an infinite separation.

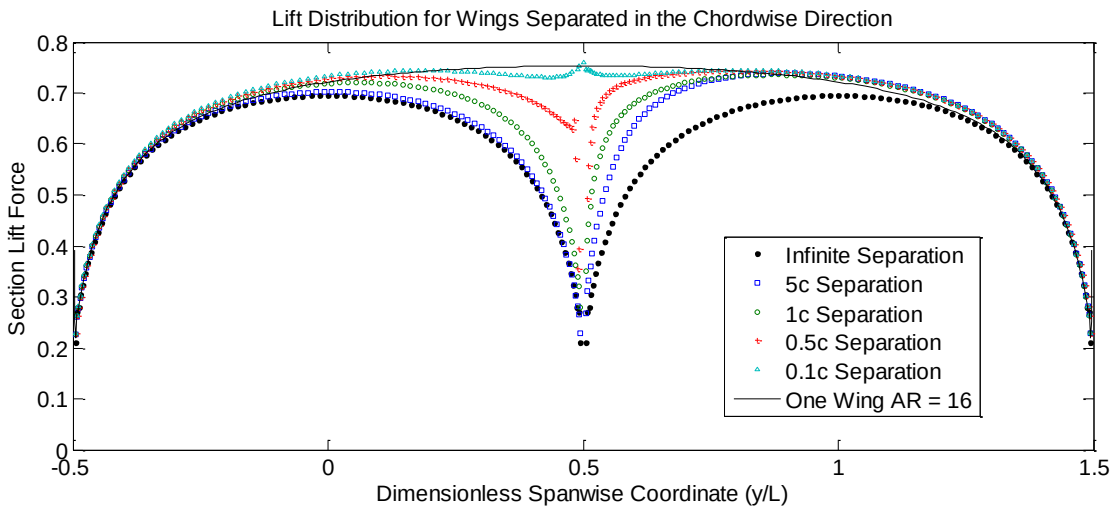

Figure. 3.4 Lift distribution for two UAV wings separated only in the chord-wise direction at different separations.

As the UAVs start getting closer to each other we see the aerodynamic coupling between the two wings gets stronger as the separation decreases. These effects can be seen from the plots in Figure 3.4 where we can see that the lift distribution around the tips of adjacent wings get by their respective proximity. Most of the aerodynamic coupling occurs around the wing tips due to vortex interactions. The lack of symmetry in the lift distributions with wings in close proximity indicates that there is a roll moment about the mid-span axis. From the results in Figure 3.4, it is clear that the total lift, which is proportional to the area under the section lift distribution curve, increases as the separation decreases for both wings. As the separation decreases to zero, where the two wings are linked, the lift distribution of the two UAV wings will approach the lift distribution of a single wing with double its aspect ratio.

Comparing the lift distributions of the left and right wings at given separation we can see that they are not symmetric. For example, for a 5 chord-lengths separation we see that the lift distribution for the left wing is about the same as of a single wing, but

for the right wing, which is flying behind the left wing, we see that there is a significant increase in the section lift distribution. The increase in aerodynamic disturbance for the UAV wing flying behind is due to the wing flying in the wing tip trailing vortex shedding from the front UAV wing. This phenomenon is similar to what is seen in formation flying where the trailing aircrafts benefits from the trailing vortex shedding of the lead aircraft [3, 4, 14]. However as the separation between the UAVs gets small, the front UAV wing is also subjected to the flow field that the back UAV induces upstream with its bound and trailing wing vortex [15]. The asymmetry in the section lift distributions between each wing disappears as the separation gets close to zero. As seen in Figure 3.4, the lift distribution for a separation of 0.1 chord lengths is symmetric and as the separation goes to zero it behave as one wing with double the aspect ratio.

The total lift coefficients for two UAV wings for the chord-wise, span-wise and vertical separation are plotted as a function of separation for an angle of attack of 6 degrees in Figure 3.5. The lift coefficient increases as the wing separation decreases. The increase in lift is especially strong after the separation is below 1 chord length, and the maximum lift occurs when then the two wings are joined, which is not surprising because joining the wings doubles the aspect ratio. As previously mentioned, we can see that lift coefficients for chord-wise separation are different for the front and back wings. The front wing starts behaving as a single wing for separation above 8 chord lengths. However, the back wing has higher lift coefficient for a larger range of separation. From Figure 3.5 we can see that the proximity effects for the back wing extend pass the 10 chord length. The effects for the back wing extend for larger range because the wing is affected by the vortex shedding from the front wing. For the span-wise and vertical separations the close proximity effects on

the lift coefficient dies out quicker than the chord-wise separation. From Figure 3.5, the close proximity effects for both the span-wise and vertical separations are negligible for separation above 4 chord lengths. Comparing the lift coefficient for a single UAV wing and two linked UAVs wings there is an increase of about 15%.

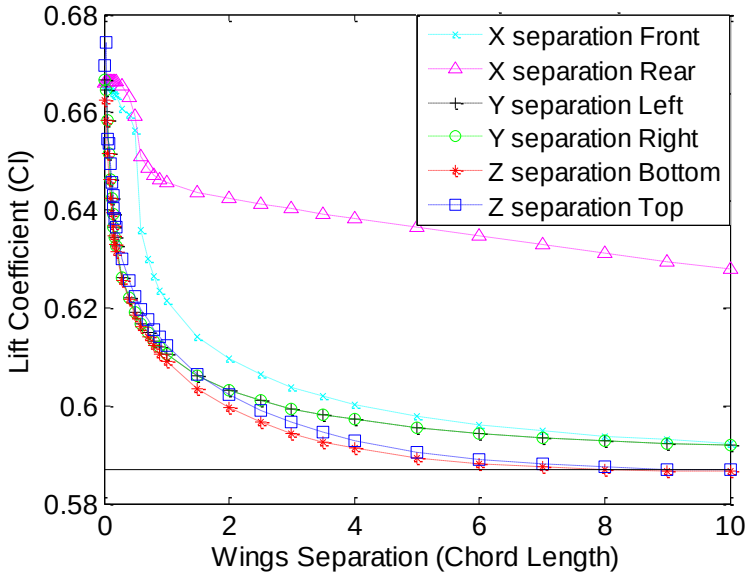

Figure. 3.5 Close proximity lift coefficient effects as a function of separation.

As seen in Figure 3.4 and 3.5, we saw that the close proximity aerodynamic effects induces an asymmetric lift distribution around the UAV wings. The asymmetry in the lift distributions will yield a roll moment about the semi axis span. The roll moment coefficients for two UAV wings for the chord-wise, span-wise and vertical separation are plotted as a function of separation for an angle of attack of 6 degrees in Figure 3.6. As the UAV wings are far away from any aerodynamic interactions the roll moment is zero, as it is for a single UAV wing without ailerons. Similar to the other aerodynamic coefficients, the roll moment coefficient magnitude increases as the wing separation decreases. As the UAV wings get closer, each will induce an opposite roll moment on each other as seen in Figure 3.6. The magnitude of roll moment coefficient for chord-

wise separation are also different for the front and back wings as seen in Figure 3.5. The range of the close proximity effects on roll moment are the same as for the lift coefficient, for the chord-wise separation it extends pass 10 chord-length and for the span-wise and vertical separation extends until about 4 chord lengths.

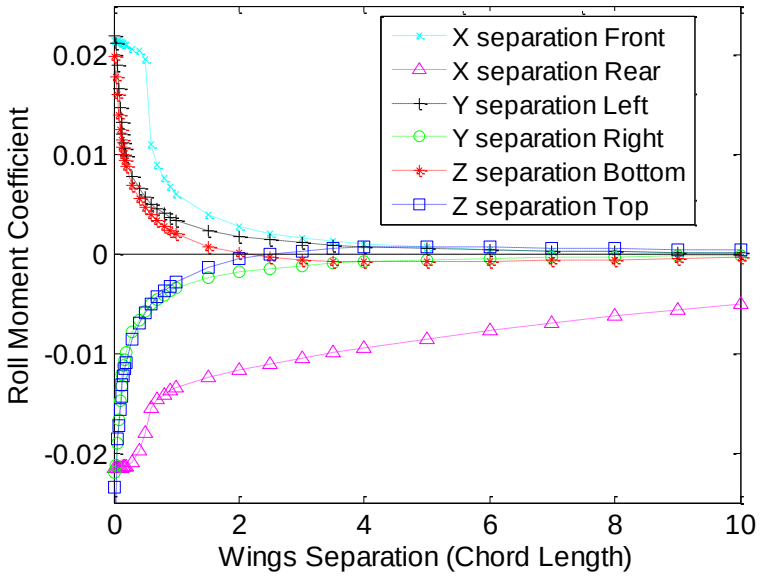

Figure. 3.6 Close proximity roll moment coefficient effects as a function of separation.

3.3.3 Model verification via wind tunnel testing

Wind tunnel tests for close proximity aerodynamic effects of two wings were performed to compare with the prediction from the lifting-line method. The wind tunnel setup consist of a full and half wing with a rectangular planform and an aspect ratio of 4.5 as seen in Figure 3.7. The wings have a chord of 3 inches and a span of 13.5 and 6.75 inches for the full and half wing, respectively. The full wing was used to measure the aerodynamic forces and moments using a 6 degree-of-freedom JR3 load cell, which measures lift to 25 lb with a resolution of less than 0.01 lb. Tests use the

Cornell University environmental wind tunnel facility, an open return wind tunnel with a 48” x 43” test section. A splitter plate was attached to the half wing to simulate a full wing. The full wing remained stationary and the half wing was able to move in all three directions chord-wise (x – direction), span-wise (y – direction), and vertical direction (z – direction).

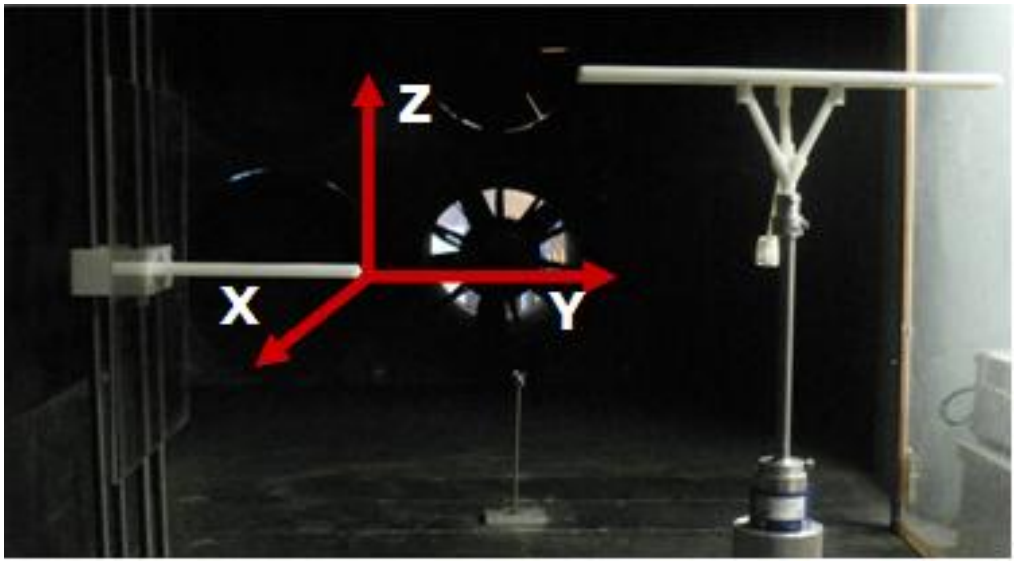

Figure. 3.7 Wind tunnel setup of the two UAV wings.

The lift coefficient for two UAV wings separated in the vertical direction for both predicted and measured values are plotted as a function of separation for an angle of attack of 9 degrees in Figure 3.8. Since only the full wing is attached to a load cell, we tested both positive and negative separation values. In Figure 3.8, positive separations corresponds for when the full wing is below the half wing and negative separations for when the full wing is above the half wing. Due to limited space in the wind tunnel testing area, tests will be performed for a range of separations between -2 and 2 chord lengths. We can see that the measured values for the lift coefficients have a good agreement with the predicted values from the lifting-line method. As expected, the lift

coefficient increases as the separation decreases, as mentioned in the previous sections. In addition, for vertical separation, the measured results verify that there is a small asymmetry in the lift coefficient between the wings that are above and below.

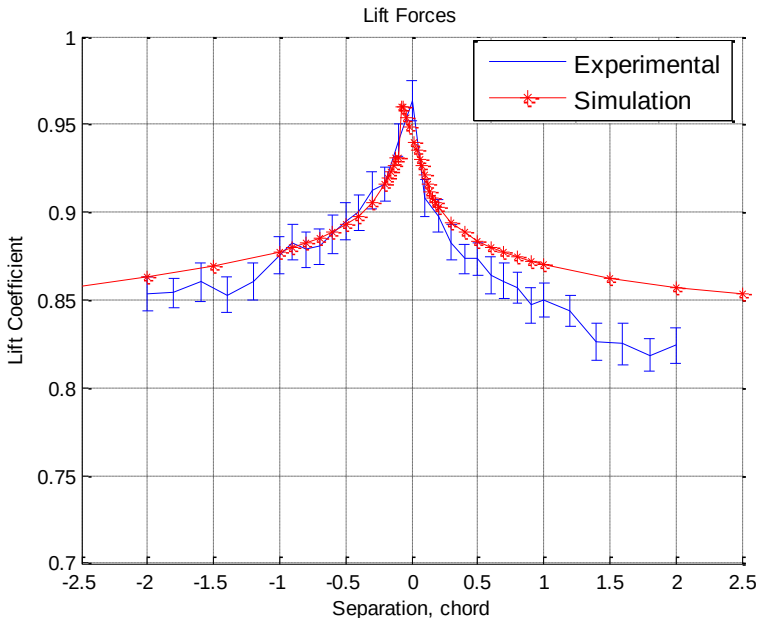

Figure. 3.8 Predicted and measured lift coefficient for two UAV wings separated in the vertical direction.

The roll moment coefficient for two UAV wings separated in the vertical direction for both predicted and measured are plotted as a function of separation for an angle of attack of 9 degrees for both wings in Figure 3.9. Figure 3.9 shows the results for both positive and negative separations, where positive separations corresponds for when the full wing is below the half wing and negative separations for when the full wing is above of the half wing. For the roll moment coefficient we can see that there is a good agreement between the measured and predicted values from the lifting-line method. Both the measured and predicted values for the roll moment have the same trends. The roll moment coefficient increases as the separation decreases.

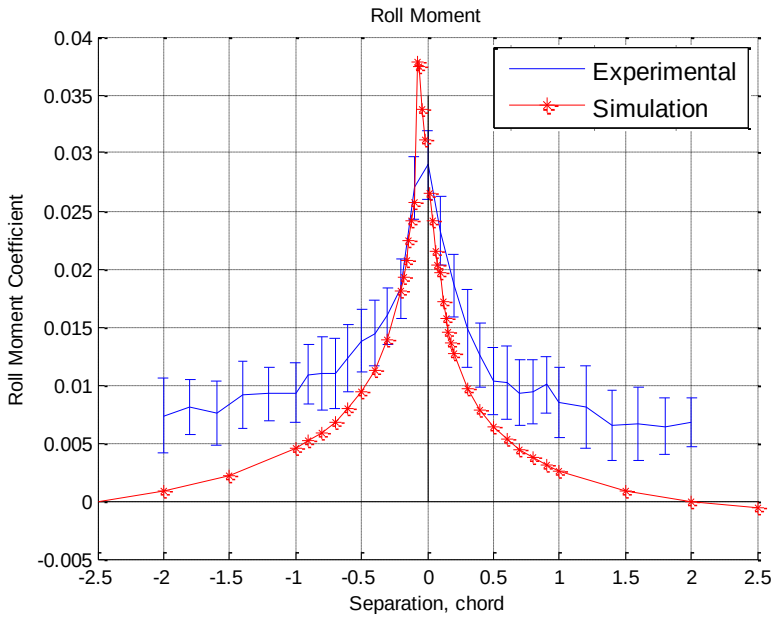

Figure. 3.9 Predicted and measured lift coefficient for two UAV wings separated in the vertical direction.

3.4 Linked UAVs Flight Simulations

This section will investigate the effects of the close proximity aerodynamic disturbances on the dynamics and stability of the two UAVs. Simulations for the two UAVs are performed in Simulink, as can be seen in Figure 3.10. The vehicle and simulation parameters for each UAV are presented in Table 3.1. The Simulink simulation includes the close proximity aerodynamic look-up library developed in the previous sections. The simulation platform consists of three main components: UAV controls, UAV Linked system and the close proximity aerodynamics. The UAV controls component gives the control inputs to each individual UAV. This section feeds the control commands to the UAV control surfaces, aileron, elevator, rudder and throttle. UAV Linked System contains the nonlinear aircraft vehicle equations of motion which are integrated to determine the states of each UAV. The close proximity

aerodynamics component will monitor the states of each UAV and applies the close proximity aerodynamics disturbances to each UAV at any given time and relative position.

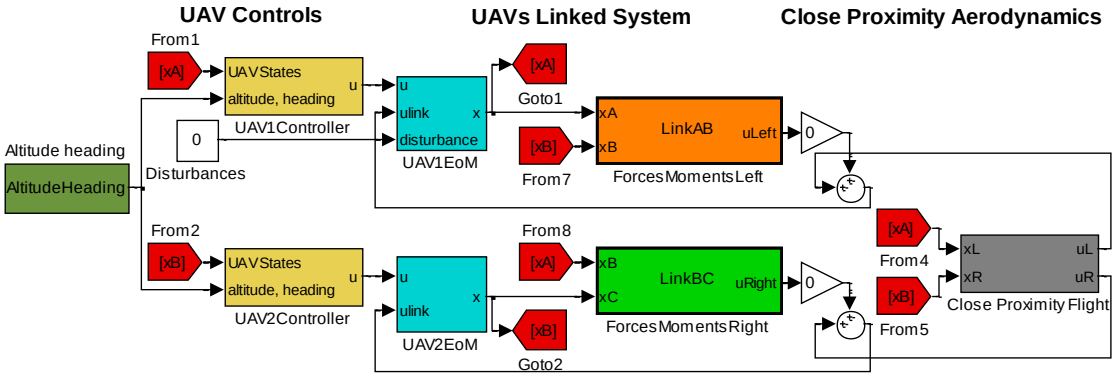

Figure. 3.10 Simulink simulation platform for two UAVs flying at close proximity

Table 3.1 UAV's vehicle and simulation parameters used in simulink vehicle model

Vehicle Parameters	**Values**
Mass	25.67 kg
Wing span	6.52 m
Aspect ratio	8
Roll moment of inertia	18.4 kg-m^2
Pitch moment of inertia	8.52 kg-m^2
Yaw moment of inertia	28.37 kg-m^2
Velocity	48.6 m/s

3.4.1 Open loop dynamics

Utilizing the Simulink platform we examined the effects of the close proximity aerodynamics disturbances on the open loop dynamics of each UAV. In this case, it simulates two UAVs undocking without any feedback control. In this scenario, the

UAVs will be linked and they undock at t=0. The plots of the inertial positions of the two UAVs are plotted in Figure 3.11. From Figure 3.11b and 3.11d, we can see that the two UAVs diverge from each other due to the close proximity aerodynamics effects. The proximity effects induces a opposite roll moment on each UAV, which leads to the UAVs to diverge from each other as seen in Figure 3.11b and 3.11d. There is also a change in altitude, as see in Figure 3.11c, which can be explained by the change in lift and pitch moment due to the proximity effects. The effects on the range are minor as it can be seen in Figure 3.11a.

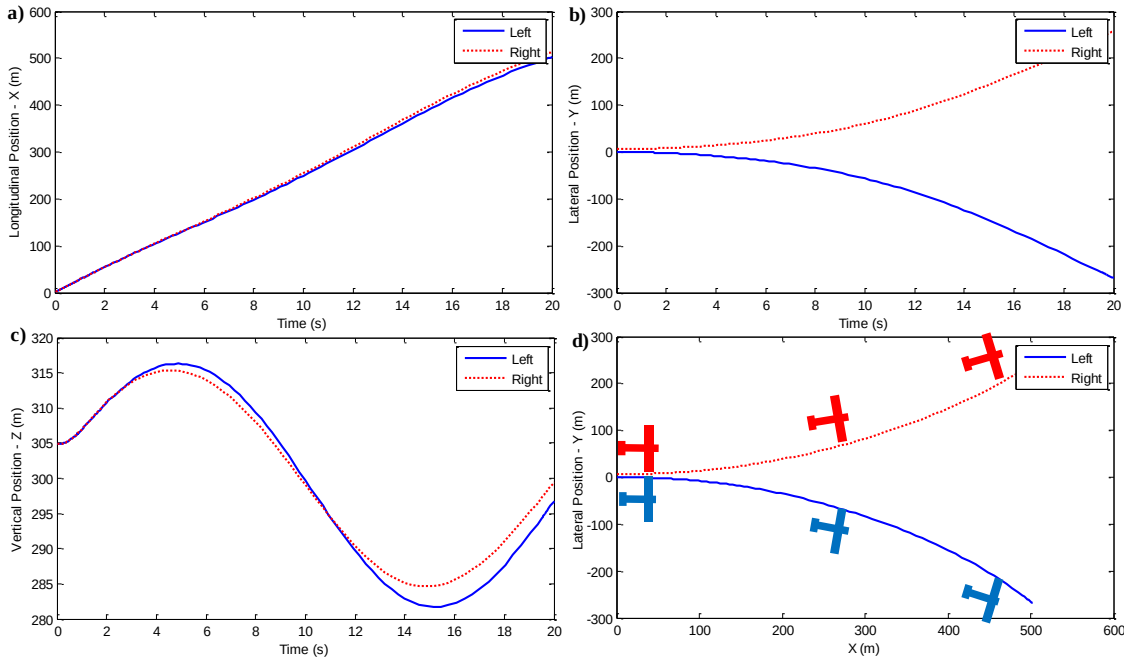

Figure. 3.11 UAVs inertial positions for two UAVs flying at close proximity.

The plots of the close proximity aerodynamic disturbances forces and moments of the two UAVs are plotted in Figure 3.12. Initially, the two UAVs are docked, with zero separation, the magnitude of proximity forces and moments are high and as they start to diverge the forces and moments decreases as it can be seen in Figure 3.12.

Figure 3.12a and 3.12b are the plots of the proximity disturbances on lift and drag. As expected, both the lift and drag disturbances for each UAV are symmetric since the separation is mainly in the span-wise direction. Figure 3.12c and 3.12d are the plots of the proximity disturbances on roll, pitch and yaw moments. From this plots we can see that the roll moments are in the opposite direction, which cause the UAVs to diverge from each other. The magnitude of the roll moments are higher than of the pitch or yaw moments, which is the reason that the divergence is mainly in the span-wise direction as show in Figure 3.12c and 3.12d.

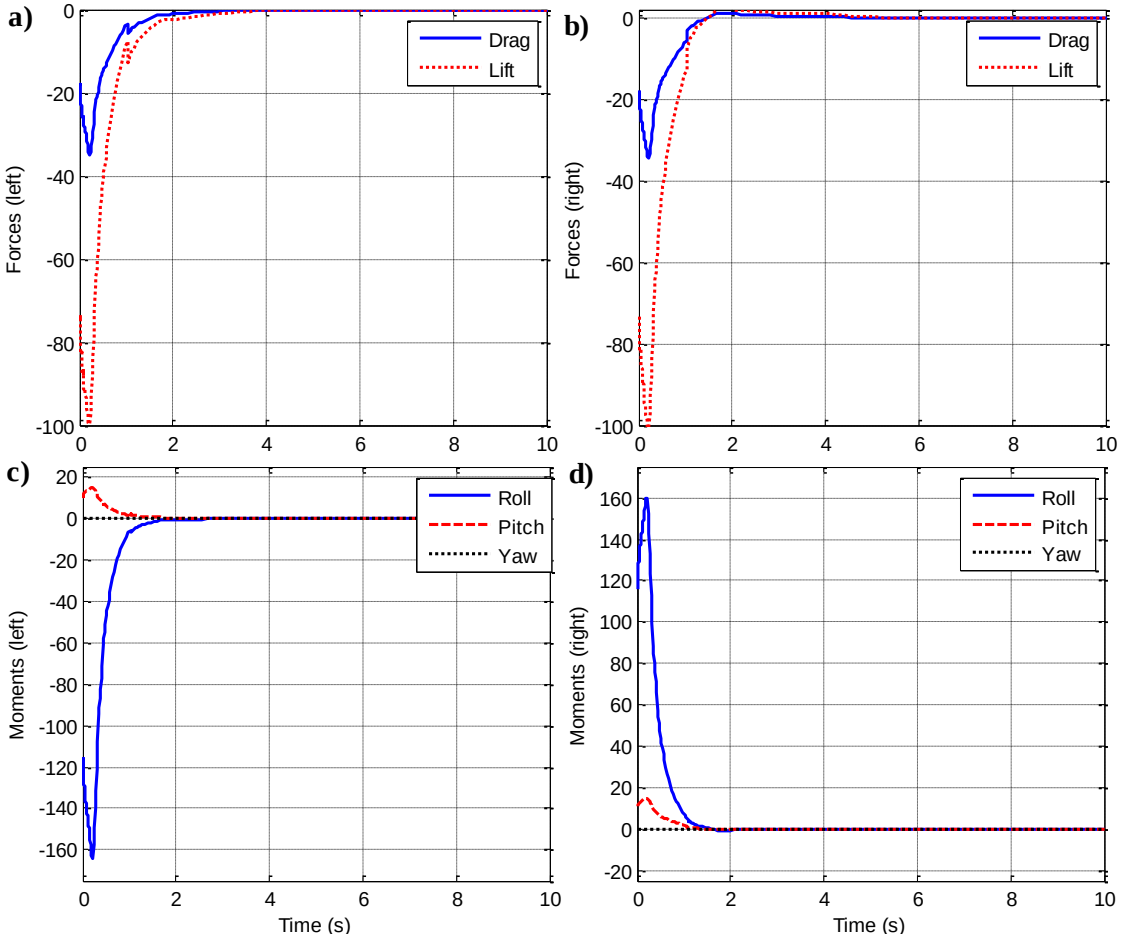

Figure. 3.12 Close proximity aerodynamic disturbances for the two UAVs flying at close proximity.

3.4.2 Docking trajectories

The main purpose of the aerodynamic intensity field study is to examine the effects from flow fields on different trajectories path for the two UAVs attempting to dock in midair. In this way we could size flight control surfaces and ultimately formulate automate control systems to aid in such a maneuver. In this section, we examined two trajectories paths, a chord-wise and a span-wise. The different trajectories will be simulated using the Simulink platform described above. Here, the left UAV will be the leader and the right UAV will be the follower. When docking, the leader will maintain straight and level flight. The follower will start at a distance far apart from the close proximity aerodynamic effects and it will track the leader and approach it for midair docking. The plot of two docking trajectory, a chord-wise and span-wise, paths are plotted in Figure 3.13.

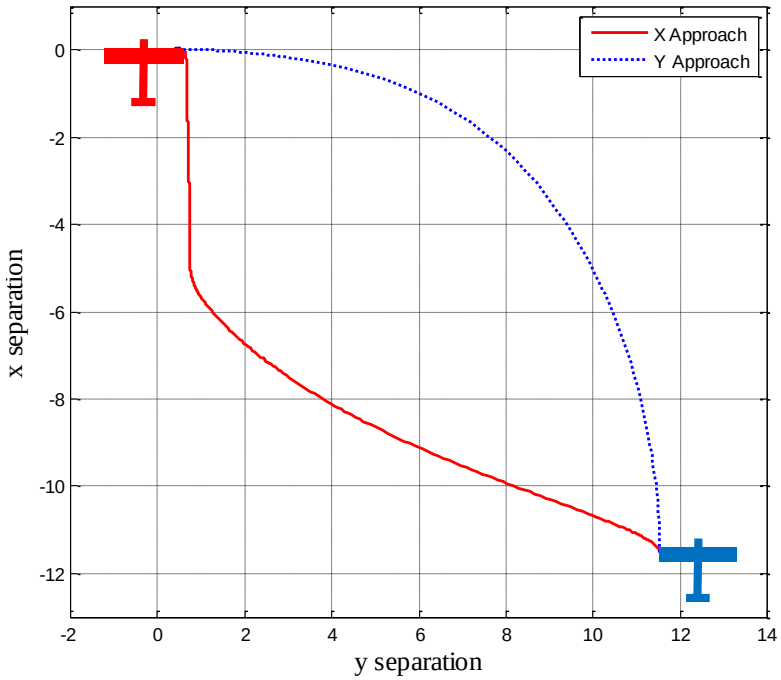

Figure. 3.13 A chord-wise and span-wise trajectory path for midair docking.

To evaluate the two trajectories we will take a look at the close proximity forces and moments acting along each trajectory. Figure 3.14 plots the forces and moments acting on the leader (left) and follower (right) UAVs for both trajectories. For the follower UAV, the forces and moment disturbances are higher for the chord-wise approach than for the span-wise approach as seen in Figure 3.14b and 3.14d. This is expected since the follower UAV for the chord-wise approach spends significant more time behind the leader. As discussed in the aerodynamic and the CFD sections this is an area of higher disturbances due to the close proximity effects in all the aerodynamic forces and moments for the follower UAV. In addition, both the close proximity forces and moments on the chord-wise trajectory act earlier than for the span-wise approach due that the proximity effects are still present more downstream in the chord-wise direction. For the leader UAV, the forces and moments act sooner for the span-wise approach, however it takes less time to complete the trajectory. So the overall amount of disturbance seen by the leader UAV for both trajectories is comparable to each other. As it was expected, for the span-wise approach the forces and moments acting on both UAVs are symmetric as discussed in the previous sections.

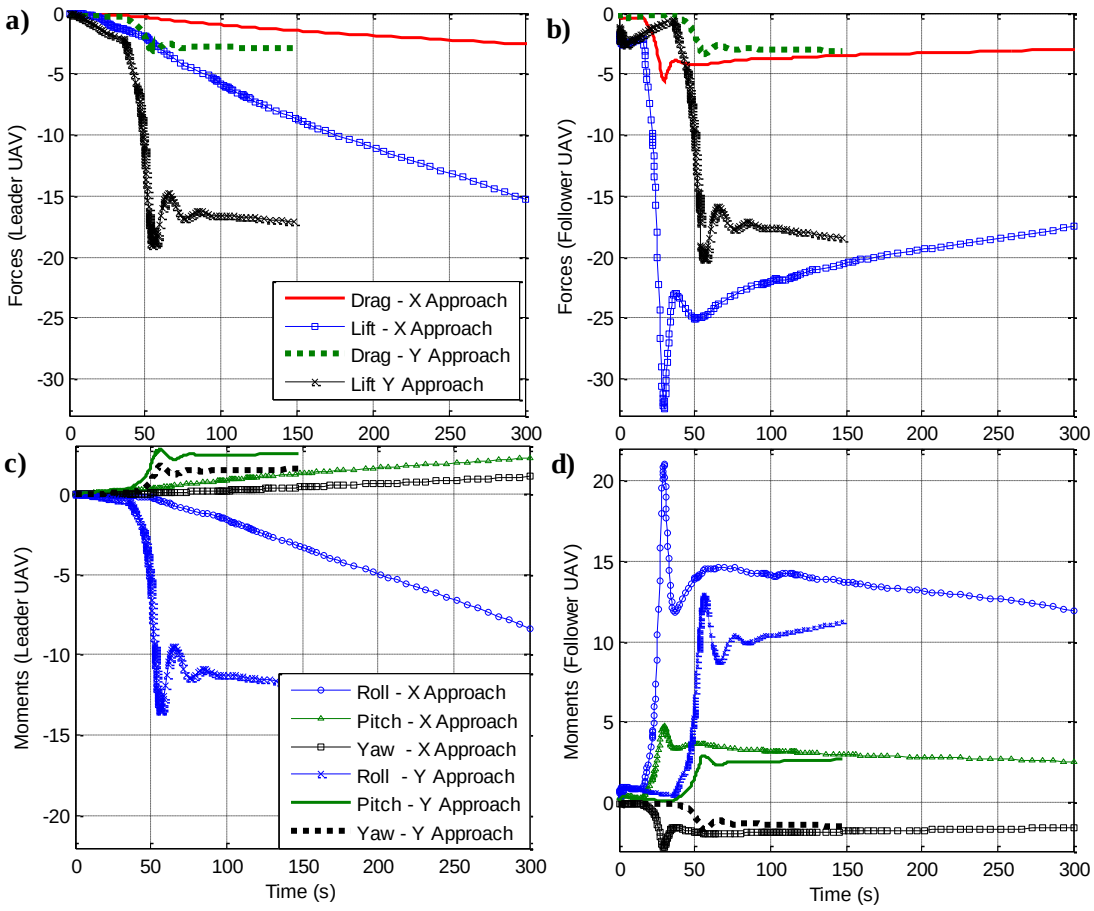

Figure. 3.14 Close proximity aerodynamic disturbance forces and moments acting on each UAV for two docking trajectories.

3.5 Conclusion

Close proximity aerodynamic analysis for two UAV wings at close proximity has been presented. A verification of the predicted aerodynamic data with wind tunnel for aerodynamic forces and moments has been presented. There is a good agreement between the predicted values calculated using the modified lifting-line method and the measured values from the wind tunnel tests. For all cases, as the separation between the two UAV wings decreases there is an increase in lift, drag, roll, pitch and yaw moment magnitudes. Close proximity induced effects on lift were significant and there

was an increase of around 15% from the nominal value of a wing by itself. Both the roll and pitch moments where also significantly affected. As the wings get closer to each other they will induce an opposite roll moment on each other. This means that as the wing approaches for docking it will tend to roll away from each other. This effect was seen in the open loop aircraft dynamics simulation presented. Also at close proximity the aerodynamic forces and moments demonstrate nonlinear behavior. This nonlinear behavior will have to be taken in to account when determining trajectories and control strategies for the UAV to link in midair to for a linked UAV platform. Two different docking trajectories, a span-wise and chord-wise paths where analyzed. The span-wise trajectory experiences less overall disturbances for both the leader and follower UAVs, which makes this trajectory more desirable for midair docking. For the span-wise approach the aerodynamics effects on both UAV wings are symmetric which help avoids the vortex mixing therefore making the path more stable.

REFERENCES

1. Pamadi, B. *Performance, Stability, Dynamics, and Control of Airplanes*, American Institute of Aeronautics and Astronautics, 1998, pp. 106–119
2. Schumacher, C., Singh, S., “Nonlinear Control of Multiple UAVS in Close-Couple Formation Flight”, AIAA Guidance, Navigation, and Control Conference 14-17 August 2000, Denver, CO
3. Blake, W., and Multhopp, D., “Design, Performance and Modeling Considerations For Close Formation Flight,” AIAA Guidance, Navigation, and Control Conference, AIAA, Reston, VA, July 1998.
4. Pachter, M., D’Azzo, J., Proud, A., “Tight Formation Flight Control”, *Journal of Guidance, Control, and Dynamics*, Vol. 24, No. 2, March–April 2001.
5. Rossow, V.J., Sacco, J.N., Askins, P.A., Bisbee, L.S., and Smith, S.M., "Measurements in 80 by 120 Foot Wind Tunnel of Hazard Posed by Lift-Generated Wakes," *Journal of Aircraft*, Vol. 32, No. 2, pp. 278-284, August 1993.
6. Pete, K.R., Smith, S.T., and Vicroy, D.D., "Model Validation of Wake-Vortex/Aircraft Encounters," AIAA paper 2000-3979, presented at the AIAA Atmospheric Flight Mechanics Conference, Denver CO, August 2000.
7. Cuji, E., Garcia, E.“Analytic Modeling of the Aerodynamics of Shape Changing Wings”, Proc. 18th International Conference on Adaptive Structures and Technologies 127, 2007.

8. Cuji, E. A. and Garcia, E. (2008) "Prediction of Aircraft Dynamics with Shape Changing Wings", Smart Structures and Materials 2008: Active and Passive Smart Structures and Integrated Systems II, March 10-13, San Diego, CA. published in: *Proc. SPIE* Vol. 6928, 2008.

9. Wickenheiser, A. M., and Garcia, E., (2007) "Aerodynamic Modeling of Morphing Wings Using an Extended Lifting-Line Analysis," *Journal of Aircraft*, 44 no.1, pp. 10-16, 2007.

10. Phillips, W. F., Snyder, D. O. (2000) "Modern Adaptation of Prandtl's Classic Lifting-Line Theory", *Journal of Aircraft ,* Vol. 37, No. 4, 2000, pp. 662-670.

11. Prandtl, L., (1918) "Aerofoil Theory, I and II Communications", *Nachr. Kgl. Gesellschaft der Wissenachaft, Math-phys. Classes,* Göttingen, 1918-19.

12. Cuji, E., Garcia, E. "Simulation and Wind Tunnel Testing of Close Proximity Aerodynamics of Two Linked UAVs", Proc. 20th International Conference on Adaptive Structures and Technologies, Hong Kong, 2009.

13. Cuji, E., Lukaczyk, T., and Garcia, E., "Aircraft Dynamics, Wind Tunnel Testing and CFD Flow Visualization of Two Linked UAVs Flying at Close Proximity", Proceedings of the Smart Structures and Materials 2008: Active and Passive Smart Structures and Integrated Systems, Vol. 7645, SPIE, San Diego, CA, March, 2010.

14. Wang, Z., Mook, D., "Numerical Aerodynamic Analysis of Formation Flight", 41st Aerospace Sciences Meeting and Exhibit 6-9 January 2003, Reno, Nevada.

15. Bramesfeld, G., Maughmer, M., “Effects of Wake Rollup on Formation-Flight Aerodynamics”, *Journal of Aircraft,* Vol. 45, No. 4, July–August 2008.

CHAPTER 4

TRAJECTORY OPTIMIZATION FOR DOCKING PATH OF TWO LINKED UAVS[*]

4.1 Abstract

This paper discusses the formulation and optimization of midair wingtip docking trajectories for two unmanned aerial vehicles (UAVs) linking in flight. The linked UAV concept, creates an aerodynamically efficient system of aircraft with long endurance capabilities and extending the ability for aircraft to cruise with significantly reduced propulsion power. Close proximity aerodynamics coupling is nonlinear and is shown to have an impact on the dynamics of the linked UAVs. The aerodynamics effects are modeled using an adaptation of a lifting-line method. Two optimal trajectories for a 2-D and 3-D docking trajectories are compared. Dynamic wind tunnel tests are performed to compare different midair wingtip docking trajectories. The results of the optimization show that a trajectory where the aircraft approach each other from a span-wise direction is more desirable since it goes through the lower aerodynamic disturbances and requires less control effort to perform the docking maneuver.

[*] To be submitted for publication to *Journal of Guidance, Control, and Dynamics* by Cuji, E. and Garcia E. "Trajectory Optimization for Docking Path of Two Linked UAVs"

4.2 Introduction

Currently, unmanned aerial vehicles (UAVs) are used mainly for Intelligence, Surveillance and Reconnaissance (ISR) missions. One advantage of using UAVs for ISR missions is that they can be rapidly deployed from any airfield due to their small wingspan. However, having a small aspect ratio wing also limits its range and endurance [1]. An effective ISR platform requires that it be rapidly deployable, and have long range and endurance. It is known that an aircraft with large aspect ratio wings has better aerodynamic efficiency due to the reduction of induce drag for the given lift [1, 2]. Wingtip docking UAVs will increase the effective aspect ratio of a system of aircraft. The larger aspect ratio of the linked UAVs leads to an improvement in overall aerodynamic efficiency due to the decrease of the induce drag as previously mentioned. The improvements in aerodynamic efficiency are similar to the improvements seen in formation flight [3, 4], but without having the trailing aircraft fly in the vortex wake of the leading aircraft which can lead to both stability and control problems [5, 6]. The linked UAV concept allows for a rapidly deployable ISR platform using individual UAVs with wingspans small enough to be deployed from small aviation airfields or even being hand launched. Individual UAVs will link at high altitude to create an aerodynamically efficient system of aircraft which has long endurance capabilities and can cruise for extended periods with significantly reduced power.

A linked UAV system requires wingtip docking of UAVs in midair. Previous works in aerodynamic analysis of the close proximity aerodynamics coupling have found that all forces and moments are impacted by the presence of the other UAV wing [7]. Previous aerodynamic analysis has showed that there are regions of higher

and lower aerodynamic disturbances. The close proximity aerodynamic disturbances affect the dynamics and stability of the UAVs [7, 8]. For example, as the two UAVs approach each other, the roll moment due to the close proximity effects are in opposite directions. In order for the UAV wings to dock in midair, the UAV controls have to have enough authority to overcome these disturbances. To minimize problems during a wingtip docking maneuver, a docking trajectory path that has the least aerodynamic resistance is most desirable. Such a path would require the least control effort, thus decreasing the energy needed to perform the docking maneuver, additional control authority is always needed for unknown disturbance rejection and robustness engineering. In addition, it reduces stability problems during the maneuver. The trajectory optimization problem is formulated as a constrained nonlinear optimization problem. The optimization problem is solved by utilizing nonlinear programming to solve the complex nonlinear optimization problem [9, 10].

In this paper, the trajectory optimization problem for midair docking path of two linked UAVs is formulated to determine an optimal docking trajectory that minimizes the aerodynamic disturbances and requires the least energy. The dynamics of the linked UAV system, as well as the incorporation of the close proximity aerodynamics coupling information into the aircraft dynamics is presented. This paper presents results of the optimization procedures for both 2-D and 3-D docking trajectories. Dynamic wind tunnel testing of an optimal and non-optimal docking trajectory is also presented.

4.3 Modeling Description and Problem Formulation

4.3.1 Linked UAV aerodynamic model

The aerodynamic model to analyze the linked UAV system is an adaptation of Prandtl's lifting-line method that we have applied to 3D aerodynamic structures [11, 12]. This method is an approach to 3D aerodynamic modeling which incorporates a modern adaptation of Prandtl's lifting-line method, based on a fully three-dimensional vortex lifting law. There are several variations of lifting-line method, for example the adaptation of the Weissinger's method present by Wickenheiser and Garcia, can be used for wings with arbitrary planforms, but cannot calculate fully 3D geometries [13]. The method that we have developed is based on the adaptation of the Prandtl's lifting-line method developed by Phillips and Snyder [14]. This method is derived from the classical lifting-line method [15], but it's generalized to correct for the violations of the classical lifting-line theory for a system of lifting surfaces with arbitrary camber, sweep and dihedral. Furthermore, with this method we can compute the aerodynamic forces for a system of lifting surfaces with arbitrary position and orientation which conventional lifting-line methods do not.

As the UAVs fly in close proximity to each other, there is strong aerodynamic interaction between them. As the UAVs approach each other, to link in midair, it experiences different aerodynamic forces and moments depending on relative position and flight condition. To determine docking trajectories, and analyze the aircraft dynamics, an understanding of the close proximity aerodynamic forces and moments that act upon the UAV wings are needed. An aerodynamic analysis for both varying relative positions between the UAVs and flight condition is needed. The lifting-line technique was use because it is a fast computational approach with a low order model

compared to CFD for aerodynamic analysis. The speed of this method allows one to determine the aerodynamic forces and moments acting on each UAV wing as a function of its relative separation in all directions and its corresponding angle of attacks.

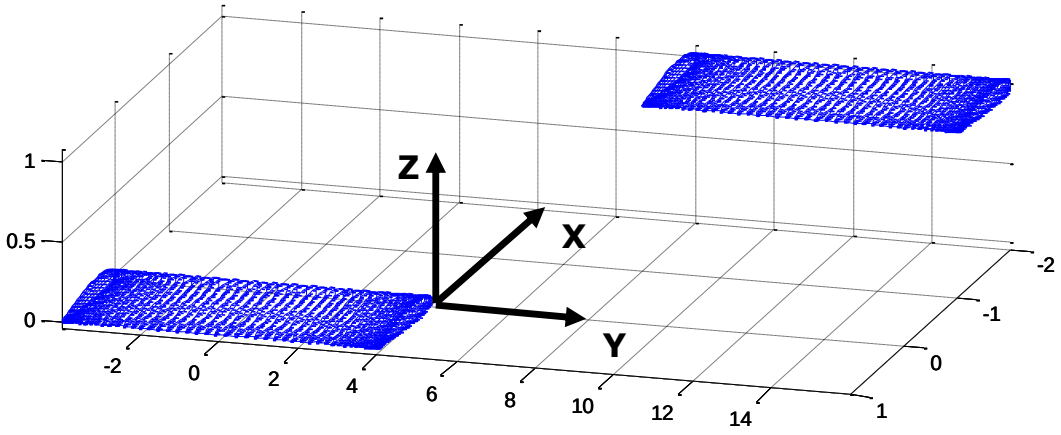

Figure. 4.1 Coordinate frame for the relative separation between the two UAV wings.

An aerodynamic intensity field between two UAVs wings has been generated as a function of its relative position in all three directions: chord-wise (x – direction), span-wise (y – direction), and vertical direction (z – direction) as seen in Figure 4.1. The lifting line method computes all the aerodynamic forces and moments, lift, drag, roll, pitch and yaw, for the two wings for different separations in all three directions and different angles of attack for each wing. In Table 4.1, contains the wing and simulation parameters used to develop the aerodynamic intensity field. The nominal angle of attack that the UAVs will fly is around 6 to 8 degrees, therefore a computing range from 2 to 12 degrees angle of attack for each wing has been chosen. For the Y and Z separation, the range computed is from 0 to 10 chord lengths. In these two directions the aerodynamic coupling between the two wings dies out by 10 chord lengths. For the x separation the computed range is from 0 to 40 chord lengths. A larger range has been

chosen for the x separation because the close proximity effects for a chord-wise separation extended pass 10 chord lengths due to the effects that trailing wake from the leading wing has on the trailing wing downfield. Table 4.1 also presents the data points computed for each of the simulation parameters. A total of 97,344 simulations were run to compile the aerodynamic intensity field.

Table 4.1 Wing and simulation parameters for the aerodynamic intensity field computed

Wing and simulation parameters		**Data points Computed**
Airfoil	LA2573A	
Planform	Rectangular	
Aspect ratio	4.5	
Angle of attack W1	2° to 12°	2, 4, 6, 8, 10, 12
Angle of attack W2	2° to 12°	2, 4, 6, 8, 10, 12
X separation	0 to 40c	0, 0.05, 0.1, 0.2, 0.4, 0.6, 1, 1.5, 2, 3, 4, 5, 10, 20, 30, 40
Y separation	0 to 10c	0, 0.05, 0.1,0 .2, 0.4, 0.6, 1, 1.5, 2, 3, 4, 5, 10
Z separation	0 to 10c	0, 0.05, 0.1, 0.2, 0.4, 0.6, 1, 1.5, 2, 3, 4, 5, 10

4.3.2 Close proximity aerodynamic analysis

The lift characteristics of the UAV wings will vary as a function of its relative separation and orientation. In addition, the lift characteristic acting on each UAV wing will be different depending on the wing position. For example, we expect a leading wing to have a different lift distribution than the wing in its wake. In this section, we are going to examine how the lift distribution, total lift, drag and roll, as well as pitch and roll moments coefficients changes for two UAV wings separated in the chord-wise, span-wise and vertical directions, as shown schematically in Figure 4.2. The

UAV wings studied have a rectangular planform with an aspect ratio of 4.5. A sample data of aerodynamic database analysis is presented here. A complete analysis has been previously presented [7, 8] and can be found in reference 7. Also, model verification for the adaptation of the lift-line method via wind tunnel experiments and CFD simulations has been presented in previous work and can be found in reference 8.

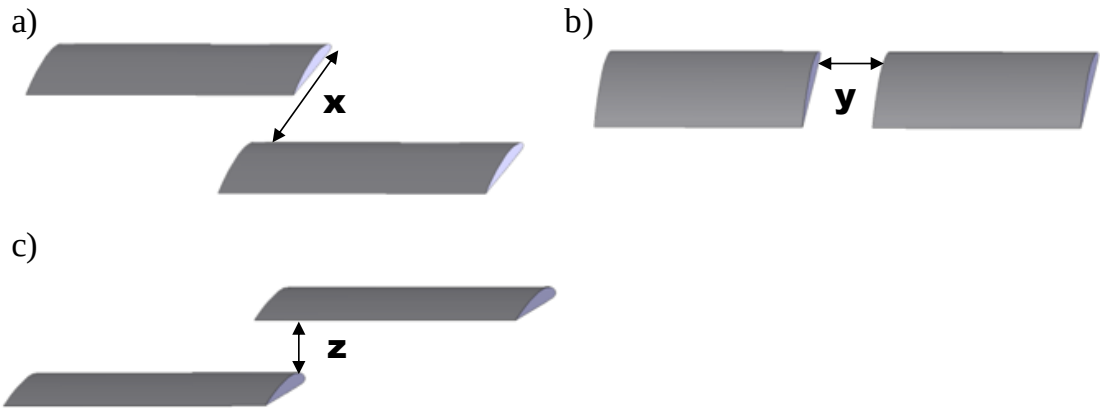

Figure. 4.2 a) UAV wings separated only in the chord-wise direction. b) UAV wings separated only in the span-wise direction. c) UAV wings separated only in the vertical direction.

The total lift coefficients for two UAV wings for the chord-wise, span-wise and vertical separation are plotted as a function of separation for an angle of attack of 6 degrees in Figure 4.3. The lift coefficient increases as the wing separation decreases. The increase in lift is especially strong after the separation is below 1 chord length, and the maximum lift occurs when then the two wings are joined, which is not surprising because joining the wings doubles the aspect ratio. The lift coefficients for chord-wise separation are different for the front and back wings. The front wing starts behaving as a single wing for separation above 8 chord lengths. However the back wing has higher lift coefficient for a larger range of separation. From Figure 4.3, we can see that the proximity effects for the back wing extend pass the 10 chord length.

The effects for the back wing extend for larger range because the wing is affected by the vortex shedding from the front wing. This phenomenon is similar to what is seen in formation flying where the trailing aircrafts benefits from the trailing vortex shedding of the lead aircraft [3, 4, 16]. However as the separation between the UAVs gets small, the front UAV wing is also subjected to the flow field that the back UAV induces upstream with its bound and trailing wing vortex [17].

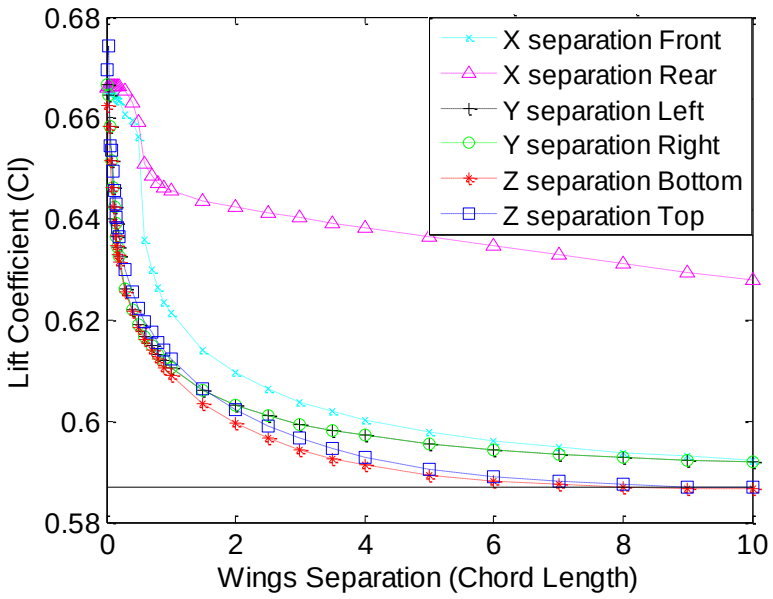

Figure. 4.3 Close proximity lift coefficient effects as a function of separation.

For the span-wise and vertical separations the close proximity effects on the lift coefficient dies out quicker than the chord-wise separation. From Figure 4.3, the close proximity effects for both the span-wise and vertical separations are negligible for separation above 4 chord lengths. Comparing the lift coefficient for a single UAV wing and two linked UAVs wings there is an increase of about 15%.

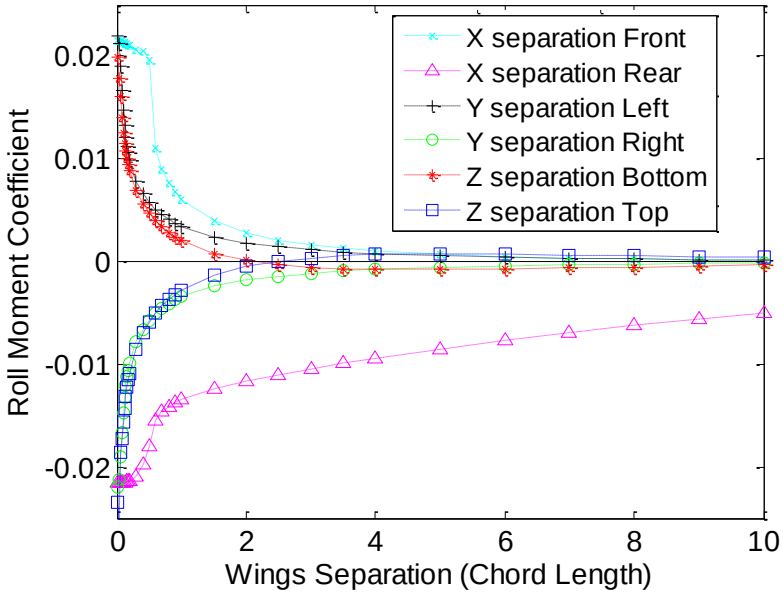

Figure. 4.4 Close proximity roll moment coefficient effects as a function of separation.

The close proximity aerodynamic effects induce an asymmetric lift distribution around the UAV wings [7, 8]. The lift distribution around the tips of adjacent wings gets disturbed by their respective proximity. Most of the aerodynamic coupling occurs around the wing tips due to vortex interactions. The lack of symmetry in the lift distributions with wings in close proximity indicates that there is a roll moment about the mid-span axis. The roll moment coefficients for two UAV wings for the chord-wise, span-wise and vertical separation are plotted as a function of separation for an angle of attack of 6 degrees in Figure 4.4. As the UAV wings are far away from any aerodynamic interactions the roll moment is zero, as it is for a single UAV wing without ailerons. Similar to the other aerodynamic coefficients, the roll moment coefficient magnitude increases as the wing separation decreases. As the UAV wings get closer, each will induce an opposite roll moment on each other as seen in Figure 4.4. The magnitude of roll moment coefficient for chord-wise separation are also different for the front and back wings as seen in Figure 4.3. The range of the close

proximity effects on roll moment are the same as for the lift coefficient, for the chord-wise separation it extends pass 10 chord-length and for the span-wise and vertical separation extends until about 4 chord lengths.

4.3.3 Linked UAVs vehicle model

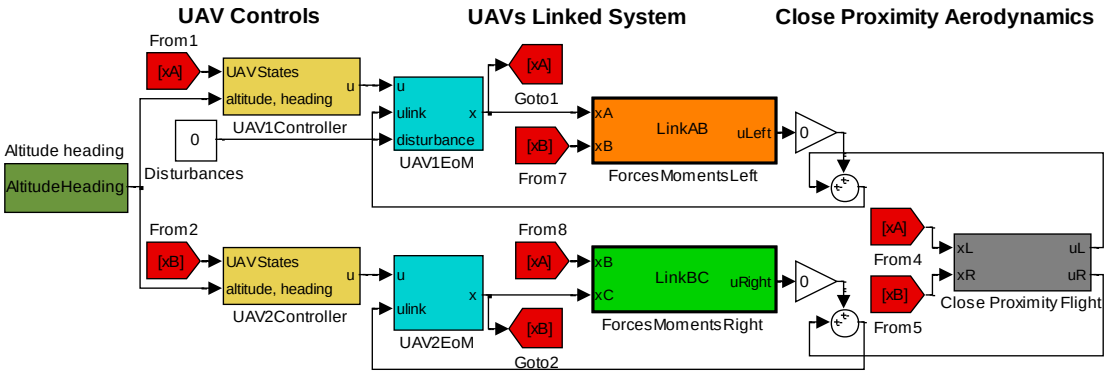

Figure. 4.5 Simulink simulation platform for two UAVs flying at close proximity

The UAVs are modeled as a standard nonlinear 6-degree-of-freedom aircraft. Each UAV are simulated utilizing the aircraft rigid body equations of motion. Simulations for the two UAVs are performed in Simulink, as can be seen in Figure 4.5. The vehicle and simulation parameters for each UAV are presented in Table 4.2. The Simulink simulation includes the close proximity aerodynamic intensity field look-up library developed in the previous work [7, 8]. The simulation platform consists of three main components: UAV controls, UAV Linked system and the close proximity aerodynamics section. The UAV are controlled individuals. The controller commands the UAV's control surfaces, aileron, elevator, rudder and throttle. The UAV linked system contains the nonlinear aircraft vehicle equations of motion which are integrated to determine the states of each UAV. The close proximity aerodynamics component monitors the states of each UAV and applies the close proximity aerodynamics

disturbances to each UAV at any given time base on their relative position and orientation.

Table 4.2 UAV's vehicle and simulation parameters used in Simulink vehicle model

Vehicle Parameters	**Values**
Mass	25.67 kg
Wing span	6.52 m
Aspect ratio	8
Roll moment of inertia	18.40 kg-m^2
Pitch moment of inertia	8.52 kg-m^2
Yaw moment of inertia	28.37 kg-m^2
Velocity	48.60 m/s

4.3.4 Optimization problem formulation

Trajectory design optimization is formulated as a constrained nonlinear 2 point boundary value problem. A schematic of the docking optimization problem can be seen in Figure 4.6. The initial positions of the two UAVs are set to be far away from the close proximity aerodynamic interactions between each other. The leader UAV is set to be traveling at a constant speed, heading and altitude. The follower UAV is set to perform the tracking and the close proximity maneuvering to approach the leading UAV in order that their wingtips make contact. This is done to simplify the optimization problem by restricting to one UAV to perform the close proximity maneuvering and therefore decreasing the convergence time of the optimal solution.

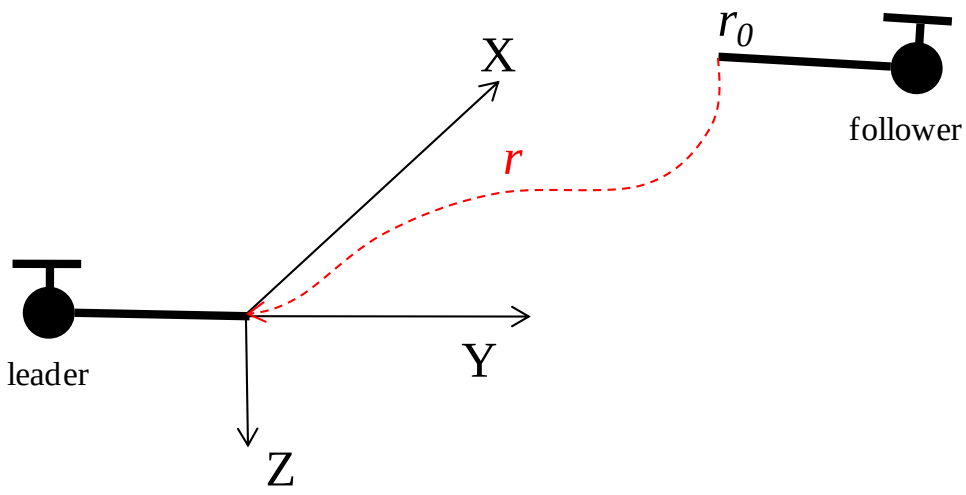

Figure. 4.6 Schematic of the wingtip midair docking trajectory optimization

The purpose of the optimization is to find a docking trajectory *r*(t) that minimizes a scalar cost function of several variables. For this study, a cost function is chosen to minimize the energy used by the combined linked UAV system. The cost function used for this study is given by the following equation:

$$J = \int_{r_0}^{0} [F_l^T(r)\Lambda_F F_l(r) + M_l^T(r)\Lambda_M M_l(r) + F_f^T(r)\Lambda_F F_f(r) + M_f^T(r)\Lambda_M M_f(r)]dr \geq 0 \quad (4.1)$$

where J is the total scalar cost function, Λ_F and Λ_M are weighting matrices, $F_{l(r)}$, $M_{l(r)}$, $F_{f(r)}$ and $M_{f(r)}$ are close proximity close proximity forces and moments for the leader and follower UAVs, respectively. The cost function takes into account all the close proximity forces and moments throughout the docking trajectory for the leader and follower UAVs. When flying close, the proximity effects on all the aerodynamic forces and moments are considered to be disturbances to the UAVs. The UAVs need to overcome those disturbances have to apply control power by deflecting their control surfaces, thus utilizing energy. Therefore, by minimizing the close proximity forces

and moments throughout a trajectory it will be essentially minimizing the total energy consumed by the overall linked UAV system. In addition, all the aircraft controls (aileron, elevator, rudder and throttle) are limited in deflection and actuation range. These ranges are included in the optimization as constraints. Thus introducing penalties in the cost function for saturating control surfaces and heavy maneuvers.

The docking trajectories are governed by the nonlinear 6 degree-of-freedom Simulink model described in the previous section. The nonlinear constraint optimization is implemented utilizing the MatLab optimization toolbox. The *fmincon* solver is utilized with the active-set optimization algorithm. This algorithm uses a sequential quadratic programming method, where it solves a quadratic programming subproblem at each iteration [18, 19]. At every iteration in the optimization, the docking trajectories are computed by simulating the nonlinear Simulink model. Therefore, the docking trajectories are generated by the UAV nonlinear vehicle dynamics model taking into account the effects of the close proximity aerodynamic interaction have on each UAV at any given time.

4.4 Optimization Results

4.4.1 2-D Docking trajectories

The main purpose of this study is to find an optimal trajectory for the two UAVs to dock with each other in midair. First, a 2-D optimization is performed. In this case the two UAVs are at the same altitude at the beginning of the docking trajectory maneuver. As the UAVs approach each other, the close proximity effects on the aerodynamic forces and moments lead to a change altitude. In order to maintain a 2-D trajectory, both UAVs are commanded to maintain a constant altitude. Therefore, each

UAV implements the necessary controls to counteract the close proximity disturbances experienced by the other. By commanding a constant altitude, we have restricted the trajectories to 2-D horizontal docking paths. The trajectories will be only in the x-y plane. The initial separation for both the x and y separations are of 40 cord length. The follower UAV is far enough downfield and to the side that no aerodynamic coupling exist between the two UAVs. By starting the UAVs outside the aerodynamic interaction range, we ensure that the initial separation does not introduce a bias to a given trajectory in the optimization. For this case, the optimization yields the trajectory with the minimum aerodynamic disturbance and therefore minimizing the energy need to perform the docking maneuver.

Figure 4.7 is the plot of the optimal 2-D docking trajectory that resulted from the optimization. A non-optimal trajectory is also presented that yielded a high values for the cost function while performing the optimization. The optimization yielded a trajectory where the aircrafts approached each other in the span-wise direction. The optimal docking trajectory took 150 seconds to complete the maneuver. The optimal trajectory path first approaches in the chord-wise direction while maintaining a relative large separation in the span-wise direction. For example at 30 seconds into the maneuver, the x separation was reduced by 80%, while the y separation has only been reduced by 30%. The final approach in the optimal docking maneuver is mainly in the span-wise direction. Thus results in the optimal trajectory being essentially from the span-wise approach.

Since the optimization only penalized the path, the optimal solution trajectory spends most of the time during the final approach of the UAVs, as seen in Figure 4.7. For example, at 60 seconds, which is 40% of the total time, almost all the separation in the x direction and 65% of the y separation are gone. While it takes an additional 90

seconds to finish the reminder of the maneuver, which is only 35% of the total y separation. The reason for the maneuver to spend most of the time when the two UAVs are close to each other is because the close proximity aerodynamic disturbances increases as the relative separation between the UAVs decreases [7,8]. As the aerodynamic disturbances increases, the UAVs require more control effort to overcome the higher disturbances thus slowing down the maneuver.

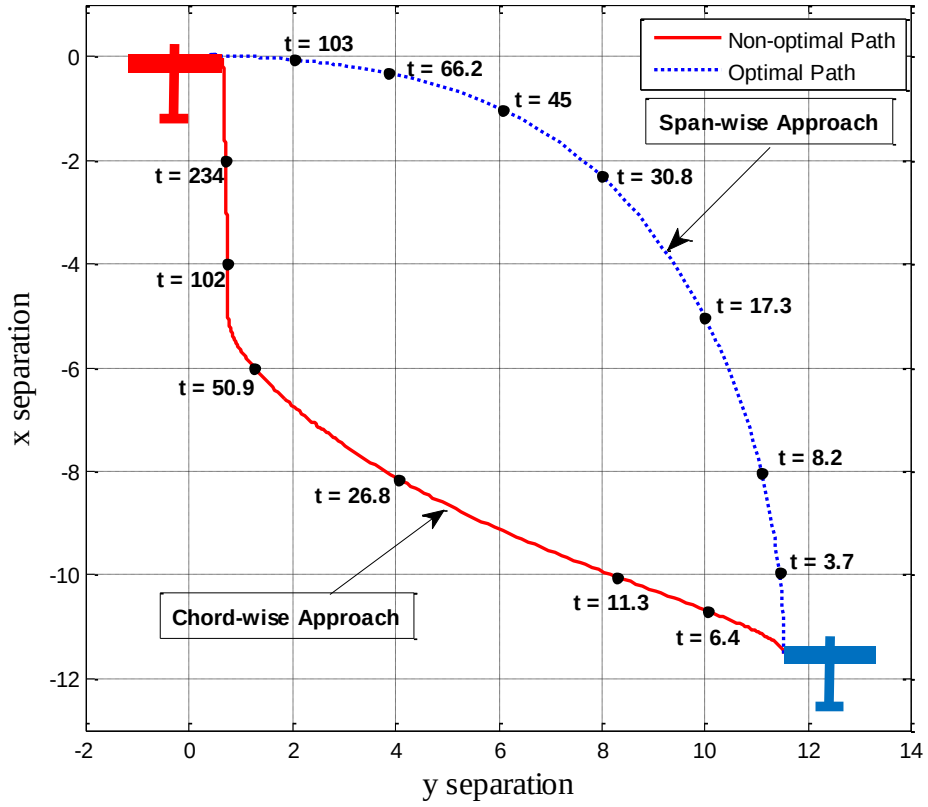

Figure. 4.7 An optimal and non-optimal trajectory path for midair docking.

A non-optimal trajectory that yielded a high cost function value is a chord-wise approach. This approach first approaches in the y direction and then in the x direction as it can be seen in Figure 4.7. From the close proximity aerodynamic analysis we can explain why this approached resulted in a high cost function value. As discussed in

the aerodynamic section, the close proximity disturbances on the trailing aircraft in the x direction extends farther downstream as compared to the y direction. Therefore, it will result in higher cost function value. Also, this trajectory took 300 seconds to complete the docking maneuver, double the time that the optimal trajectory took. Even though the optimization did not explicitly optimize for time, the optimization yielded a trajectory with a fast time to complete the maneuver. This can be explain because the cost function is a measurement of the energy needed to complete the docking maneuver. If a certain maneuver takes longer, it consumes more energy resulting in a higher cost function value.

To evaluate the two trajectories we will take a look at the close proximity forces and moments acting along each trajectory. Figure 4.8 plots the forces and moments acting on the leader (left) and follower (right) UAVs for both trajectories. For the follower UAV, the forces and moment disturbances are higher for the non-optimal approach than for the optimal approach as seen in Figure 4.8b and 4.8d. This is expected since the follower UAV for the chord-wise (non-optimal) approach spends significant more time behind the leader. As discussed in the aerodynamic section, this is an area of higher disturbances due to the close proximity effects in all the aerodynamic forces and moments for the follower UAV. In addition, both the close proximity forces and moments on the non-optimal trajectory act earlier than for the optimal approach due that the proximity effects are still present more downstream in the chord-wise direction. For the leader UAV, the forces and moments act sooner for the optimal approach, however it takes less time to complete the trajectory. So the overall amount of disturbance seen by the leader UAV for both trajectories is comparable to each other. As expected, the optimal approach the forces and moments

acting on both UAVs are symmetric because it is mainly a span-wise approach as discussed in the previous sections.

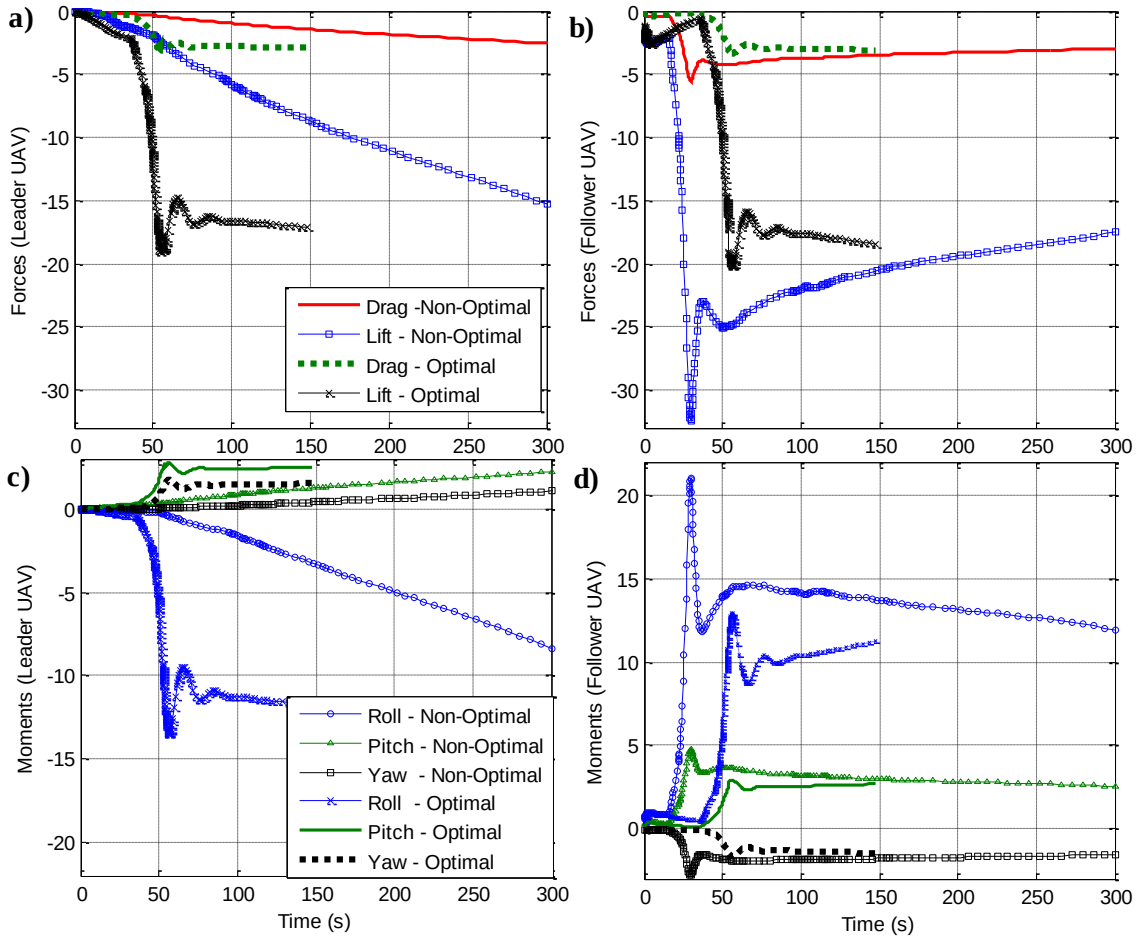

Figure. 4.8 Close proximity aerodynamic disturbance forces and moments acting on each UAV for an optimal and a non-optimal trajectory

4.4.2 Dynamic wind tunnel experiments

A dynamic wind tunnel model has been built and tested to evaluate the docking trajectories. The model consists of a full and half wing with a rectangular planform, with an aspect ratio of 4.5 as seen in Figure 4.9. The wings have a chord of 3 inches and a span of 13.5 and 6.75 inches for the full and half wing, respectively. The full

wing was used to measure the aerodynamic forces and moments using a 6 degree-of-freedom JR3 load cell, which measures lift to 25 lb with a resolution of less than 0.01 lb. Tests use the Cornell University environmental wind tunnel facility, an open return wind tunnel with a 48" x 43" test section. A splitter plate was attached to the half wing to simulate a full wing. The full wing remained stationary, while the half wing is attached to dynamic 3-axis system. The 3-axis system can move in the chord-wise (x – direction) for 18 inches, in the span-wise (y – direction) for 14 inches and vertical direction (z – direction) for 18 inches. Each independent axis is driven by lead screw/lead nut and stepper motor. The stepper motors are controlled by an ATMega32 Atmel microcontroller. Docking trajectories paths are programmed into the microcontroller to dynamically test the trajectories in the wind tunnel.

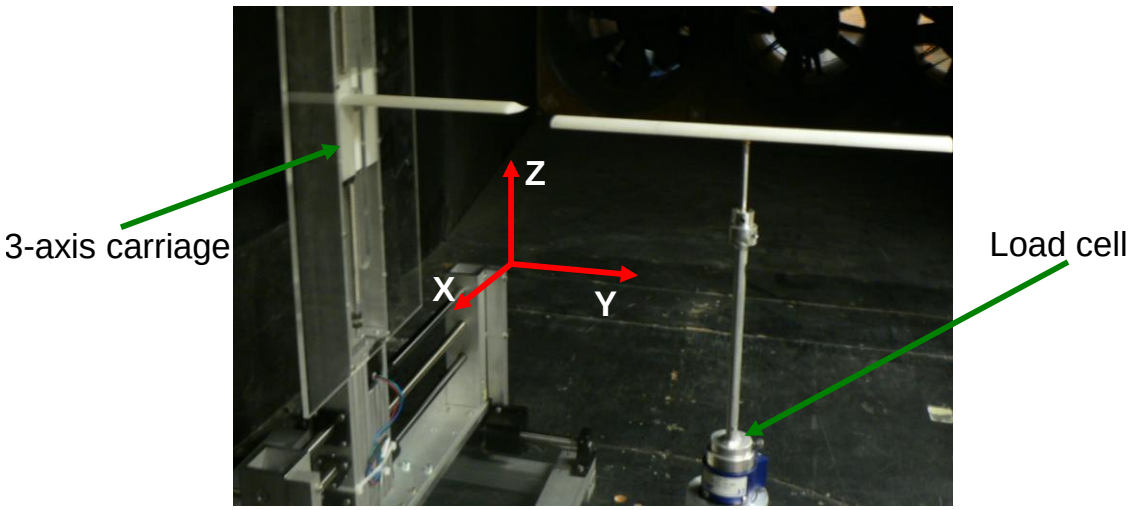

Figure. 4.9 Dynamic wind tunnel setup to test docking trajectories

The two docking trajectories discussed in the previous section, the optimal and non-optimal trajectories, where tested in the wind tunnel. The lift coefficients for the follower UAV wing for both predicted and measured values are plotted as a function of separation for the two trajectories in Figure 4.10. We can see that the measured

values for the lift coefficients are in good agreement with the predicted values from the lifting-line method. For both trajectories the measured values follows the same trends and the error is about 6 %, which is within the expected error for the lifting-line approximation. The wind tunnel tests also corroborate the results from the optimization. The test clearly shows that the optimal span-wise approach experiences less overall disturbances in the lift coefficient.

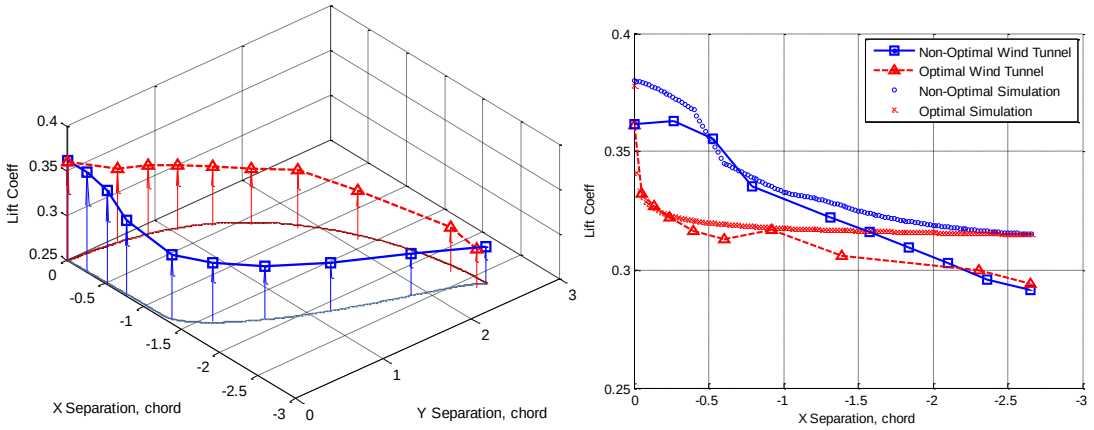

Figure. 4.10 Lift coefficient for both the optimal and non-optimal docking trajectories

The roll moment coefficients for the follower UAV wing for both predicted and measured values are plotted as a function of separation for the two trajectories in Figure 4.11. We see that the measured values for the roll moment coefficients have a good agreement with the predicted values from the lifting-line method. For both trajectories the measured values follows the same trends. From the plot we see that there is an offset between the measured and simulated values. This offset can be attributed to wall effects due to the presence of the two wings. The test clearly shows that the optimal span-wise approach experiences less overall disturbances in the roll moment coefficient.

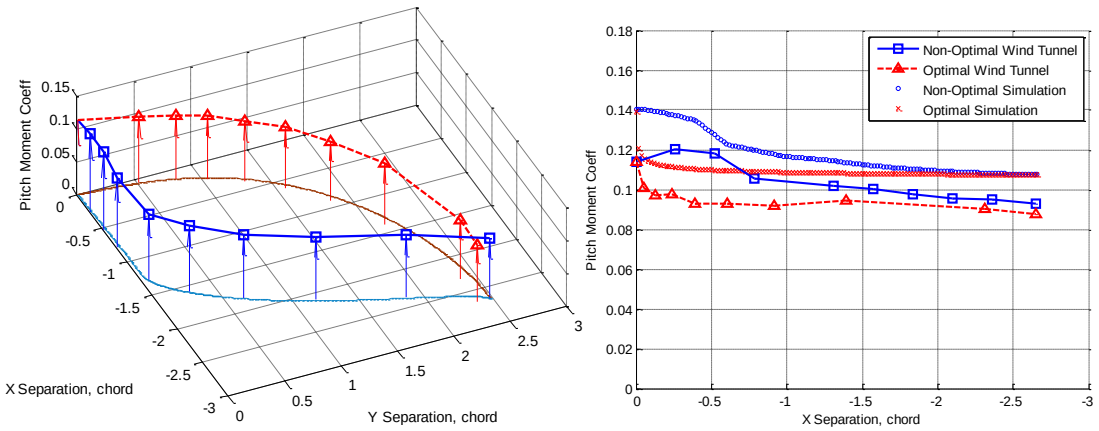

Figure. 4.11 Pitch moment coefficient plot for both the optimal and non-optimal docking trajectories

4.4.3 3-D Docking trajectories

In this section, we present the results of a full 3-D optimization. For this case the restriction for both UAVs to start at the same altitude and maintain a constant altitude is removed from the optimization. Therefore the trajectories simulated by the Simulink model are free to move in any direction in the 3-D space. The initial separations for all three directions (x, y and z separation) are 40 cord lengths. As in the previous case, the follower UAV is far enough downfield, to the side and in the vertical position that there is no aerodynamic coupling between the two UAVs. Similar to the 2-D optimization, this optimization is performed with the same optimization algorithm, dynamic model and cost function. For this case, the optimization yields a 3-D optimal trajectory with the minimum aerodynamic disturbance and consequently minimizing the energy need to perform the docking maneuver.

Figure 4.12 is the plot of the optimal 3-D docking trajectory that resulted from the optimization and the 2-D optimal trajectory from the previous section. The 3-D optimization yielded a similar span-wise approach as the 2-D optimal docking

trajectory. The optimal trajectory path, first approaches both in the chord-wise and vertical direction while maintain a relative large separation in the span-wise direction. The final approach in the 3-D optimal docking maneuver is mainly in the span-wise direction thus resulting in the optimal trajectory being a span-wise approach. If the 3-D optimal trajectory is collapsed to a 2-D plane it mainly follows the 2-D optimal trajectory presented in the previous section.

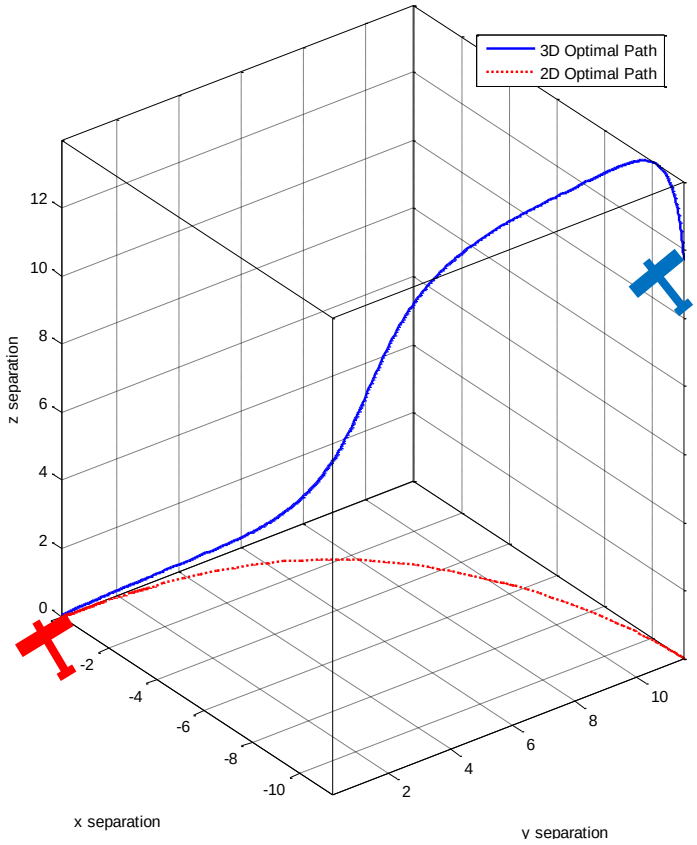

Figure. 4.12 3-D and 2-D optimal docking trajectories

4.5 Conclusions

The problem of modeling and computing a trajectory optimization for wingtip midair docking of a Linked UAV system has been formulated and solved. A 2-D and 3-D optimal trajectories have been presented and analyzed. These trajectories both lead to a span-wise approach for wingtip midair docking as being the optimal path. These results are expected as the close proximity disturbances are smaller in the span-wise direction as compared to chord-wise approach. The span-wise approach not only leads to a lower cost function and lower energy consumption but also to faster times to complete the docking maneuver. A comparison of the 2-D optimal trajectory and a non-optimal trajectory has been presented. Dynamic wind tunnel tests of the optimal trajectory and non-optimal trajectory to correlate the optimization results have been presented.

REFERENCES

1. Pamadi, B. *Performance, Stability, Dynamics, and Control of Airplanes,* American Institute of Aeronautics and Astronautics, 1998, pp. 106–119
2. Schumacher, C., Singh, S., “Nonlinear Control of Multiple UAVS in Close-Couple Formation Flight”, AIAA Guidance, Navigation, and Control Conference 14-17 August 2000, Denver, CO
3. Blake, W., and Multhopp, D., “Design, Performance and Modeling Considerations For Close Formation Flight,” AIAA Guidance, Navigation, and Control Conference, AIAA, Reston, VA, July 1998.
4. Pachter, M., D’Azzo, J., Proud, A., “Tight Formation Flight Control”, *Journal of Guidance, Control, and Dynamics,* Vol. 24, No. 2, March–April 2001.
5. Rossow, V.J., Sacco, J.N., Askins, P.A., Bisbee, L.S., and Smith, S.M., "Measurements in 80 by 120 Foot Wind Tunnel of Hazard Posed by Lift-Generated Wakes," *Journal of Aircraft*, Vol. 32, No. 2, pp. 278-284, August 1993.
6. Pete, K.R., Smith, S.T., and Vicroy, D.D., "Model Validation of Wake-Vortex/Aircraft Encounters," AIAA paper 2000-3979, presented at the AIAA Atmospheric Flight Mechanics Conference, Denver CO, August 2000.
7. Cuji, E., Garcia, E. “Simulation and Wind Tunnel Testing of Close Proximity Aerodynamics of Two Linked UAVs”, Proc. 20th International Conference on Adaptive Structures and Technologies, Hong Kong, 2009.

8. Cuji, E., Lukaczyk, T., and Garcia, E., “Aircraft Dynamics, Wind Tunnel Testing and CFD Flow Visualization of Two Linked UAVs Flying at Close Proximity”, Proceedings of the Smart Structures and Materials 2008: Active and Passive Smart Structures and Integrated Systems, Vol. 7645, SPIE, San Diego, CA, March, 2010.

9. Enright, P. J., and Conway, B. A., “Discrete Approximations to Optimal Trajectories Using Direct Transcription and Nonlinear Programming,” *Journal of Guidance, Control, and Dynamics*, Vol. 15, No. 4, 1992, pp. 994–1002.

10. Stengel, R. F., *Optimal Control and Estimation*, Dover, Mineola, NY, 1994, pp. 421–432.

11. Cuji, E., Garcia, E.“Analytic Modeling of the Aerodynamics of Shape Changing Wings”, Proc. 18th International Conference on Adaptive Structures and Technologies 127, 2007.

12. Cuji, E. and Garcia E. "Analysis of Turning Performance of Symmetric and Asymmetric V-Shape Morphing Wings", International Review of Aerospace Engineering Journal, Vol 4, No 1, February, 2011.

13. Wickenheiser, A. M., and Garcia, E., (2007) “Aerodynamic Modeling of Morphing Wings Using an Extended Lifting-Line Analysis,” *Journal of Aircraft*, 44 no.1, pp. 10-16, 2007.

14. Phillips, W. F., Snyder, D. O. (2000) “Modern Adaptation of Prandtl’s Classic Lifting-Line Theory”, *Journal of Aircraft ,* Vol. 37, No. 4, 2000, pp. 662-670.

15. Prandtl, L., (1918) “Aerofoil Theory, I and II Communications”, *Nachr. Kgl. Gesellschaft der Wissenachaft, Math-phys. Classes*, Göttingen, 1918-19.

16. Wang, Z., Mook, D., “Numerical Aerodynamic Analysis of Formation Flight”, 41st Aerospace Sciences Meeting and Exhibit 6-9 January 2003, Reno, Nevada.

17. Bramesfeld, G., Maughmer, M., “Effects of Wake Rollup on Formation-Flight Aerodynamics”, *Journal of Aircraft,* Vol. 45, No. 4, July–August 2008.

18. Gill, P.E., W. Murray, and M.H. Wright, *Practical Optimization, London*, Academic Press, 1981.

19. Han, S.P., "A Globally Convergent Method for Nonlinear Programming," Vol. 22, *Journal of Optimization Theory and Applications*, p. 297, 1977.